Investigating the mechanisms of the formation of spiral grain and interlocked grain in wood

A thesis submitted in partial fulfilment of the requirements for the Degree

of Master of Science

in Plant Biotechnology

in the University of Canterbury

by Stephanie M. Dijkstra

University of Canterbury

2020

Acknowledgements

Firstly, I would like to thank my supervisory team. To my original senior supervisor Dr David Collings – thank you for your crazy ideas that made this thesis possible. To Dr Ashley Garrill, thank you for your tireless support during this journey. To Dr Clemens Altaner, thank you for

Secondly, I would like to acknowledge the Ngāi Tahu Research Centre, both for the two scholarships that I received from them and for the whanaungatanga and mātauranga that being part of their scholars brought.

I would like to acknowledge the technical staff from the school of biological sciences, the school of forestry and the school of geology for their support. Thank you for going along with the many left-field ideas that I often arrived with, and the generosity that each of you had with your time and knowledge.

Thanks to the most amazing lab group (both past and present) that I could have asked for. Not only have you been fantastic co-workers, but I feel privileged to count you among my close friends (Cell bio Jedi for life!). Special thanks to Liz, Louise, Azy and Annabella for coffee, tea, chocolate and laughter when it was most needed

Thanks to my family for always believing in me and providing support in all its forms.

To my Argentinian sister, I finally submitted! Thank you for always being there for me. This thesis would not have been possible without your hugs and support. I look forward to all the spare time we will now have together.

Finally, thank you to my long-suffering husband Tony Dijkstra. You have helped me through many difficult parts of my postgraduate journey, and I wouldn't be the person I am today without you.

Table of Contents

I. Abstract

Spiral grain is the deviation of grain angle away from the stem axis, where the grain forms a helical array around the pith. In radiata pine, trees are initially straight-grained but develop a left-handed twist in the first year of growth that increases in severity in the several subsequent growth rings until reaching a maximum angle that is often above 5^{o} from vertical. After this, grain angles slowly decrease and sometimes shift to right-handed (Cown et al., 1991; Harris, 1989). Most northern hemisphere gymnosperms follow this pattern in which grain is initially left-handed (Harris, 1989), and they retain this left-to-right pattern when grown in the southern hemisphere suggesting that spiral grain formation is under genetic control. Genetic control of grain direction is also supported by the partial heritability of grain angle severity in radiata pine (Gapare et al., 2007).Suggestions have, however, been made that southern hemisphere gymnosperms develop an initially right-handed twist before shifting back towards the left (Edwards et al., 2007; Kubler, 1991; Ohkura, 1958), although these suggestions are based on observation of only two Australian species, and none that are indigenous to New Zealand. It has been further suggested that any difference in spiralling direction between trees originating in different hemispheres might be caused by an interaction between predominant wind directions, and growth of the young trees towards the sun (Gapare et al., 2007).

While serial sectioning approaches are traditionally used to observe cell development, they are time consuming in both technique and data analysis and can generally only be applied to smaller samples. Additionally, 3D reconstructions can be confounded by section distortion, misalignment or tearing, severely reducing the accuracy of the model generated. A novel method for measuring grain in whole stems of young trees that utilises X-ray microtomography (μCT) has been developed. This technique allows whole stem sections of young trees to be imaged and reconstructed, thereby allowing *in-situ* tracheid angle measurements. Using this technique, several northern hemisphere species grown in New Zealand were analysed and no changes were observed in the grain patterns from the change in hemisphere suggesting that spiral grain is under strong genetic control. Additionally, the analysis of southern hemisphere gymnosperms with this technique demonstrated that the left-handed to right-handed pattern is common among all coniferous species regardless of hemisphere

II. List of Figures

III. List of Tables

Chapter 1 General Introduction

1.1 Overview

Timber and other wood derived products are extensively utilised throughout many aspects of human life; including structural applications, appearance products, furniture and infrastructure, as well as being processed for pulp and paper. For each of these purposes the timber utilised must meet certain wood quality parameters to ensure that it is fit for purpose. These parameters include shrinkage, density, moisture content, stiffness, grain pattern and the presence of knots. In this thesis the development of two grain patterns will be investigated in two different species, the gymnosperm (softwood) *Pinus radiata* (radiata pine) and the angiosperm (hardwood) *Eucalyptus bosistoana* (coast grey box).

Radiata pine is a gymnosperm species native to California, USA, where it is known as the Monterey pine. The maturation period for radiata pine is relatively short, taking 6 years to reach sexual maturity and 20-35 years to harvest when grown in New Zealand (Carson, 1987). This, coupled with its hardiness, even texture and medium density wood has resulted in radiata pine becoming the most important commercial timber species in New Zealand, with plantations covering 1.5 million hectares (ha) and exports totalling $5.47 billion over the 2016-2017 financial year (Forest Owners Association & Industries, 2017). Additionally, radiata pine has become a significant commercial crop in Australia (773 000 ha) and Chile (1.5 million ha) (Mead, 2013). Despite numerous decades of selective breeding and extensive silviculture development, wood quality issues persist within radiata pine. One such wood quality issue is spiral grain, the offset of the wood cells from the vertical axis so that the grain forms a spiral around the pith of the tree (Harris, 1989).

Eucalyptus bosistoana is an angiosperm species native to coastal regions of New South Wales and Victoria, Australia. It is drought tolerant and has a high degree of natural durability to biodegradation and fungal disease, reducing the need for chemical treatment when used for timber. It has, therefore, been selected as an appropriate species for commercial forest development in the dryland areas of New Zealand (Van Ballekom & Millen, 2017). In contrast to radiata pine, *E. bosistoana* exhibits an interlocked grain pattern, where the twisting of the wood grain rapidly switches direction (Harris, 1989).

1.2 Radiata pine and New Zealand forestry

Radiata pine is a native of the coast of California, USA, where it grows in three discrete populations in Santa Cruz, Monterey and San Luis Obispo Counties. While it grows mainly in pure stands, it can also be found comingled with other conifers, such as redwood, Douglas fir, ponderosa pine and macrocarpa (Burdon & Bannister, 1973). The wood produced by these native radiata pine trees is of very poor quality, containing a large number of knots, a high degree of spiral grain and high resin content and is not utilised commercially in the USA (Kininmonth & Whitehouse, 1991).

1.2.1 Introduction to New Zealand

Radiata pine was first introduced to New Zealand in 1859 and planted at Mt Peel Station, Mid-Canterbury, in a private garden. However, the rapid growth and hardiness of radiata pine led Canterbury farmers to utilise it for shelterbelt formation. These traits were also recognised as desirable for timber production, and dwindling indigenous timber supplies, coupled with favourable trials, resulted in the establishment of radiata pine as a commercial species in New Zealand in the 1920s. Trees from the first plantations can be traced back to Año Nuevo Point and Monterey, California and, therefore, originated from a similar latitude to locations where the species is now grown in New Zealand, although the climate is markedly different (Burdon & Bannister, 1973).

1.2.2 Improvement of radiata pine

Since the introduction of radiata pine as a commercial species to New Zealand, the development of superior clonal lines has been of high importance. However, much of this has been focused at the bulk timber and tree level and has neglected to explore the cellular development of undesirable wood traits such as spiral grain.

Early plantings of wild-type trees produced wood with a high proportion of knots, a large number of branches, great variation in height and the propensity to form a forked trunk (Burdon & Bannister, 1973). To combat these undesirable phenotypes, initial lots were planted close together, preventing branch formation which reduced knots present in the wood (Kininmonth & Whitehouse, 1991). This resulted in trees

that, overall, provided large, straight logs and wood of high density. However, this method resulted in significant loss of young trees during thinning, as only those deemed suitable remained to harvest.

In the early 1950s, the genetic improvement of radiata pine as a crop species began. Due to stakeholder pressure, emphasis was placed on rapid growth and stem formation (Burdon, 2010). While this resulted in high yield over a relatively short period, the wood harvested from these plantings was of reduced quality, due to an increase in corewood and structural wood defects. This was due to wood properties largely being ignored by breeders in favour of volume production, resulting in limitations of use for structural and high-grade appearance products.

1.2.3 Spiral grain in radiata pine

Spiral grain is an anatomical feature that is found in the vascular tissue of most trees, and is the deviation of grain angle away from the stem axis such that the grain forms a helical array around the pith (Bannan, 1966; Harris, 1989). The direction of the spiral is defined with respect to the observed angle from the ground: when the helix deviates up to the left it is denoted as left-handed, and conversely, when it deviates up to the right it is denoted as right-handed (Figure 1.1). In older literature, left- and right-handed grain are often described as the S and Z grain patterns, respectively, based on the orientation of the diagonal in these letters.

In severe cases of spiral grain, the grain can be observed through spiral cracks that occur on the outside of the tree or visible twisting in the bark. An example of this is the spiral cracks often observed in electricity poles. However, even minor deviations in the grain angle can result in twisting of milled timber (Harris, 1989). Further information on spiral grain, and its prevalence in radiata pine, is included in Section 1.5.

1.3 *Eucalyptus* trees and New Zealand forestry

Eucalyptus is a genus of 900 angiosperm tree and shrub species found predominantly in Australia, and to a limited extent in Papua New Guinea, Indonesia and Southeast Asia. *Eucalyptus* species can be found in most Australian climates,

and the genus exhibits a large degree of diversity between species. While only a subset of species is utilised in commercial wood production, these timber species have been selected for their strength, rapid growth and natural durability. This natural durability is due to the presence of extractives that exhibit anti-fungal, anti-microbe and insecticide properties (Batish et al., 2008) reducing the need for chemical treatment and fumigation of eucalypt timber products and increasing their longevity when utilised in wet conditions and below ground.

1.3.1 New Zealand utilisation of Eucalyptus

It should be noted that while there are no *Eucalyptus* species native to New Zealand, this was not always the case. Numerous fossils containing *Eucalyptus* leaves have been found in Miocene (5 to 23 million years ago) deposits in Gondwana derived locations such as New Zealand and Patagonia (South America) indicating that *Eucalyptus* distribution used to be more widespread (Gandolfo et al., 2011; Pole, 1994).

Eucalypts were among the first exotic trees to be planted in New Zealand by the early settlers, with over 100 species of the genus planted around the country in private gardens. The rapid growth and durability of *Eucalyptus globulus* led to its utilisation in shelterbelt formation and general farm usage, becoming the most commonly planted eucalypt species in the 1900s. However, the susceptibility of *E. globulus* to insect attack resulted in its usage being largely abandoned (Fry, 1983; Wilcox, 1980). This, coupled with the dominance of radiata pine in New Zealand, has resulted in a general lack of interest in the development of eucalypts as a commercial timber resource.

In recent years concerns around the usage and disposal of chromated copper arsenate (CCA) treated radiata pine has resulted in a demand for the development of a naturally durable timber resource. CCA-treated posts are extensively utilised for trellising throughout the New Zealand viticulture industry. Disposal of these posts produces hazardous waste and is costly. Additionally, improperly treated posts can leach arsenic, copper and chromium into the surrounding soils resulting in concerns about soil toxicity and grapevine uptake (Ko et al., 2007). The natural durability and strength of eucalypts make their timber ideally suited to replace CCA-treated radiata

pine in agricultural and horticultural settings, as well as replacing imported hardwood utilised in critical infrastructure (power poles, railway sleepers) (Van Ballekom & Millen, 2017).

To this end, the New Zealand Dryland Forests Initiative (NZDFI) commenced a large-scale research trial in 2008, focused on the development of eucalypt timber resources, in New Zealand. This research has focused primarily on three species, *Eucalyptus bosistoana* (Coast Grey Box), *Eucalyptus globoidea* (White Stringybark) and *Eucalyptus quadrangulata* (White-topped Box), which were chosen for their high natural durability, drought and frost tolerance, pest tolerance, fast growth and straight stems. As a part of this trial this thesis will investigate the prevalence and severity of interlocked grain in *E. boisistoana*.

1.3.2 Interlocked grain in Eucalyptus

Interlocked grain is a similar phenomenon to spiral grain, where spiral grain will reverse systematically, cycling between a left and right-handed form (Figure 1.1c). The severity of the interlocked grain is dependent on the periodicity of this shift and the maximum grain angle (Harris, 1989; Thinley et al., 2005). Whereas spiral grain is universally regarded as undesirable, as it makes sawn timber prone to warping, the rapid changes in grain angle from interlocked grain result in a cross-laminate structure and cause an increase in timber stability and, when sawn, produces a ribbon stripe effect. Interlocked grain can therefore be seen as a desirable trait for product when either log strength or appearance is prioritised (Fry, 1983; Hernández & Almeida, 2007).

1.4 The Plant Cell Wall

1.4.1 Cell wall and plant cell structure

A plant cell is surrounded by a rigid cell wall that maintains cell shape, allows the generation of turgor pressure and provides stability to the entire plant. The cell wall is composed of three layers, the middle lamella, the primary cell wall and, in some cells, a secondary cell wall (Figure 1.1). The middle lamella is the external layer of the cell wall that links adjacent plant cells and is mainly composed of the polysaccharide pectin (see Section 1.4.2). This layer is the remains of the cell plate

that initially divides a plant cell into two during cytokinesis (Aloni, 1987). Inside the middle lamella, the primary and secondary cell walls provide structure to the individual cell and are discussed further below.

1.4.1.1 Primary cell wall

The primary cell wall is a thin, flexible layer that is composed of cellulose microfibrils (25-30%), hemicellulose (20-30%), pectin (30%), structural proteins and other ancillary molecules (Albersheim, 2011). These compounds are defined in Section 1.4.2. Cellulose microfibrils provide the tensile strength within the cell wall and their orientation within the wall determines cell shape and the direction of expansion. A random orientation of the microfibrils will cause isotropic cell expansion, equal in all directions, and result in a spherical cell. Instead, plant cells contain a primary cell wall with an ordered orientation of the microfibrils to constrain expansion to one direction (anisotropic cell expansion). This direction will be perpendicular to the cellulose microfibrils, as the cellulose itself cannot elongate. (Baskin, 2001; Chan, 2012).

1.4.1.2 Secondary cell wall

The secondary cell wall develops inside, and subsequent to, the primary cell wall, and is only produced by some cell types. This wall consists of three distinct layers that differ both in structure and function. The outermost layer, S_1, is the first to be deposited and is the thinnest of the three as it is only 0.1-0.35 µm thick. This layer contains transverse cellulose microfibrils which limit further radial expansion, thereby fixing the width of the developing plant cell. The middle layer, S_2, is the thickest layer (1-10 µm) and is highly lignified. This layer therefore provides the mechanical support to the plant cell. Additionally, the cellulose microfibrils reorient during the deposition of this layer, from a transverse orientation to a longitudinal arrangement. This orientation strengthens the cell wall parallel to the direction of growth and therefore provides mechanical support against the effects of gravity. The third layer, S_3, is deposited closest to the lumen of the cell. While this layer is thin (0.5 -1.1 µm) it is highly lignified; more so than the S_2 layer in radiata pine. This allows the S_3 layer

to function as a barrier between the lumen and the rest of the plant cell wall (Mellerowicz et al., 2001; Ptashnyk & Seguin, 2016).

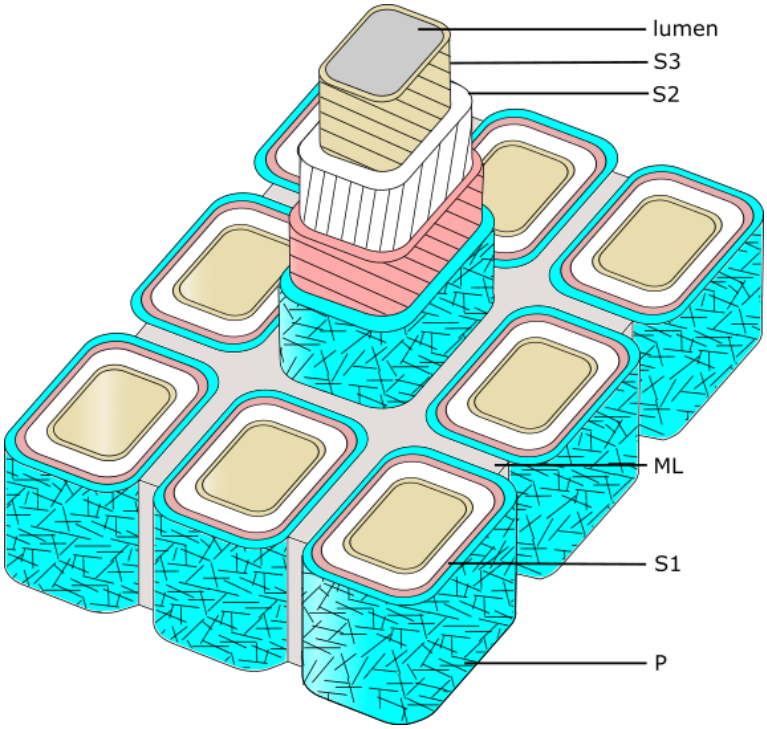

Figure 1.1: Organisation of the cell wall layers in a tracheid

ML – middle lamella, **P** – Primary wall showing random microfibril arrangement, **S1** – outer layer of secondary wall with transverse microfibrils, **S2** – middle layer of secondary wall with longitudinal microfibrils, **S3** – inner layer of secondary wall with transverse microfibrils, **lumen** – the cavity inside the tracheid

1.4.2 Cell wall components

As detailed in the previous section, the plant cell wall is composed of cellulose, hemicellulose, pectin, lignin and various cell wall proteins. Cellulose is the main component of the plant cell wall and is a polysaccharide homopolymer made from repeating 1-4 linked β-D-glucose units attached into long chains. Eighteen of these polymer chains are bundled into microfibrils about 10-25 nm in diameter (Newman et al., 2013). Within this microfibril the individual strands interact with each other through tight noncovalent bonding, and it is this that imparts significant tensile strength into the plant cell wall (Ptashnyk & Seguin, 2016).

Hemicellulose is another polysaccharide whose composition varies, with different hemicellulose components found in different plants and in different cell walls. Hemicellulose is, therefore, a general term for all heterogeneous glycan polymers. In many dicotyledons, the most abundant hemicellulose is xyloglucan, a branched polymer containing a backbone of 1-4 inked β-D-glucose residues with short attached side chains containing xylose, galactose and fucose residues. Xyloglucan has been shown to bind to the surface of the cellulose microfibrils in the primary cell wall, thereby linking adjacent microfibrils together and further increasing the rigidity of the plant cell wall (Cosgrove, 1997; Strabala & MacMillan, 2013). In the secondary cell wall, galactoglucomannan is more common, making up 10-30% of total cell wall polysaccharides. The backbone of galactoglucomannan consists of alternating glucose and mannose residues with galactose side chains. In compression wood, a type of reaction wood formed in gymnosperms on the lower side of tilted trunks and in side branches, the cell wall has a reduced quantity of galactoglucomannan, making it more brittle (Nanayakkara et al., 2005).

Pectins are a gel-like heteropolymer found in high concentrations in the primary cell wall and the middle lamella, and lower or negligible concentrations in secondary cell wall layers. It surrounds the cellulose-hemicellulose network, stabilising it. Pectin characteristically contains acidic sugars such as glucuronic acid and galacturonic acid and is therefore, highly hydrophilic, attracting water into the plant cell wall. This imparts plasticity to the growing plant cell wall, allowing for expansion of the plant cell (Cosgrove, 1997; Mellerowicz et al., 2001).

Lignins are polymers formed from three phenolic compounds: *p*-coumaryl (H), coniferyl (G) and sinapyl (S) alcohols. The ratios of these differ depending on the fraction of the cell wall, functionality of the cell and the species of the plant. The lignification of the secondary cell wall strengthens it against compressive forces, with the S monolignols interacting with crosslinking glycans in the hemicellulose. Compression wood formation in gymnosperms drastically increases the lignin concentration of cell walls, whereas in tension wood, the analogous reaction wood formed in angiosperms on the upper side of leaned stems, lignin content is greatly reduced or eliminated (Joseleau et al., 2004; Timell, 1986). The second crucial function that lignin provides is waterproofing the plant cell. Cellulose, hemicellulose and pectin are all hydrophilic and therefore promote water conduction, both in and out of the plant cell. Lignin, however, is hydrophobic and, by crosslinking the hemicellulose and pectin, prevents water from entering the plant cell wall. This increases the efficiency of water conduction through the lumen of the plant cell (Donaldson, 2001).

1.4.3 Wood anatomy

The trunk of a tree consists of five main elements which are, from the outside of the tree, the outer bark, phloem, cambium, secondary xylem and pith. The bark acts as a physical barrier that protects the tree from the environment, insects and pathogens, while the phloem is located underneath the outer bark and is composed of sieve elements and associated cells for nutrient conduction from source tissues to sink tissues, parenchyma cells for storage and sclerenchyma for support. Inside the phloem is the vascular cambium, a lateral meristem that contains mother cells, and is where wood cell development begins through specific cell divisions and then cell differentiation. On the inside of the vascular cambium, is located the secondary xylem, the tissue that is commonly referred to as “wood” and which in angiosperms contains vessel elements (broad, open-ended conducting cells), fibre cells and ray parenchyma cells. In gymnosperms, however, the secondary xylem contains tracheids (narrow, closed end conducting cells), resin canals and ray parenchyma cells. Finally, the pith at the centre of the tree is composed of parenchyma cells that can store nutrients and waste products. In trees, the pith is only present in young growth and this storage functionality is eventually replaced by the xylem cells (Esau,

1965). The vascular cambium and secondary xylem will be discussed in further detail in the following sections.

1.4.3.1 The vascular cambium

The vascular cambium contains highly vacuolated meristematic cells and is formed at the cessation of primary growth from procambial cells. There are two main cell types present in the vascular cambium: longitudinally oriented fusiform initials and radially oriented ray initials. The fusiform initials are significantly longer than they are wide, while the ray initials are short and squarish in appearance. From these initials new phloem and cambial cells are formed through longitudinal proliferative cell divisions in the periclinal plane (parallel to the stem surface). If the new cell is produced toward the outside of the stem, it will become a phloem cell but if the new cell is produced towards the pith, then it will differentiate into a xylem cell (Altamura et al., 2001; Chaffey et al., 2002).

There are two types of vascular cambia; storied and non-storied (Larson, 1994). A non-storied cambium is the most common type and is where the ends of the fusiform initials overlap so that there is no discrete pattern to the cambial cells when viewed in a tangential longitudinal section. These fusiform initials increase in number (necessary for a vascular cambium that progressively increases in circumference) through anticlinal divisions of existing fusiform cells. Whereas the divisions that give rise to new xylem and phloem divide the fusiform initial lengthwise, in the non-storied cambium, the divisions that produce daughter fusiform cells do not occur fully lengthwise. Instead, the divisions form partially across the cell, and are thus known as pseudo-transverse divisions. Non-storied cambial initials extend to their full length through the process of intrusive growth, where the tip of the cell squeezes between existing cell files (Kojs et al., 2004; Mazur & Kurczynska, 2012; Włoch et al., 2013).

A storied cambium, in contrast, is considered as an evolutionarily more advanced feature, and has evolved separately multiple times (Wyatt et al., 2010). It consists of fusiform initials that are aligned in the horizontal plane so that when the vascular cambium is sectioned longitudinally in a tangential plane, the ends of the fusiform initials are all aligned. These fusiform initials are significantly shorter that their non-storied counterparts. A significant difference between the storied and no-storied

cambia is that formative divisions in the anticlinal plane that produce new fusiform initials can occur though full, longitudinal cytokinesis. Thus, these daughter cells are the same length as the parent cells, and do not have to undergo significant intrusive growth. It has been suggested that this storied structure provides an adaptive advantage for tropical trees as short initials allow for fast growth and rapid reorientation of the initials to form interlocked grain that will increase the stability of the tree (Altamura et al., 2001; Bannan, 1968; Kojs et al., 2004; Kojs et al., 2003). The cambia present in radiata pine and *E. bosistoana* are non-storied (Dickson et al., 2016; Medhurst et al., 2011), therefore both species undergo intrusive growth during expansion of the fusiform cells.

In trees from temperate regions, a seasonal difference in cambial activity can be observed manifesting as distinct bands of earlywood and latewood. Earlywood has proportionally thinner cell walls and wider cells and latewood has proportionally thicker cell walls and narrower cells. The change from earlywood to latewood is gradual and is not discernible to the naked eye. However, the change from latewood to early wood is abrupt and it is this change that is observed as tree rings (Kininmonth & Whitehouse, 1991). Both radiata pine and *E. bosistoana* have observable growth ring patterns, however they are often more visible in radiata pine (Dickson et al., 2016; Medhurst et al., 2011).

1.4.3.2 Wood organisation

The woody part of a tree consists of different elements depending on whether the tree is an angiosperm or gymnosperm. The woody area of angiosperms contains fibre cells, vessel elements, and ray parenchyma cells whereas the woody area of gymnosperms contains tracheids, ray cells, and resin canals.

Vessels, the wide conducting cells found in most angiosperms and some gymnosperms, are built up from individual vessel elements (dead cells) that are connected end-to-end and which provide a pipe-like system to transport water and nutrients from the roots to the apex of the tree. To facilitate this function, the ends of each vessel element are open and have perforation plates, multiple openings in the end walls that align with those in the adjoining vessel element. Additionally, the side walls of vessel elements often contain pits, both to facilitate inter-vessel connections

and to connect vessels to other cell types within the xylem. The vessels are surrounded by fibre cells which are long narrow cells (generally 1-2 mm long, but in some species up to 6mm long, and 10µm - 50µm in diameter) with pointed ends and a highly lignified cell wall. Their primary function is to provide stability to the tree, and they are only found in angiosperms. Like the vessels, these cells are also dead at maturity (Butterfield, 2006; Butterfield & Meylan, 1980).

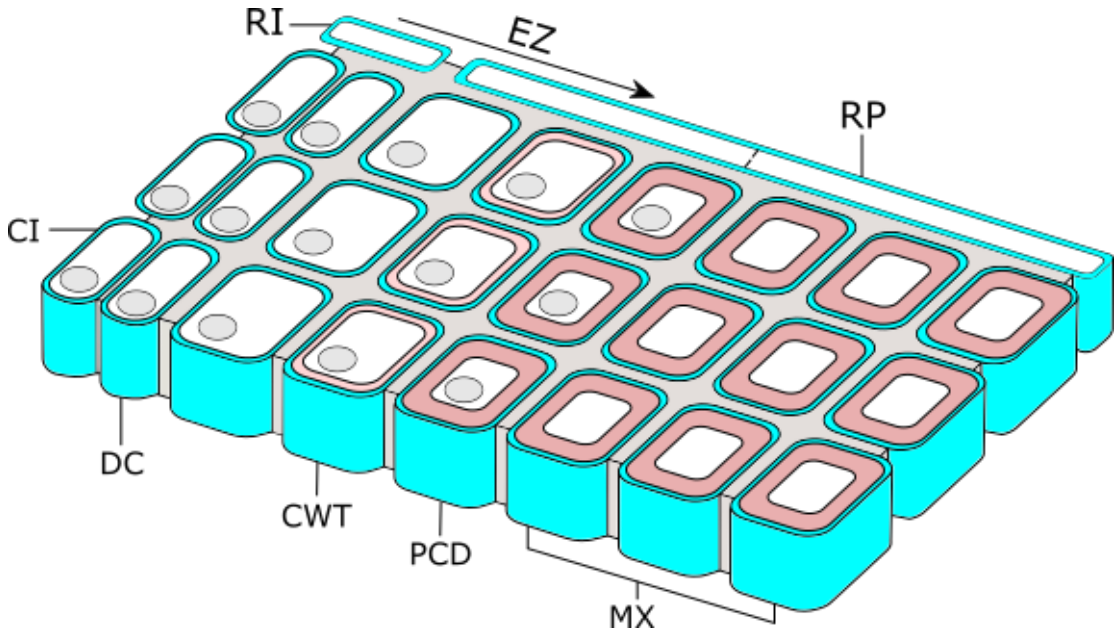

Figure 1.2: Wood organisation within the cambial domain of a gymnosperm

CI – cambial initial (mother cell), **DC** – daughter cell, **CWT** – cell wall thickening, **PCD** – programmed cell death, **MX** – mature xylem, **RI** – ray initial, **EZ** – expansion zone, **RP** – ray parenchyma cell

In contrast to the vessels, the tracheids, which are the conducting cells found in gymnosperms, are narrow although they also die once they mature. These tracheids also conduct water and nutrients from the roots to the tree crown, as well as providing structural support to the tree. Tracheids contain a lignified secondary cell wall and connect to each other through bordered pits. Unlike the vessel elements, the ends of the tracheids are tapered and closed, meaning that water must flow through the lateral bordered pits (Butterfield, 2006). In radiata pine, the tracheids are highly asymmetric and have average dimensions of 38 µm in diameter and 3 mm in length (Patel, 1971).

With their significantly larger diameter, 94-135 µm in trees such as *E. bosistoana*, the vessels of angiosperms are considered evolutionarily more advanced than the narrow tracheids of gymnosperms, and actually evolved from tracheids (Dadswell, 1972). Due to the large diameter and open ends of the vessels, water can move more efficiently. However, vessels are susceptible to air embolisms and freezing damage from ice crystal formation in winter. The narrow diameter of tracheids reduces the likelihood of freezing damage and air embolisms in gymnosperms and therefore has an advantage in extreme climates (Esau, 1965).

The properties of wood and the grain are determined by the angle of the fibre cells in angiosperms and the tracheids in gymnosperms. Therefore, the development of tracheids and fibre cells need to be understood to predict and improve wood properties

Ray cells are a part of the radial system and allow movement of nutrients from the phloem to the xylem and water from the xylem to the phloem. They also serve as storage sites for starch, proteins and lipids. In angiosperms, the rays tend to be larger than those in gymnosperms and often form multiseriate bundles (Butterfield & Meylan, 1980). There are three types of ray cells: ray parenchyma, ray tracheids and ray epithelial cells. Ray parenchyma cells generally have only a thickened primary cell wall and are alive at maturity, allowing them to dedifferentiate upon injury (Aloni, 1987). They are present in both angiosperms and gymnosperms. Ray tracheids are similar to axial tracheids in that they are dead and they are located at the margins of the ray cells in gymnosperms (Butterfield & Meylan, 1980). Ray epithelial cells line

the radial resin canals that are formed in some gymnosperms (Butterfield & Meylan, 1980; Yamanaka, 1984).

The final cell type present in wood are the resin canals. Resin canals are only present in some gymnosperms and are part of the axial system. In most plants, resin canals are formed in response to wounding, as the resin has anti-fungal and insecticide properties (Yamanaka, 1984). However, resin canals can be formed in the absence of wounding in radiata pine and some other conifers. The distribution of resin canals within radiata pine is modulated by external factors that are separate to wounding, with canals being less frequent in reaction wood and in wind-stimulated wood (Thomas & Collings, 2016)

1.4.4 Wood formation

Wood formation begins with the division of the cambial initial cells, and as described above, division of the fusiform initials can occur in either of two planes and occurs at a ratio that allows both the radial and circumferential growth of the stem (Figure 1.3). Periclinal divisions, parallel to the vascular cambium and the stem surface, occur longitudinally and result in daughter cells that are added to the radial file of existing xylem (or phloem) cells. Anticlinal cell divisions, however, add to the circumference of the stem, as the fusiform initials divide at right angles to the stem surface (Bannan, 1968; Larson, 1994).

In a non-storied cambium, the division plate during anticlinal divisions is more oblique than longitudinal, adopting a partially transverse orientation. These divisions are often referred to as pseudo-transverse. As the new daughter cells, which are shorter than the mother cell, undergo cell expansion the tips of the cells intrude between the existing cells, potentially reorienting the longitudinal orientation of the new fusiform cells (Bannan, 1966; Karczewska et al., 2009; Mazur & Kurczynska, 2012). An equilibrium between radial and circumferential growth is maintained through the elimination of ~10% of anticlinal daughter cells, either by differentiation to phloem or xylem element cells, or into ray cambial cells (Harris, 1973; Iqbal & Ghouse, 1990). This maintains the equilibrium between radial and circumferential growth.

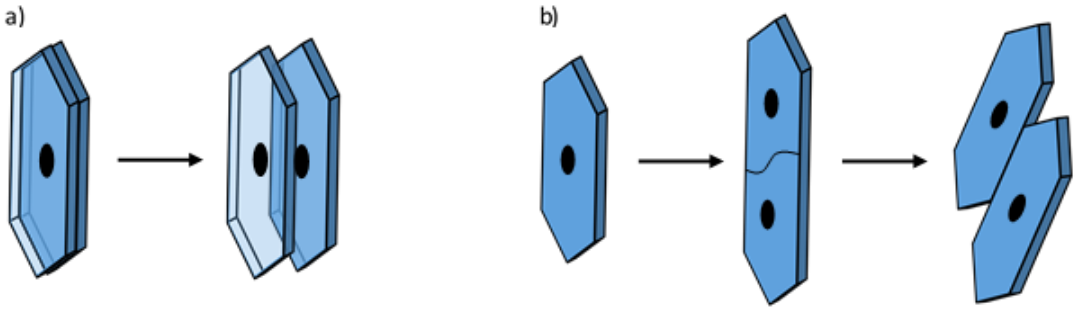

Figure 1.3: Cambial cell division **a)** periclinal divisions add to the cell file, **b)** anticlinal divisions add to the stem circumference

Once the fusiform initials have divided, the daughter cells produced expand both longitudinally and radially to their final dimensions. These cells possess only a primary cell wall, and therefore have the necessary plasticity for wall expansion to occur. The longitudinal growth involves the same intrusive growth process as found in newly forming fusiform initials. During intrusive growth, the tips of the expanding daughter cells grow between the neighbouring xylem cells. This is driven by turgor pressure and the middle lamella of the neighbouring cells is loosened at the tip of the expanding cell (Lev-Yadun, 2001; Schoch-Bodmer & Huber, 1952).

Following cell expansion, secondary wall deposition occurs. In addition to lignification and deposition of the S1 and S2 layers, the developing axial cell also undergoes bordered pit formation. These pits align between tracheids and allow movement of materials between xylem cells (Chaffey et al., 1997). Once this process is completed the cell undergoes programmed cell death, only retaining its cell wall (Mellerowicz et al., 2001).

1.5 Spiral Grain, and related grain phenomena

Spiral grain, the helical twisting of the wood grain around the pith, is a growth pattern that can be observed in both gymnosperms and angiosperms growing in both plantations and natural forests. It is, therefore, a natural phenomenon and the

tendency for many tree species to form spiral grain would suggest it confers an evolutionary advantage to the tree (Braun, 1854; Harris, 1989; Northcott, 1957; Ohkura, 1958).

While spiral grain may be advantageous for the living tree, the presence of spiral grain in cut timber is problematic for human utilisation. Thus, the propensity of sawn timber containing spiral grain to twist, warp, and/or split has led to the classification of spiral grain as a wood defect by foresters. The link between spiral grain and these undesirable wood properties has long been known to those working with timbers and has long been a subject of academic interest. In the third century BC, the Greek philosopher Theophrastus, considered to be the father of "Modern Botany", wrote in his work "*Enquiry into Plants*" that

> ὅσα δὲ ὑποπαράβορρα καὶ ἐν περίπνῳ, ταῦτα στρέφει καὶ παραλλάττει παρὰ μικρὸν ὁ βορέας, ὥστε εἶναι παρεστραμμένην αὐτῶν τὴν μήτραν καὶ οὐ κατ᾽ ὀρθόν. ἔστι δὲ ὅλα μὲν τὰ τοιαῦτα ἰσχυρὰ τμηθέντα δὲ ἀσθενῆ διὰ τὸ πολλὰς ἔχειν παραλλαγάς. καλοῦσι δὲ οἱ τέκτονες ἐπίτομα ταῦτα διὰ τὸ πρὸς τὴν χρείαν οὕτω τέμνειν
>
> But if a tree stands sideways to the north with a [draft] round it, the north wind by degrees twists and contorts it, so that its core becomes twisted instead of running straight. The timber of such a tree while still in one piece is strong, but, when cut, it is weak, because the grain slants across the several pieces. Carpenters call such wood 'short lengths,' because they thus cut it up for use.

While Theophrastus attributed the formation of spiral grain to the action of the wind, the actual causes of spiral grain, and how the patterns develop, remain a mystery.

1.5.1 Spiral grain

Spiral grain is more commonly found in gymnosperm than angiosperm species. In most gymnosperms a left-handed twist is the most common initial form, and radiata

pine provides an excellent example of this. The wood immediately adjacent to the pith is always straight grained, but the wood that is formed in the first year of growth develops a left-handed twist. The grain angle then steadily increases within the first eight to ten growth rings, after which the angle decreases often reaching 0° or becoming steadily more right-handed (Cown et al., 1991; Harris, 1989; Schulgasser & Witztum, 2007). In radiata pine, trees will frequently achieve a left-handed twist between 1 - 9°, with some trees exceeding this and reaching values as high as 18° (Cown et al., 1991; Moore et al., 2015). This pattern, with the central tree rings being left-handed and with the outer rings being vertical or right-handed, is called the LR pattern (figure 1.4a).

The reverse of this pattern, where the grain is initially right-handed and eventually becomes left-handed, is the RL pattern (figure 1.4b) and has been observed in some Japanese and Australian species (Harris, 1989; Ohkura, 1958).This has led to the hypothesis that there is a hemispherical difference in the direction of spiral grain formation (Kubler, 1991; Schulgasser & Witztum, 2007; Skatter & Kucera, 1998, 1997). The impacts of the environment on spiral grain formation will be discussed further in section 1.5.6.

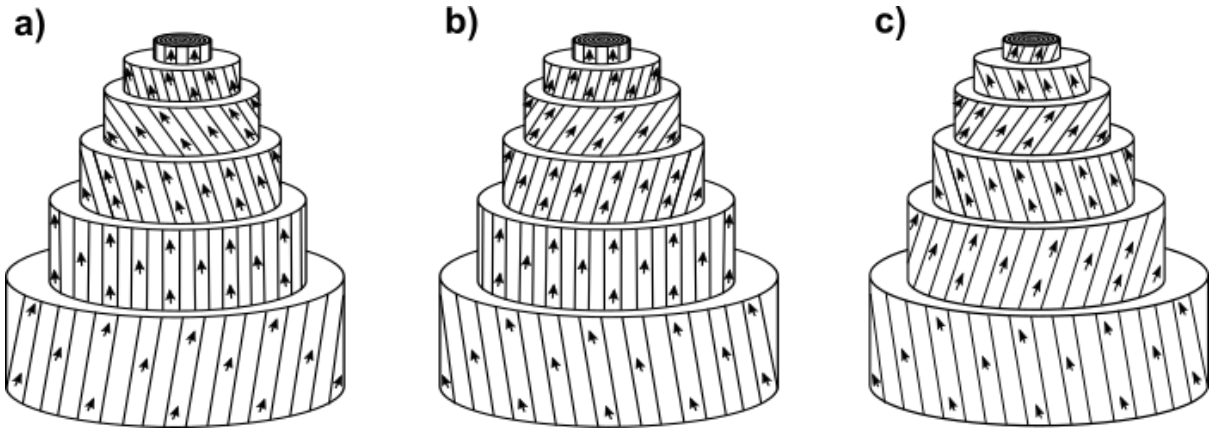

Figure 1.4: Spiral and interlocked grain

- **a)** Left to right-handed spiral grain pattern
- **b)** Right to left-handed spiral grain pattern
- **c)** Interlocked grain

1.5.2 Interlocked grain

Interlocked grain is often viewed as a modification of spiral grain, as the grain angle switches between left-handed and right-handed between growth rings or even within a growth ring (figure 1.4c). This alternating pattern results in wood that, when the radial face is sawn, exhibits a ribbon stripe pattern (Krawczyszyn, 1972; Kubler, 1991). This is caused by the cellulose microfibrils inclined either towards or away from the observer, thereby reflecting the light at different angles and is desirable for furniture making. However, interlocked grain can also cause warping, cracking and grain tear out during processing and therefore can limit timber utilisation (Harris, 1989; Hernández & Almeida, 2007).

Wavy grain is a variation on interlocked grain where the grain angle oscillates down the stem axis, producing a wavy figure when the timber is radially sawn. Curly grain is a more irregular form of wavy grain (Harris, 1989). Both these grain patterns are highly prized and are utilised in musical instrument and fine furniture production.

1.5.3 The economic impacts of grain angle

Spiral grain classified as a wood defect due to the negative impact it has on wood properties, primarily strength and shrinkage issues upon drying, and therefore the human utilisation of timber (Harris, 1989; Thinley et al., 2005).

Due to the anisotropic grain angle, cut timber will have a non-longitudinal grain, reducing the strength of the timber. A grain angle between 5° and 10° results in a 10% decrease in compressive, tension and bending strength and grain angles exceeding 15° result in a 20-80% reduction in strength (Kollmann & Côté, 1968) Additionally, it has been shown that grain angles above 2° severely reduce the impact strength of timber (Boas, 1933; Koehler, 1924).

Cut timber containing spiral grain is susceptible to both board warping and shrinkage following kiln drying. While board warping can be mitigated through controlled drying under restraint, this requires the moisture content to be lowered to the conditions that the board will be subjected to in situ and is therefore impractical and time consuming. It has been also demonstrated that boards containing 5° of spiral grain can undergo shrinkage double that of straight-grained timber (Harris, 1969).

These effects result in the downgrading of timber or rejection for structural utilisation, causing significant economic losses within the forestry industry. During the 1990s, the presence of spiral grain was estimated to devalue harvested radiata pine by $100 million per year in New Zealand (Sorensson & Lausberg, 1996), and more recent estimates suggest that the European softwood industry suffers from a devaluation of about €1 billion per year (Tarvainen, 2005). Thus, there is a clear need to understand the mechanisms through which spiral grain may develop.

1.5.4 Cellular development of spiral grain

For the cellular development of spiral grain, the plant cell wall must have enough plasticity to distort (Kubler, 1991; Schulgasser & Witztum, 2007). Therefore, spiral grain formation is most likely to occur before secondary cell wall deposition. The three stages of cell development that would have the greatest impact on cell shape determination are:

- Formation of the preprophase band and phragmoplast
- Intrusive growth
- Cell expansion

As mentioned in section **Error! Reference source not found.**, the organisation and orientation of the cytoskeleton is important for the regulation of cell shape and anisotropy at any of these three stages could result in cell shape variation, including spiral grain development.

1.5.4.1 Anisotropic plant cell division

The cell division plane is initially defined by the preprophase band, a ring of microtubules that bisect the nucleus during prophase. Studies have shown that the preprophase band accurately predicts both the symmetry and axis of the new cell wall (Gunning & Wick, 1985; Nick, 2007).

The Arabidopsis mutant *ton1* lacks a preprophase band but can form a normal mitotic spindle and phragmoplast. The daughter cells resulting from these divisions show severe cellular anisotropy and microtubule misalignment in both hypocotyl and root cells, with cells varying in size, shape and orientation throughout all plant organs. This indicates that the preprophase band is integral in the positioning of the

cell plate and suggests that cell plate positioning is a key determining factor in cell shape (Azimzadeh et al., 2008; Traas et al., 1995).

Phragmoplast formation and alignment can also impact cell shape. The *mor1-1* mutant contains a defective microtubule associated protein involved in formation of the preprophase band, mitotic spindle and phragmoplast. This mutation results in temperature-dependent microtubule disorganisation, which leads to left-handed twisting and radial swelling in organs. Imaging of phragmoplast formation at the restrictive temperature showed it to be obliquely oriented in some cells, indicating that phragmoplast orientation may also have a role in determining the cell axis (Kawamura et al., 2006; Twell et al., 2002; Whittington et al., 2001).

1.5.4.2 Asymmetric intrusive growth

Intrusive growth occurs before cell maturation and therefore the surrounding cells have enough plasticity to deform when the cell tips elongate into the middle lamella between neighbouring cells. Włoch et al. (2002) observed that asymmetric intrusive growth of cambial initials, where the cell ends grew from one cell file to another, resulted in asymmetric periclinal divisions. They suggested that this could be a mechanism of cambial initial reorientation, resulting in spiral grain formation.

Furthermore, it has been observed that intrusive growth of fibre cells in the xylem generally follows the direction set by pseudotransverse divisions (Hejnowicz & Romberger, 1979; Włoch & Zagorskamarek, 1982). This has led to the hypothesis that spiral grain arises from the reorientation of the cambial initials during intrusive growth, and subsequent periclinal divisions and maturation of the xylem cells result in this orientation becoming “fixed” (Harris, 1973; Schulgasser & Witztum, 2007; Włoch et al., 2013).

1.5.4.3 Asymmetric cell expansion

Cell elongation and expansion occurs primarily through intrusive growth in developing xylem cells. However, immediately following cytokinesis, the daughter cell needs to expand radially to its final size (as detailed in section 1.5.4). While this

expansion is constrained by the neighbouring cells, the plasticity of the cambial zone will allow a degree of cellular reorientation (Albersheim, 2011; Harris, 1989).

As discussed in section **Error! Reference source not found.**, the orientation of cytoskeleton guides the direction of cellular expansion. Thus, coupled with the cambial plasticity, a change in the cytoskeletal arrangement in expanding cambial cells could cause a change in the overall cell orientation.

1.5.5 Heritability

The heritability of certain traits within a species is influenced by both environmental and genetic factors and can be utilised to predict the phenotypic variation within a population. Broad-sense heritability (H) is the ratio of total genetic variance to total phenotypic variance and therefore includes the effects of dominance and epistasis. Narrow-sense heritability is the ratio of additive genetic variance to the total phenotypic variance, this is important in plant selection programs as the response to selection pressures depends on additive generic variance. Additionally, the resemblance between relatives is mostly driven by additive genetic variance (Wray & Visscher, 2008).

The likelihood of a phenotypic trait to be inherited from the parents of an individual can be calculated by using a regression of the progeny phenotypic variation vs the parental phenotypic variation (H^2 and h^2). A low heritability value (0.1) shows that there is high environmental variation in phenotypic expression, whereas a high heritability value (1.0) shows that there is no environmental variation and the phenotype is therefore under genetic control (Cornelius, 1994).

There are a significant number of studies regarding the heritability of spiral grain in gymnosperms. Hansen and Roulund (1998) reported that the narrow-sense heritability of spiral grain in *Picea sitchensis* (Sitka spruce) was 0.7, therefore demonstrating that spiral grain can be inherited. Spiral grain was also shown to be heritable in radiata pine ($h^2 = 0.44 \pm 0.12$) and *Picea abies* (Norway spruce) ($H^2 = 0.42$) (Gapare et al., 2007; Hannrup et al., 2002). Many other timber species have also been investigated to determine the genetic control of spiral grain, including *Picea roxburghii* (Chir pine) (Paul et al., 2015) and *Pinus taeda* (Loblolly pine) (Zobel et al., 1968). In these studies, heritability was observed in both clonal and sexually

propagated progeny, strengthening the argument that spiral grain development is under genetic control.

There have also been a small number of heritability studies conducted on species exhibiting interlocked or wavy grain. Fan et al. (2013) discovered that curly grain (an extreme form of wavy grain) in curly poplar (*Populus canescans x P.* alba) is heritable, but the frequency of trait inheritance suggests that curly grain is not simply controlled by a dominant or recessive gene. Thinley et al. (2005) observed that both the tendency to develop interlocked grain and the amplitude of the grain oscillations are heritable in *Eucalyptus dunnii* (Dunn's white gum) (h^2= 0.99 and h^2=0.63 respectively). However, the periodicity of interlocked grain oscillations was not found to be heritable (h^2=0.0) and it was therefore posited that this is under environmental control.

1.5.6 Environmental causes of spiral grain

Environmental factors are also thought to play a supporting role in spiral grain formation, and it has been proposed that spiral grain might be an adaptive response to and strong winds. The premise of this theory is that due to the phototropic response on trees, systemic crown asymmetry will naturally develop within most forest trees.

In the northern hemisphere, where the Sun tracks through the southern sky, growth will occur preferentially on the southern side of the tree. This phototropic effect would result in longer branches forming on the equatorial-side, and shorter branches forming on the poleward side of the tree. This pattern would also occur in the southern hemisphere, with the difference being that growth would preferentially be on the northern side of the tree (Skatter & Kucera, 1998, 1997)

According to the proposal by Skatter and Kucera, most Northern Hemisphere coniferous forests are subjected to a prevailing westerly wind and this, combined with the crown asymmetry, results in the tree being subjected to a strong right-handed torque. This would be stronger in younger trees where the growth asymmetry is more pronounced. Southern hemisphere coniferous forests are also subjected to a westerly wind. However this, combined with an increasingly northern crown asymmetry, will instead result in a left-handed twist (Skatter & Kucera, 1998). The response of the tree would be to counter this torque through the generation of spiral grain, with this being

preferentially left-handed in northern hemisphere species and right-handed in southern hemisphere species

The correlation between the direction of tree crown asymmetry, wind direction, and grain angle was further examined by Eklund and Säll (2000). Their results showed a correlation between the angle of the tracheids compared to the axis, with trees exhibiting a left-handed angle if the crown was asymmetric to the north and a right-handed angle if the crown was asymmetric to the south.

The hypothesis that spiral grain direction is linked to hemisphere location, fails however to account for the findings that a northern hemisphere species grown in the southern hemisphere will not reverse its grain angle. It has been suggested that this could be due to long term selection of those trees that exhibit a left-to-right pattern and that this grain angle trend is therefore under genetic control. However, if this is the is the case Southern Hemisphere conifers should still exhibit an initial right-handed twist, followed by a shift in to left-handed in mature wood. This has yet to have been characterised, with no grain angle currently available for those species indigenous to the Southern Hemisphere and is therefore one of the objectives of this thesis.

1.6 Aims in this thesis

In this thesis, spiral grain and interlocked grain will be investigated through a variety of systems and techniques, including X-ray microtomography and wood splitting techniques. Additionally, the environmental causes of spiral grain will be investigated through the analysis of northern hemisphere species grown in New Zealand, and the characterisation of the grain patterns of New Zealand native gymnosperms.

Chapter 2 Hemispheric trends in twisting of indigenous gymnosperm species

The research in this chapter was funded by a grant from the Brian Mason Trust to Dr DA Collings entitled "*Investigating spiral grain in New Zealand gymnosperms*"

Research in this chapter involved the use of native species and was approved by the University of Canterbury Māori Research Advisory Group.

Research in this chapter has been presented at conferences:

Dijkstra S and Collings DA. "Global trends in the initiation of spiral grain in gymnosperms." February 21st, 2017, New Zealand Cell wall symposium, Rotorua.

2.1 Introduction

Spiral grain is the deviation of grain angle away from the stem axis, where the grain forms a helical array around the pith. The direction of this spiral is defined with respect to the observed angle from the ground: when the helix deviates up to the left it is denoted as left-handed, and conversely, when it deviates up to the right it is denoted as right-handed. The direction of spiral grain is also dynamic, with radiata pine exhibiting straight grain in the first year of growth before developing a left-handed twist that reaches it maximum angle in the second or third growth ring. Subsequently, the angle then steadily decreases towards zero and then shifts to right-handed (Cown et al., 1991; Moore et al., 2015; Skatter & Kucera, 1997). This is defined as a left-to-right grain development, sometime abbreviated as LR. Most Northern Hemisphere conifers show either this LR pattern, or have an L pattern in which no reversal occurs (Harris, 1969; Harris, 1989; Skatter & Kucera, 1997)

It is, perhaps, significant that several authors have noted a reversal of this LR pattern to an RL patterns in Southern Hemisphere gymnosperms (Harris, 1989; Skatter & Kucera, 1998). However, this conclusion is based on the observation of just two Australian species, *Agathis robusta* (Queensland kauri pine) and *Araucaria cunninghamii* (hoop pine) (Balodis, 1971). As noted by Skatter and Kucera (1998), analysis of other Southern Hemisphere species would be required to test the robustness of this theory. To this end, the research in this chapter will focus on the characterisation of grain angle in young trees of New Zealand gymnosperms species.

2.1.1 Potential causes of a hemispherical difference in grain direction

While the mechanisms of spiral grain formation are not generally understood, a persistent assumption is that such development has a function and therefore confers a survival benefit to the tree. One primary proposed function of spiral grain is that it allows the trunk to withstand mechanical forces applied by wind. As suggested by Skatter and Kucera (1998), the spiral grain phenotype may result from exposure to persistent torsional forces created by an asymmetric crown perpendicular to the prevailing wind direction (see section 1.5.6).

This initial hypothesis that spiral grain direction is linked to hemisphere location fails to explain why a northern hemisphere species grown in the southern hemisphere

would not reverse its grain angle even though the phototropic growth asymmetry would be reversed. It has therefore, been concluded that this could be due to long term selection of those trees that exhibit a left-to-right pattern and that this grain angle trend is therefore under genetic control. However, if this were to be the case, then New Zealand native gymnosperm species should exhibit an initial right-handed twist, followed by a shift to left-handed in mature wood while their Northern Hemisphere relatives should retain their LR pattern.

This model is open to numerous additional objections. Firstly, as explained above, the southern hemisphere data used to support this model is based on only two Australian species. Secondly, it ignores the extensive but somewhat obscure data set compiled by Ohkura (1958) in which numerous southern hemisphere species were measured, many which exhibited a left-right pattern. And thirdly, the model might be criticised for the generic assumption that wind directions are predominantly in a westerly direction in both hemispheres and all locations that significant forestry plantations are situated. In fact, were the model to be correct, local variations in wind direction might be expected to generate differential grain responses that vary by locality.

Nevertheless, the availability of new methods to investigate grain at high resolution allows differences between grain in northern and southern hemisphere species to be investigated in detail, and to determine whether there might be some validity to the model proposed by Skatter and Kucera (1998).

2.1.2 Measuring spiral grain in trees

A significant barrier to research into wood grain development is the tree itself. The density of the wood and size of the samples prevent *in situ* analysis of cambium and xylem. While grain angle can be detected through splitting, scribe tests and other macroscopic techniques (Bannan, 1966; Harris, 1989; Koehler, 1960; Ogata et al., 2003), these fail to elucidate the mechanisms of grain deviations at a cellular level and instead only confirm the presence or absence of spiral grain and the degree of severity. Therefore, to further any hypotheses on the mechanisms of spiral grain formation, a cellular approach must be taken.

Traditional approaches to observing spiral grain at a cellular level involve embedding and serial sectioning approaches (Ogata & Fujita, 2005). While these methods allow high resolution imaging at the cellular level, they are also constrained by the area that can be covered by sectioning, and the mixture of tissue types that exist within the tree. The cambium of trees consists of cells with a primary cell wall, giving them a high degree of plasticity during cell expansion and intrusive growth. However, the xylem of trees consists of cells with a rigid lignified secondary cell wall and therefore is much harder than the cambium. The interface of these two tissue types results in significant cambium compression at the beginning of the section and significant cambium tearing at the terminus (Dickson et al., 2016).

While this can be accommodated for by choosing a more rigid embedding medium, this will reduce the maximum section thickness possible and therefore increase the number of sections required to image grain angle over a relevant scale. Additionally, serial sectioning relies on image reconstruction, either manually or with computer software to align each individual section into a 3D volume before grain analysis can be conducted. All grain angle values obtained through this method would therefore be subject to error from section misalignment or distortion.

To overcome these limitations in conventional serial sectioning, this study has used X-ray computed microtomography to image wood samples at near cellular resolution, and to measure wood grain. This allowed grain analysis in whole stem sections that were 1-2 cm in height, and thus covering several orders of magnitude more volume of cells than conventional approaches.

2.1.3 X-ray microtomography and analyses of wood samples

X-ray computed microtomography is a technique that allows three-dimensional (3D) *in situ* imaging of sample blocks with minimal preparation. To achieve this, the sample is illuminated by a conical X-ray source and a two-dimensional (2D) detector collects the resulting X-ray transmission image. This projection shows the differing levels of X-ray absorbance in the sample, which is directly proportional to radio density and chemical composition of the sample. Typically, elements with a higher atomic number (that is, further down the periodic table) are stronger X-ray absorbers (Flannery et al., 1987). By affixing the sample to a stub and rotating the sample through 180°, around

a fixed axis and with a constant step size of 0.2° to 1°, all structural angles of the sample are collected (Figure 2.1). This generates a series of 2D images that can be reconstructed into a 3D virtual volume using a Filtered Back Projection algorithm.

In the last decade, X-ray microtomography has been used to visualise xylem connectivity in a range of plants including ferns and (Brodersen et al., 2011; Brodersen et al., 2012), and xylem organisation in *Arabidopsis* (Dhondt et al., 2010). The approach has been used to observe wood structure. Xylem anatomy has been investigated in the gymnosperms *Picea abies* (Fuhr et al., 2012; Trtik et al., 2007), *Pinus taeda* (loblolly pine) and *Pseudotsuga menziesii* (Douglas fir) (Mayo et al., 2010) and *Pinus sylvestris* (Scots pine) (Van den Bulcke et al., 2009), and in the angiosperms *Fagus sylvatica* (beech), *Disthemoanthus benthamianus* and *Afzelia bipindensis* (Van den Bulcke et al., 2009), *F. sylvatica* and *Quercus robur* (oak) (Steppe et al., 2004), *Q. robur* (Stuppy et al., 2003) and unidentified species of eucalyptus and teak (Mayo et al., 2010).These experiments have investigated the shapes of individual cells (fibres and vessels) and have confirmed that X-ray microtomography images match traditional sectioning approaches.

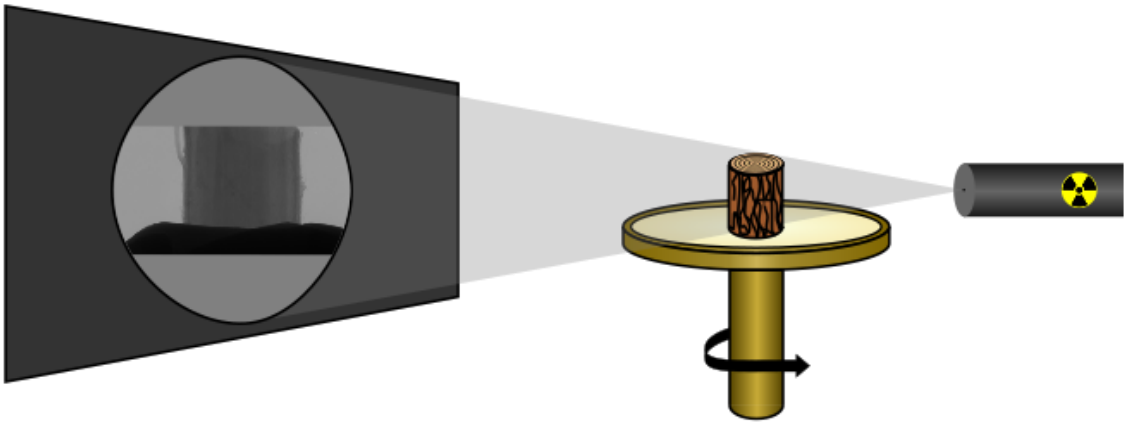

Figure 2.2: X-ray microtomography set up. A sample was affixed to a stub and an X-ray image collected. The sample was then rotated progressively through 180°, with X-ray transmission images collected by a detector at every 0.4º. Such images can then be used to calculate the structures present within the sample

To date, there are no published studies in which X-ray microtomography has been used for the analysis of wood grain at a cellular level, beyond some introductory analyses (Thomas & Collings, 2017). Unpublished data has, however, confirmed that radiata pine shows increasingly left-handed grain in the first year of growth, with grain developing from an average of several degrees right-handed to several degrees left-handed (Thomas *et al*., *manuscript in preparation*). Similar unpublished experiments have also investigated the changes in wood grain associated with interlocked grain in the tropical hardwood, African mahogany (Collings *et al*., *manuscript in preparation*). X-ray microtomography, therefore, represents a tool through which many samples can be processed for wood grain measurements at high resolution, and in a relatively short period of time.

2.1.4 Aims in this chapter

The work conducted in this chapter aims to assess the suitability of X-ray microtomography for analysis of grain patterns in gymnosperms species, investigate the relationship between spiral grain direction and hemispherical location, and characterise the grain patterns of native New Zealand gymnosperms

2.2 Methods

2.2.1 Collection of plant samples

A total of 24 gymnosperm species were investigated in this study, with 18 being northern hemisphere species that come from 3 different families (Cupressaceae, Pinaceae, Podocarpaceae) and a total of eight native species from 3 different families (Araucariaceae, Cupressaceae, Podocarpaceae) (Table 2.1). To reduce the influence of environmental factors, as these have been indicated as factors in grain pattern development, all northern hemisphere trees were purchased from Southern Woods (Templeton, Canterbury, New Zealand) at roughly 6 months of age and were therefore subjected to similar environmental pressures. Southern hemisphere trees were 1-3 years old, were purchased from Taupo Native Plant Nursery (Kumara, Westland, New Zealand).

Table 2.1. Gymnosperm species investigated in this study.

Family	Species	Common Name	N [1]	Supplier
New Zealand natives				
Araucariaceae	*Agathis australis*	Kauri	9	Southern Woods
				Taupo Native
Cupressaceae	*Libocedrus bidwillii*	Pāhutea	6	Taupo Native
Podocarpaceae	*Dacrydium cupressinum*	Rimu	5	Taupo Native
	Dacrycarpus dacryoides	Kahikatea	6	Taupo Native
	Prumnopitys ferrugineus	Miro	6	Taupo Native
	Prumnopitys taxifolia	Mātai	9	Taupo Native
				Southern Woods
	Podocarpus totara	Tōtara	5	Taupo Native
	Podocarpus hallii	Halls Tōtara	4	Taupo Native
Northern hemisphere species				
Cupressaceae	*Cupressus leylandii*	Leyland cypress	5	Southern Woods
	Cupressus macrocarpa	Monterey cypress	5	Southern Woods
	Cupressus torulosa	Himalayan cypress	5	Southern Woods
	Cryptomeria japonica	Japanese cedar	5	Southern Woods
	Juniperus chinensis	Chinese juniper	5	Southern Woods
	Sequoiadendron giganteum	Giant sequoia	5	Southern Woods
	Sequoia sempevirens	Coastal redwood	4	Southern Woods
Pinaceae	*Abies vejarii*	Silver fir	5	Southern Woods
	Cedrus deodara	Deodara cedar	5	Southern Woods
	Larix decidua	European larch	5	Southern Woods
	Picea abies	Norway spruce	5	Southern Woods
	Pinus coulteri	Coulter pine	5	Southern Woods
	Pinus pinaster	Maritime pine	5	Southern Woods
	Pinus radiata	Radiata pine	5	Southern Woods
Podocarpaceae	*Podocarpus macrophyllus*	Buddhist pine	5	Southern Woods

[1] Replicate number varied depending on availability and cost.

Sections (10 cm long) were excised from the stems near the base of each tree. Care was taken to avoid nodes and structural defects within the sample as these areas may contain changes in grain angle that are not due to spiral grain. Samples were then fixed with FAA fixative solution (10% (v/v) formaldehyde, 5% (v/v) acetic acid and 50% (v/v) ethanol) and stored in this solution for a minimum of 24 h.

2.2.2 X-ray microtomography

For use, samples were washed extensively with tap water. The samples were then cut to ensure height did not exceed 2 cm and then washed in 50% ethanol for 24 h under vacuum. They were then placed through an ethanol series of 50%, 70%, 90% and 100% for 2 h each. Finally, the stem sections were air-dried to minimise vascular collapse in the cambium and placed in an airtight container with silica beads to maintain desiccation.

Samples were analysed using a Bruker µCT Skyscan 1172 (Kontich, Belgium) at Otago Micro and Nanoscale Imaging (the University of Otago, Dunedin). To prevent movement during scans, samples were affixed to the stub with plasticine. As the plasticine will significantly absorb X-rays, and therefore reduce the reconstruction quality, care was taken to ensure that a small quantity was used to stack samples and, where possible, reconstructions were conducted away from this area. All samples were scanned with an average voltage of 40 kV, a current of 250 µA, a rotation step size of 0.39° and a magnification of 3.99 µm/px.

Shadow images generated by X-ray tomography were reconstructed through the NRecon program and output as 16-bit tiff files. With the above settings, the reconstructed images had a resulting voxel size of 3.99 x 3.99 x 3.99 µm. Pre-processing was conducted in Photoshop to convert files from 16 bit to 8 bit to reduce processing memory requirements. In imageJ (version 1.51i), a stack of 500 images was created, corresponding to a sample depth of 2 mm. This stack was then cropped to remove excess space around the trees. A three-dimensional Gaussian blur was run with values of x=1, y=1 and z=5 to smooth any misalignment due to the reconstruction process. Brightness and contrast of the stack was altered to ensure a bright image and reduce any background interference.

The pith was then blacked out and the centre marked with a 10 px white circle providing a mark for grain angle calculations. Strips 1mm wide were selected at 0°, 45°, 90° and 180° and resliced to give an optical tangential stack (Figure 2.2). These vertical slices through the sample showed the angle of the tracheids within the wood sample. Grain angle was then calculated in each of the stacks using the directionality plugin (Tinevez, 2017). The directionality algorithm detects the orientation of structures in each image, returning the average angle, standard deviation, amount of structures that have an orientation within the standard deviation, and goodness of fit of the model. This plugin was applied to each virtual radial slice and the amount, and goodness values were used to screen the resulting data, ensuring that only the vertical xylem cells were measured.

Using a custom-developed excel spreadsheet, these four measurements were then averaged to ascertain the grain angle of the whole stem. As the sections were all placed by hand on the stub, there was some variance in vertical alignment. To account for this samples were optically radially sectioned, and the offset angle was measured using the directionality algorithm. This was then subtracted from the calculated initial asymmetry and the difference applied to sections orthogonal to this.

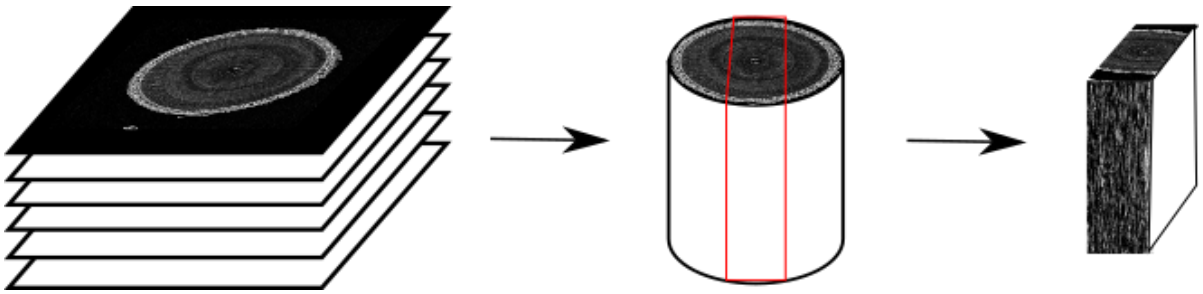

Figure 2.2: Samples were reconstructed into a 3D virtual volume and then a strip taken through the centre. The grain angle was then measured in the optical longitudinal sections through a Fast Fourier transform. In actual measurements, 1 mm slices were also collected at 45º, 90º and 135º rotations to get 4 strips across the wood sample.

2.3 Results

2.3.1 X-ray microtomography of Northern hemisphere gymnosperms

Due to the commercial significance of many northern hemisphere gymnosperms, the grain patterns they develop have been well characterised. The analysis of the fourteen selected Northern Hemisphere species therefore achieved two purposes; firstly, due to natural variance in grain patterns within a species, and the unknown genetic provenance of the trees utilised, it was important to ensure that consistent grain patterns could be observed. Secondly, these trees were used to validate the X-ray microtomography technique through comparison with literature values.

Spiral grain development was categorised depending on the maximum left-handed and/or right-handed angle reached in the sample. Grain angles ≤0.5° were classified as straight grained, grain angles between 0.5 – 1.0° as weak spiral grain, grain angles between 1.0 – 5.0° as moderate spiral grain, and grain angles ≥5.0° as severe spiral grain. The weak spiral grain classification was based on work conducted by Cown et al. (1995), that determined that an increase in grain angle of 1° resulted in a 3.3% reduction in tensile strength and a 1.2% reduction in bending stiffness. Spiral grain angles greater than 5° are classified as severe, the resulting loss of strength and increase in warping makes it unsuitable for structural applications, resulting in the downgrading of timber (Cown et al., 1991).

2.3.2 General trends in the grain pattern of northern hemisphere gymnosperms

The effect of growth in the southern hemisphere on northern hemisphere species was investigated. The overall spiral grain direction in the northern hemisphere species was determined using X-ray microtomography, and the results compared to literature values (table 2.2).

Silver fir (*A. vejarii*) is a medium sized fir, native to North-eastern Mexico, where it grows at high altitudes (Esteban et al., 2009). No literature could be found discussing grain patterns or the general figure of the wood in silver fir. Analysis of five silver fir trees gave an overall grain pattern of initial right-handed grain that shifted to left-handed (figure 2.3a)

Table 2.2 Grain observations in northern hemisphere gymnosperms

Species	Common Name	Pattern (measured)[1]	Pattern (literature)[1]	Reference
Pinus radiata	Radiata pine	weak L	L – R	(Cown et al., 1991)
Pinus pinaster	Maritime pine	weak L	L – O	
Pinus Colteri	Coulter pine	O		
Picea abies	Norway Spruce	weak R -L	L – R	(Ohkura, 1958) (Säll, 2002)
Abies vejariii	Silver Fir	R-L		
Sequoia sempervirens	Coast redwood	O	R	(Ohkura, 1958)
Cedrus deodara	Deodar cedar	O		
Cryptomeria Japonica	Japanese cedar	O	weak R	(Ohkura, 1958)
Cupressus x leylandii	Leyland Cypress	O	O	(Low et al., 2005)
Cupressus torulosa	Himalayan Cypress	O		
Cupressus macrocarpa	Monterey Cypress	O	O	(Harris, 1989)
Larix decidua	European Larch	weak L	L – R	(Burger, 1950)
Juniperus chinensis 'Kaizuka'	Chinese Juniper	O	L	(Jacot, 1931)
Podocarpus macrophyllus	Buddhist pine	O	R	(Ohkura, 1958)

[1] Grain direction: L=left-handed, R=right-handed, O=straight grained

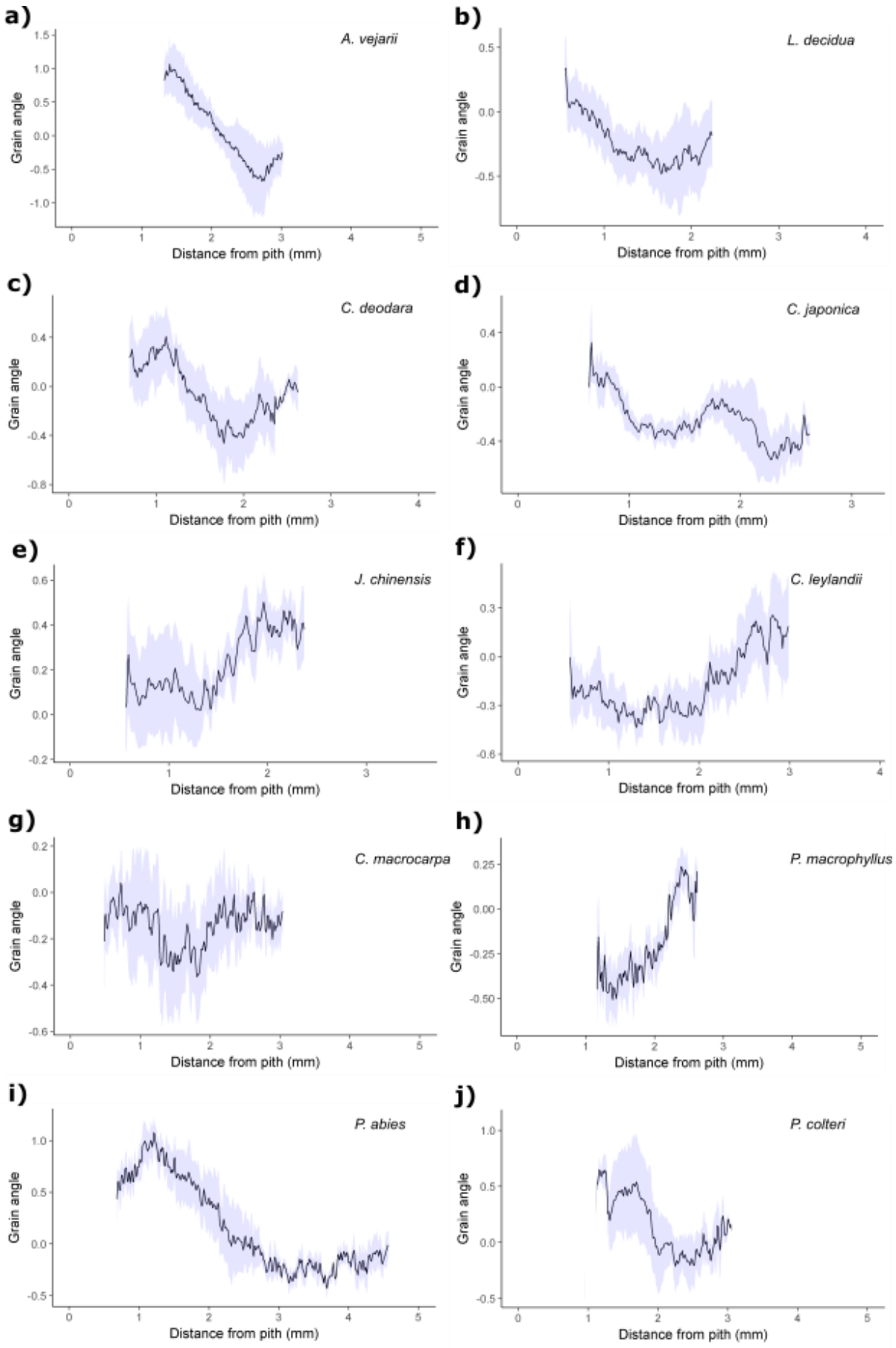
a)
A. vejarii
b)
L. decidua
c)
C. deodara
d)
C. japonica
e)
J. chinensis
f)
C. leylandii
g)
C. macrocarpa
h)
P. macrophyllus
i)
P. abies
j)
P. colteri
Grain angle
Distance from pith (mm)

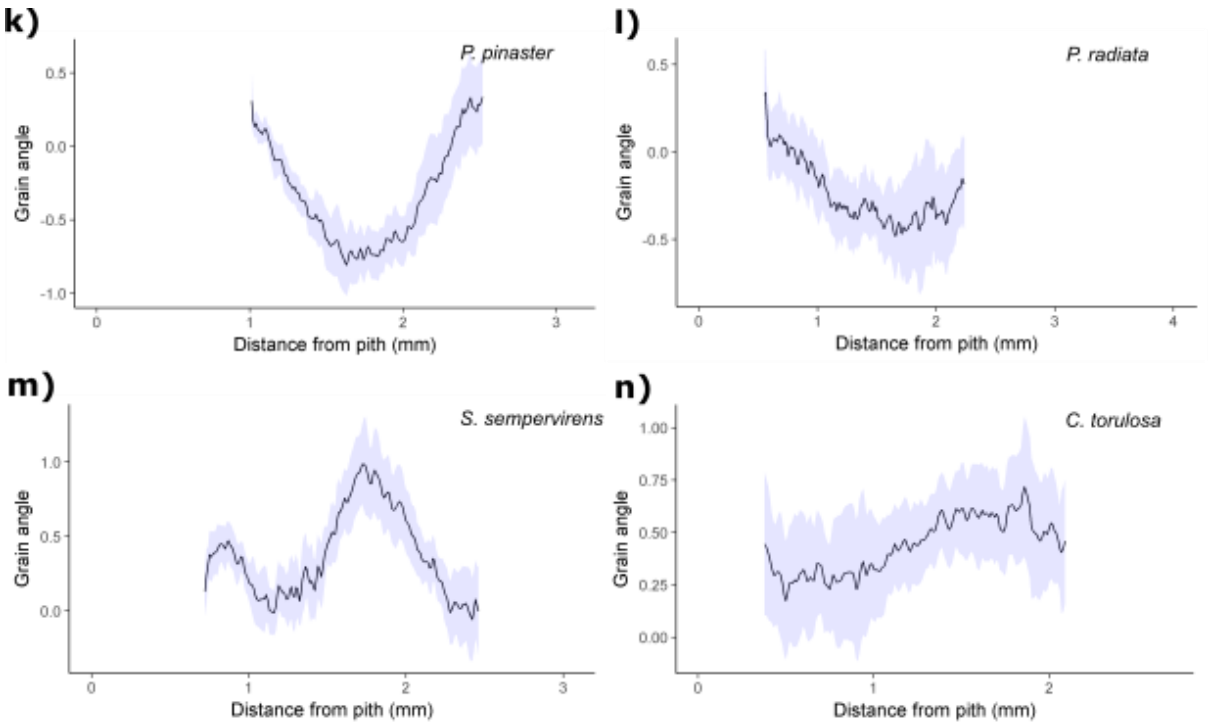

Figure 2.3: Average grain pattern for the fourteen northern hemisphere gymnosperms analysed with X-ray microtomography. Except for *S. sempervirens* (n = 4), replicate number = 5.

European larch (*L. decidua*) is a medium – large sized deciduous conifer that is native to the mountainous regions of central Europe (Moser et al., 2009). It was introduced to New Zealand for erosion control measures, but has become invasive in high country areas (Ledgard, 2008). Spiral grain has been well characterised in this species, with Burger (1950) conducting a study with 1774 individuals and discovering that european larch has left-handed spiral grain in youth, switching to right-handed spiral grain in maturity (100-200 years). The five european larch trees analysed, when averaged, had initial straight grain that shifted to weak left-handed spiral grain (figure 2.3b).

Deodar cedar (*C. deodara*) is a medium sized, evergreen conifer that is native to the Himalayan region. Its drooping branches make it a popular ornamental throughout the world, and oil extracted from deodar cedar is utilised for a variety of uses due to its

fungicidal, antibacterial and pesticide properties (Tewari, 1994). No literature could be found discussing the predominant grain patterns in deodar cedar, however, the five trees analysed (figure 2.3c), when averaged, had straight grain, with minor fluctuations in grain angle (≤0.4°).

Japanese cedar (*C. japonica*) is a large evergreen conifer, that is native to Japan. It is extensively used in forestry plantations in Japan, China and the Azores Islands and is a naturally durable timber (Ohba, 1993). Studies completed by (Ohkura, 1958) discovered that Japanese cedar has a weak right-handed twist (less than 1°). The five trees analysed when averaged, had straight grain, with minor fluctuations in grain angle up to 0.5° left-handed (figure 2.3d).

Chinese juniper (*J. chinensis*) is an evergreen conifer that grows 1-20 m tall and is native to northeast Asia, including China, Mongolia, Japan, Korea and the southeast of Russia. It is primarily used as an ornamental and is an important bonsai species (Thurn et al., 2018). A study conducted by Jacot (1931) of 38 trees discovered that over half had left-handed spiral grain (Harris, 1989). The five trees analysed in this thesis, when averaged, had straight grain with minor fluctuations in grain angle up to 0.4° right-handed (figure 2.3e).

Leyland cypress (*C. x leylandii*) is a hybrid of the Monterey cypress and the Nootka cypress and is utilised extensively in shelterbelts throughout New Zealand and in limited plantations. It is reported to be straight grained and produces high quality timber (Low et al., 2005). The five trees analysed in this thesis had overall straight grain (figure 2.3f).

Monterey cypress (*C. macrocarpa*) is a medium sized evergreen conifer that is native to the central coast of California, USA. It is used in shelter belts throughout New Zealand and its attractive timber is utilised in the manufacture of fine furniture (Low et al., 2005). Monterey cypress is reported to have straight grain, however, when grown as a shelter belt, can develop severely interlocked or curly grain (Harris, 1989). The five trees analysed in this thesis, when averaged, had even, straight grain (figure 2.3g).

Buddhist pine (*P. macrophyllus*) is a small – medium sized evergreen conifer that is native to southern Japan and eastern China and is a highly valued ornamental (Silba, 1983). Work conducted by Ohkura (1958) discovered that buddhist pine has right-handed spiral grain, with a maximum twist angle of 3.50°.The average of the five

buddhist pine trees analysed in this thesis concurred with this finding, with initial right-handed grain developing in the first 1mm of growth (figure 2.3h).

Norway spruce (*P. abies*) is a medium sized evergreen conifer endemic to northern Europe. It is the most commercially important timber species in Europe and is utilised for paper and timber production. Säll (2002) discovered that spiral grain in Norway spruce is initially left-handed, reaching a maximum angle in growth rings 4-8, before shifting to become right-handed. The average of the five trees analysed in this thesis matches this pattern, with a minor variation, there is initial weak right-handed grain closest to the pith, that then shifts to left-handed (figure 2.3i).

Coulter pine (*P.coulteri*), or big-cone pine, is native to the southern Californian mountains (USA) and is a large sized evergreen conifer. It has the largest cone of any pine tree and is therefore valued as an ornamental. The wood is weak and extremely soft and the timber therefore has limited usage (Chase, 1911). No literature could be found on the wood grain properties of the coulter pine, however, the five trees analysed in this thesis had an overall trend of straight grain with minor fluctuations in grain angle ±0.4° (figure 2.3j).

Maritime pine (*P. pinaster*) is a fast growing, medium sized conifer endemic to the Mediterranean basin and is one of the most important plantation trees in France, Spain and Portugal. Maritime pine has been characterised as having moderate left-handed spiral grain, that shifts to become straight grained (Harris, 1989). The average of the five trees analysed in this thesis match this pattern, with the grain rapidly becoming left-handed before returning to straight grain (figure 2.3k)

Radiata pine (*P. radiata*) is a moderate sized conifer that is of great importance to the New Zealand forestry industry (see section 1.2). The development of spiral grain is well characterised in radiata pine, with left-handed spiral grain developing in growth rings 2-4 (Gapare et al., 2007). The five radiata pine trees analysed in this thesis had an average weak left-handed twist begin development 2 mm from the pith, which coincided with commencement of the second growth ring (figure 2.3l).

Coast redwood (*S. sempervirens*) is native to the California area (USA), and is among the tallest trees on earth, easily reaching over 100 m in height. It is highly prized for its durable timber and is utilised in exterior timber applications (Olson et al., 1990). The grain is reported to be predominantly straight, with occasional wavy grain (Koehler &

Luxford, 1951). The four trees analysed in this thesis showed a development of weak right-handed grain (figure 2.3m).

Himalayan cypress (*C. torulosa*) is a large evergreen conifer native to southeast Asia. Like most other cypress species, it has naturally durable wood and is therefore resistant to most fungal diseases (Yue & Feng, 1984). Its primary use in New Zealand is for shelterbelt formation. No literature could be found on the grain patterns of Himalayan cypress, however, the five trees analysed in this thesis had an overall trend toward weak right-handed grain with subsequent growth (figure 2.3n).

Overall, there was a high degree of agreement between the accepted spiral grain patterns of the selected Northern Hemisphere species, and the spiral grain patterns obtained through X-ray microtomography, strengthening the argument for the use of this technique as an alternative to current high-resolution grain analysis techniques.

2.3.2.1 Intraspecies phenotypic variation of grain angle

Due to natural phenotypic variation within a species the presence ,or absence of spiral grain, and the severity of the grain angle can differ between members of the same species (Gapare et al., 2007; Harris, 1969; Harris, 1989). Additionally, while some species, such as radiata pine, have a consistent grain pattern throughout individuals; other species, such as *Pinus caribaea*, have no discernible common grain pattern, resulting in grain angles that are highly variable and unpredictable (Cown et al., 1983; Cown et al., 1991). It was therefore essential to investigate the variation in grain patterns between members of the same species.

Silver fir (Abies vejarii)

There was some variation between the five Silver fir individuals (figure 2.4). Tree 1 (figure 2.4a) and tree 2 (figure 2.4b) both show initially straight grain that then becomes steadily more left-handed, reaching a maximum of 0.6° at 2.75 mm in tree 1 and 2.8° at 2.73 mm in tree 2. The grain angle then reverses in both tree 1 and tree 2, passing through zero and ending up weakly right-handed at the bark side. Conversely, tree 3 (figure 2.4c) and tree 4 (figure 2.4d) show an initial right-handed grain angle, reaching a maximum of 2.35° at 1.4 mm in tree 3 and 1.69°at 1.35 mm in tree 4. The grain then

reverses direction in both trees, passing through zero and becoming weakly left-handed, with a maximum of 1.04° at 3.38 mm for tree 3 and 1.02° at 3.24 mm for tree 4. Another reversal of grain angle is then observable in the final millimetres towards the bark, with both trees reaching a grain angle of 0°. Tree 5 (figure 2.4e) also shows an initial right-handed grain angle with a maximum of 1.41° at 1.22 mm. While the grain angle decreases towards 0° over the rest of the tree 5 section, the pattern fluctuates significantly between the pith and cambium.

European Larch (Larix decidua)

The five European larch trees analysed show minor variation (± 1°) between individuals (figure 2.5). The initial sharp increase in grain angle in tree 1 (figure 2.5a), from 0° to 0.8° can be attributed to the proximity of these first two measurements to the pith. The initial grain direction of tree 1 is therefore right-handed, with a maximum of 1.10° at 0.48 mm from the pith. The grain the slowly reverses direction towards 0°, reaching this at 1.58 mm and then slowly increasing to become more right-handed towards the cambium. Tree 2 (figure 2.5b) shows a moderately straight grain pattern with minor fluctuations in the first 1.4mm of growth. The grain then changes to become weakly right-handed, reaching a maximum of 0.76° at 1.91mm, before switching back to straight-grained. Tree 3 (figure 2.5c) follows a similar pattern to tree 2, showing straight grain with minor fluctuations for the first 2.25 mm of growth and then developing a weak right-handed twist. This reaches a maximum right-handed angle of 0.79 ° at 2.71 mm. Tree 4 (figure 2.5d) and tree 5 (figure 2.5e) show a similar pattern, with both becoming increasingly left-handed in the first millimetres of growth. Tree 4 reaches a maximum left-handed angle of 1.67° at 1.86 mm of growth, whereas tree 5 reaches a maximum of 0.63° at 1.99 mm of growth. The grain then reverses direction in both trees, reaching a maximum right-handed grain angle of 0.43° at 3.72 mm in tree 4 and 0.85° at 2.94 mm in tree 5.

Deodar Cedar (Cedrus Deodara)

Of the four Deodar cedar trees analysed, there were two distinct grain patterns observed (figure 2.6). Tree 1 (figure 2.6a) and tree 3 (figure 2.6c) both exhibited

straight grain with minor fluctuations throughout the stem. Tree 2 (figure 2.6b) and tree 4 (figure 2.6d) showed increasingly right-handed grain in the first millimetre of growth, reaching a maximum of 0.41° at 0.66 mm in tree 2 and 1.20° at 0.93mm in tree 4. The grain then switches in tree 2, becoming increasingly left-handed and reaching a maximum of 1.1° at 1.77 mm before returning to the straight-grained form. While tree 4 has a similar reversal of grain, it does not become left-handed. Rather, the grain becomes straight at 2 mm from the pith, with minor fluctuations in the last 0.5 mm of the stem.

Japanese Cedar (Cryptomeria japonica)

There was little variation between the five Japanese cedar trees analysed, with all trees showing an initial straight grain and four of the five trees developing a left-handed twist (figure 2.7). Tree 1 (figure 2.7a), tree 3 (figure 2.7c) and tree 5 (figure 2.7e) all showed a pattern of increasingly left-handed grain up to 2 mm from the pith, where there is a brief reversal and then a return to the left-handed form. This pattern is exaggerated in tree 1, with the grain reaching a maximum left-handed angle of 0.56° at 1.57 mm, before reversing to a maximum right-handed angle of 0.85° at 2.09 mm. The grain direction then reverses a second time, reaching a maximum of 0.54° at the cambium. Tree 2 (figure 2.7b) had the same initial pattern of an increase towards left-handed grain, where the grain angle started weakly right-handed close to the pith (0.67° at 0.42 mm) and then reaches a left-handed maximum grain angle of 1.32° at 2.16 mm. There is then a reversal in grain direction as the grain angle approaches 0°towards the cambium. Tree 4 (figure 2.7d) shows minor fluctuations in grain angle ±0.5° from straight grained.

Chinese Juniper (Juniperus chinensis)

There was little variation in the grain pattern of the five Chinese juniper trees analysed, with all trees showing a predominantly straight grain (figure 2.8). Tree 1 (figure 2.8a) and tree 2 (figure 2.8b) both exhibited minor fluctuations in grain angle, with the grain becoming weakly left-handed around 1 mm of growth reaching a maximum angle of 0.5° in tree 1, and 0.6° in tree 2. Trees 3 to 5 (figure 2.8c-e) showed no significant

variation in grain angle. Rather, the grain in all three of these trees is predominantly straight grained with fluctuations >±0.5°.

Leyland Cypress (Cupressus x leylandii)

The five Leyland cypress trees analysed showed significant variation (figure 2.9). Tree 1 (figure 2.9a) reached a maximum right-handed grain angle of 0.33° at 2.71 mm and a maximum left-handed angle of 0.29° at 1.11 mm. These values do not represent local maxima within the graph profile of the grain angle, rather, they represent the spread of the fluctuations in grain angle around 0°. Tree 2 (figure 2.9b) has an initial weak left-handed grain, reaching a maximum of 0.76° at 0.64 mm from the pith. The grain then shifts to 0° at 1mm of growth, before switching back the weak left-handed form for the remainder of the stem section, reaching a maximum of 0.99° at 2.75 mm. Tree 3 (figure 2.9c) shows a similar straight-grained pattern as tree 1, with fluctuations in grain angle ±0.5°. Tree 4 (figure 2.9d) has an initial week left-handed grain, reaching a maximum of 0.72° at 0.6 mm before slowly shifting to a right-handed form. A maximum right-handed angle of 0.69° is observed at 2.59 mm. Tree 5 (figure 2.9e) follows a similar pattern as tree 4

Monterey Cypress (Cupressus macrocarpa)

The five Monterey cypress trees analysed showed a moderate variation in grain patterns (figure 2.10). Tree 2 (figure 2.10b) and tree 3 (figure 2.10c) both have a similar grain pattern. The grain is initially left-handed reaching a maximum angle of 1.25° at 0.45 mm in tree 2 and 0.9° at 0.48 mm in tree 3. The grain direction then reverses, and switches to straight grained at 3.42 mm in tree 2 and 3.11 mm in tree 3. The grain then remains straight, with minor fluctuations in angle ±0.3°. Tree 1 (figure 2.10a) is straight grained for the first 2mm of growth, before switching to a weak left-handed grain angle, reaching a maximum of 0.58° at 2.36 mm. The grain continues to be left-handed up to 3.77 mm, where it switches to become weakly right-handed, reaching a maximum of 0.54° at 4.91 mm. Tree 4 (figure 2.0d) starts out straight grained, but then abruptly switches to left-handed grain at 1.28 mm from the pith. The grain reaches a maximum left-handed angle of 0.61° at 1.77 mm before abruptly returning to the

straight-grained form. The grain in tree 5 (figure 2.10e) is initially right-handed reaching a maximum angle of 0.77° at 1.12 mm. The grain then shifts to an increasingly left-handed form at 2.78 mm. The left-handed grain angle continues to increase towards the cambium, reaching a maximum grain angle of 0.67° at 4.1 mm.

Buddhist pine (Podocarpus macrophyllus)

There is some variation in the grain patterns of the five Buddhist pine trees analysed (figure 2.11). Tree 1 (figure 2.11a), tree 2 (figure 2.11b), tree 4 (figure 2.11d) and tree 5 (figure 2.11e) all follow the same grain pattern, development of left-handed grain within 1 mm of the pith, followed by a return to straight grain at 2.19 mm in tree 1, 2.33 mm in tree 2, 2.20 mm in tree 4 and 2.20 mm in tree 5. The maximum left-handed angles reached are 0.93° at 1.29 mm in tree 1, 0.65° at 1.29 mm in tree 2, 0.74° at 0.84 mm in tree 4, and 1° at 1.07 mm in tree 5. Tree 3 (figure 2.11b) is straight grained with minor fluctuations in grain angle ±0.5°.

Norway spruce (Picea abies)

All five Norway spruce trees followed the same grain pattern (figure 2.12). The grain initially forms a right handed twist, reaching a maximum of 0.96° at 0.69 mm in tree 1 (figure 2.12a), 0.95° at 1.6 mm in tree 2 (figure 2.12b), 1.74° at 1.71 mm in tree 3 (figure 2.12c), 0.83° at 1.51 mm in tree 4 (figure 2.12d) and 1.8° at 1.07mm. The grain then reverses direction, becoming straight grained in tree 1. The grain in the other four trees becomes left-handed, reaching a maximum left-handed angle of 0.65° at 3.38 mm in tree 2, 0.66° at 3.55 mm in tree 3, 1.47° at 2.33 mm in tree 4 and 0.8° at 4.25 mm in tree 5. The grain then reverses again, back to right-handed, in trees 2 and 3 reaching a maximum right-handed angle of 0.42° at 4.94 mm in tree 2, 0.72° at 4.83 mm in tree 3.

Coulter Pine (P. Coulteri)

There is significant variation in the grain patterns of the five Coulter pine trees analysed (figure 2.13). Tree 1 (figure 2.13a) has an initial right-handed grain angle of 0.55° at 1.17 mm, which then reverses direction, reaching a maximum left-handed grain angle

of 1.04° at 2.03 mm before slowly reversing direction and tending towards straight grain. Tree 2 (figure 2.13b), has an initial right-handed grain of 0.99° at 0.85 mm, but then the grain becomes increasingly right-handed, reaching a maximum of 2.07° at 1.64 mm. The grain angle then decreases back towards 0° in the remaining 1mm of the sample. Trees 3-5 (figure 2.13c-e) all show a similar grain pattern, where there are minor fluctuations in the grain (± 0.4°), but they are predominantly straight-grained.

Maritime Pine (P. pinaster)

The five Maritime pine trees analysed show some intraspecies variation (figure 2.14). Tree 1 (figure 2.14a) has an initial right-handed grain angle develop at 1mm from the pith, reaching 0.54°. The grain direction then reversed, becoming increasingly right-handed and reaches a maximum right-handed angle of 0.88° at 1.81 mm. The direction then switched again, reaching a maximum left-handed angle of 0.71° at 2.84 mm. Tree 2 (figure 2.14b), tree 3 (figure 2.14c) and tree 5 (figure 2.14d) all exhibit the same grain pattern. The grain rapidly became increasingly left-handed and reached a maximum angle of 1.41° at 1.58 mm in tree 2, 1.38° at 2.14 mm in tree 3, and 0.66° at 1.62 mm in tree 5. The grain then reversed direction, reaching a maximum right-handed angle of 1.13° at 2.52 mm in tree 2, 0.29° in tree 3 and 0.83° at 2.5 mm in tree 5. Tree 4 exhibited a straight grained pattern with inflections in grain ±0.3°.

Radiata pine (Pinus radiata)

The four radiata pine trees analysed showed little variation in grain patterns (figure 2.15). Except for tree 2 (figure 2.15b) the grain was initially right-handed in all the trees analysed. A maximum right-handed grain angle of 0.84° was reached at 1.17 mm in tree 1 (figure 2.15a), 1.47° was reached at 1.35 mm in tree 3 (figure 2.15c) and 1.64° was reached at 1.13 mm in tree 4 (figure 2.15d). The grain then changed direction, and became left-handed in trees 1, 3, and 4. The maximum left-handed angle was 1.24° at 2.48 mm in tree 1, 1.19° at 3.03 mm in tree 3, and 1.18° at 2.89 mm in tree 4. Tree 2 had a left-handed grain deflection at of 1.14° 1.02 mm, but then had a rapid shift back to straight grain in the following 0.10 mm. The grain then remained straight for the remainder of tree 2.

Coast redwood (Sequoia sempervirens)

There was little variation between the four Coast redwood species analysed (figure 2.14). Tree 1 (figure 2.16a) and tree 2 (figure 2.16b) had a moderately straight grain with minor fluctuations in grain angle ±0.5°. Tree 3 (figure 2.16c) and tree 4 (figure 2.16d) had initial straight grain, which then shifted to right-handed grain in both trees. A maximum right-handed grain angle of 1.31° at 1.95 mm in tree 3, and 2.02° at 1.74 mm in tree 4 was reached. The grain then reversed direction, becoming straight-grained in tree 3 and left-handed in tree 4, reaching a maximum left-handed grain angle of 1.38° at 2.63 mm.

Himalayan cypress (Cupressus torulosa)

The five Himalayan cypress trees analysed showed disparate growth patterns. While there was significant variation in grain angle and grain pattern between the five trees tested, the overall tendency was for the development of right-handed grain (figure 2.17). Tree 1 (figure 2.17a) had predominantly straight grain throughout the sample, however there is a significant increase in the error between 1 mm and 2 mm from the pith. Tree 2 (figure 2.17b) had consistent right-handed grain throughout the sample, reaching a maximum left-handed angle of 1.26° at 0.94 mm. Tree 3 (figure 2.17c) was straight grained for the first 1 mm of growth. The grain angle shifted to become increasingly right-handed, reaching a maximum right-handed angle of 2.04° at 2.27 mm from the pith. Tree 4 (figure 2.17d) also had initial right-handed grain, reaching a maximum right-handed angle of 1.18° at 2.36 mm. Tree 5 (figure 2.17e) had weakly left-handed grain, reaching a maximum left-handed angle of 0.79° at 0.9 mm.

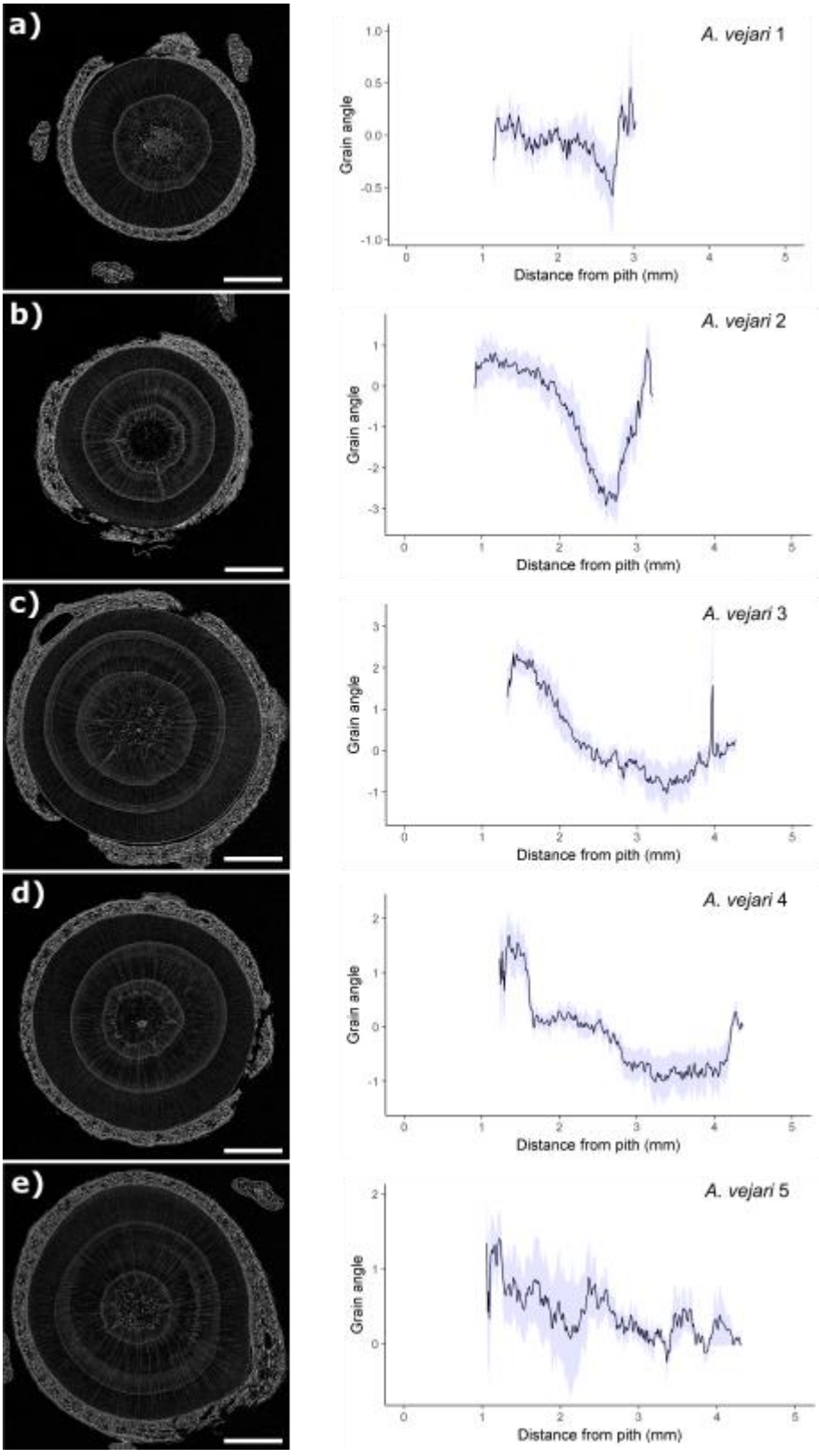
a)
b)
c)
d)
e)
A. vejari 1
A. vejari 2
A. vejari 3
A. vejari 4
A. vejari 5
Grain angle
Distance from pith (mm)

Figure 2.4 A vejarii

Analysis of five Silver fir trees (A vejarii) trees allows identification of intraspecies grain trends. Scale bar equals 2mm. Negative grain angle values denote left-handed grain angles; positive grain angle values denote right-handed grain angles. The solid black line in each graph represents the measured grain angle, whereas the light blue area shows the standard error of the mean. a) Silver fir tree 1. b) Silver fir tree 2. c) Silver fir tree 3. d) Silver fir tree 4. e) Silver fir tree 5.

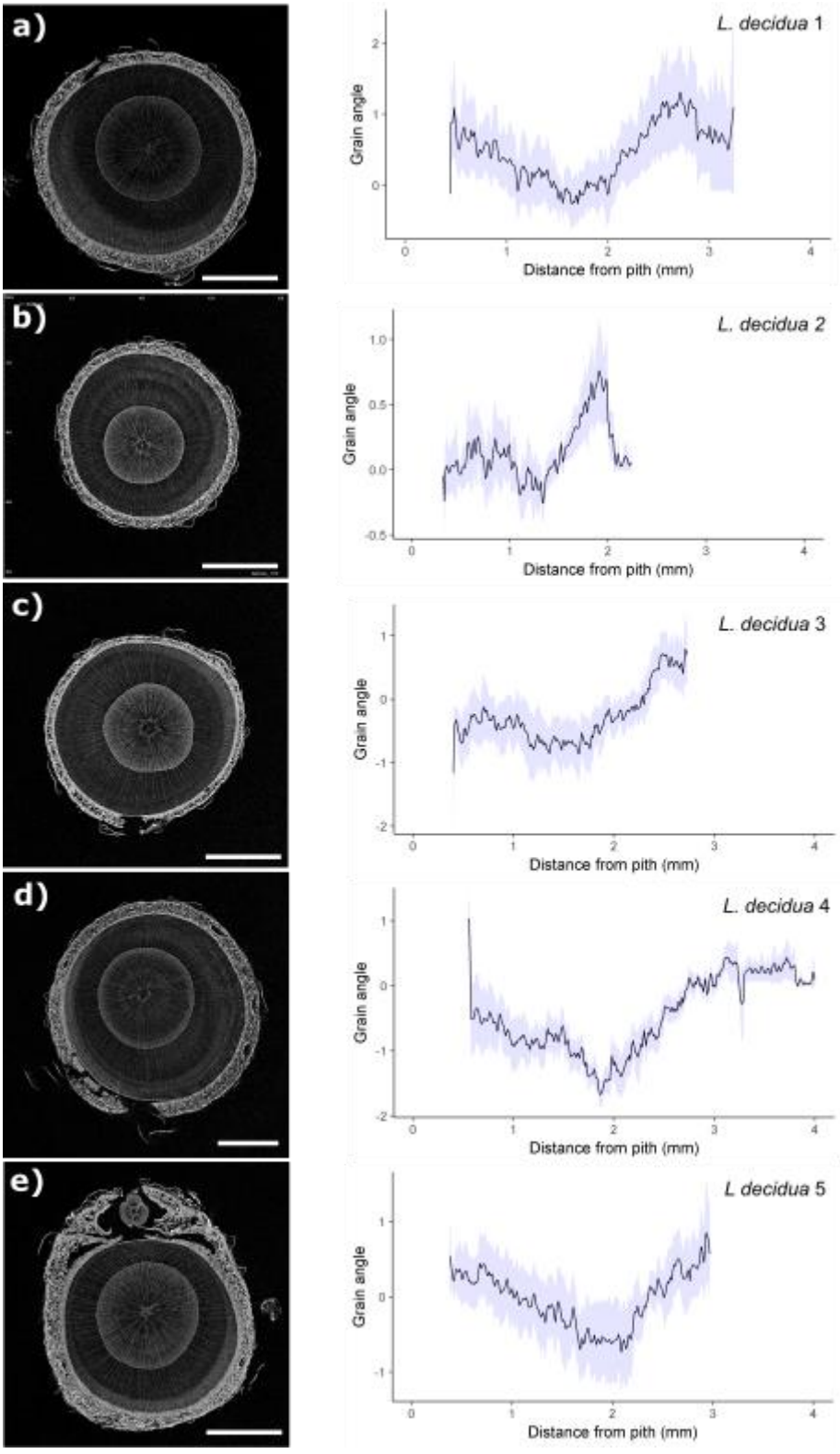
a)
b)
c)
d)
e)
L. decidua 1
L. decidua 2
L. decidua 3
L. decidua 4
L. decidua 5
Grain angle
Distance from pith (mm)

Figure 2.5 L. Decidua

Analysis of five European larch trees (*L. decidua*) trees allows identification of intraspecies grain trends. Scale bar equals 2mm. Negative grain angle values denote left-handed grain angles; positive grain angle values denote right-handed grain angles. The solid black line in each graph represents the measured grain angle, whereas the light blue area shows the standard error of the mean. a) European larch tree 1. b) European larch tree 2. c) European larch tree 3. d) European larch tree 4. e) European larch tree 5.

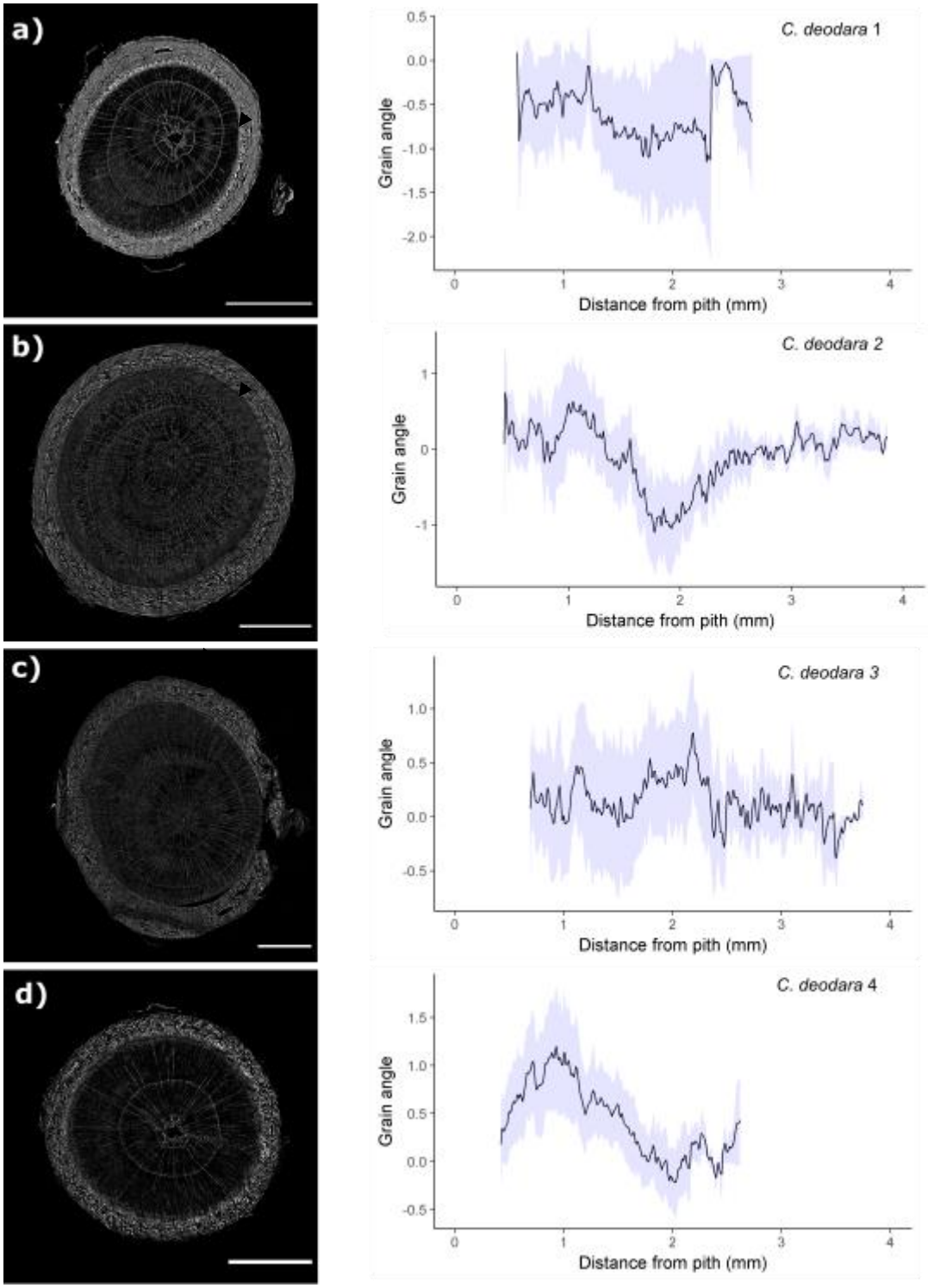
a)
b)
c)
d)
C. deodara 1
C. deodara 2
C. deodara 3
C. deodara 4
Grain angle
Distance from pith (mm)

Figure 2.6

Analysis of four Deodar cedar (*C. deodara*) trees allows identification of intraspecies grain trends. Scale bar equals 2mm. Negative grain angle values denote left-handed grain angles; positive grain angle values denote right-handed grain angles. The solid black line in each graph represents the measured grain angle, whereas the light blue area shows the standard error of the mean. a) Deodar cedar 1. b) Deodar cedar 2. c) Deodar cedar 3. d) Deodar cedar 4.

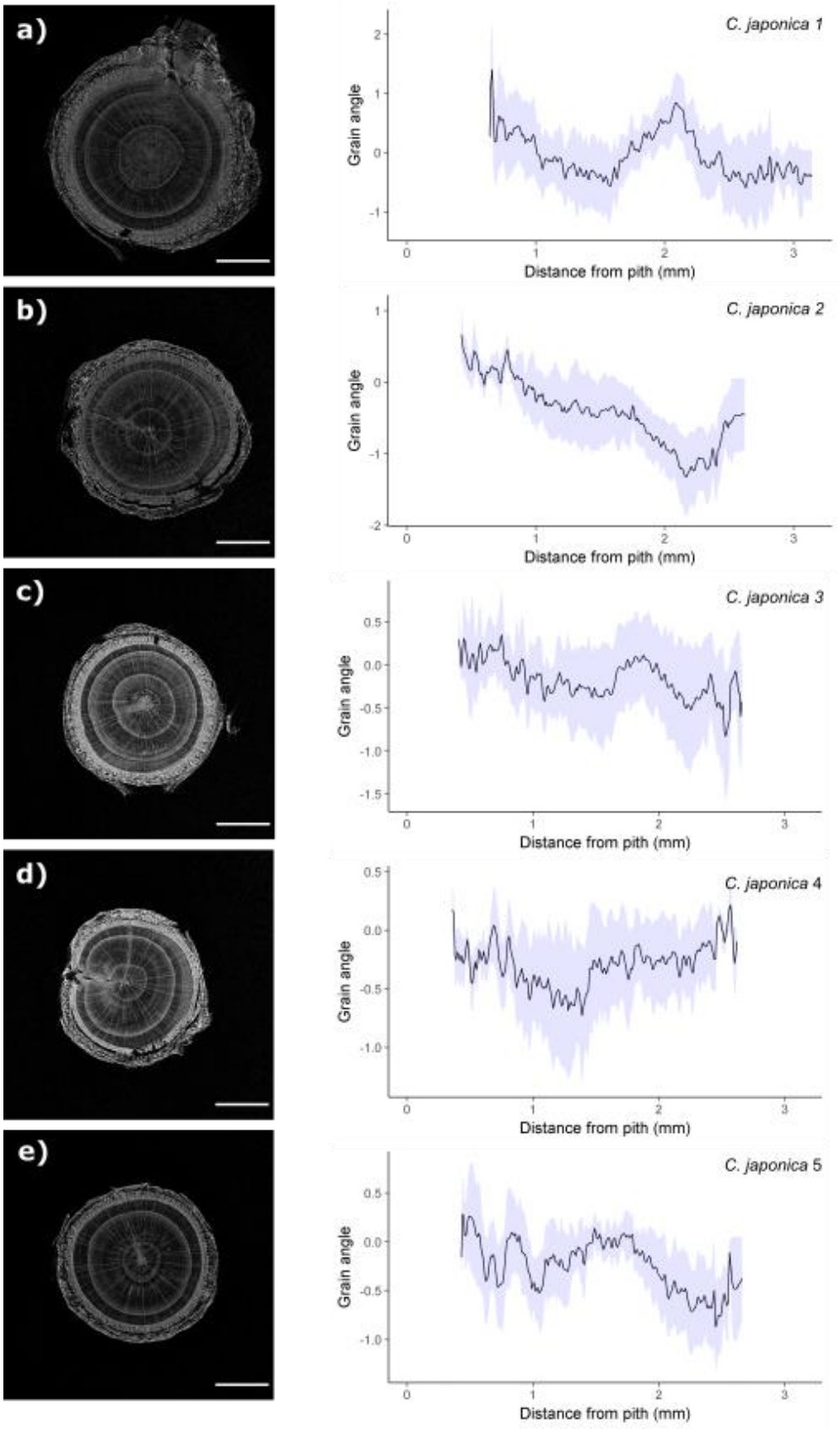
a)
b)
c)
d)
e)
C. japonica 1
C. japonica 2
C. japonica 3
C. japonica 4
C. japonica 5
Grain angle
Distance from pith (mm)

Figure 2.7

Analysis of five Japanese cedar (*C. japonica*) trees allows identification of intraspecies grain trends. Scale bar equals 2mm. Negative grain angle values denote left-handed grain angles; positive grain angle values denote right-handed grain angles. The solid black line in each graph represents the measured grain angle, whereas the light blue area shows the standard error of the mean. a) Japanese cedar 1. b) Japanese cedar 2. c) Japanese cedar 3. d) Japanese cedar 4. e) Japanese cedar 5.

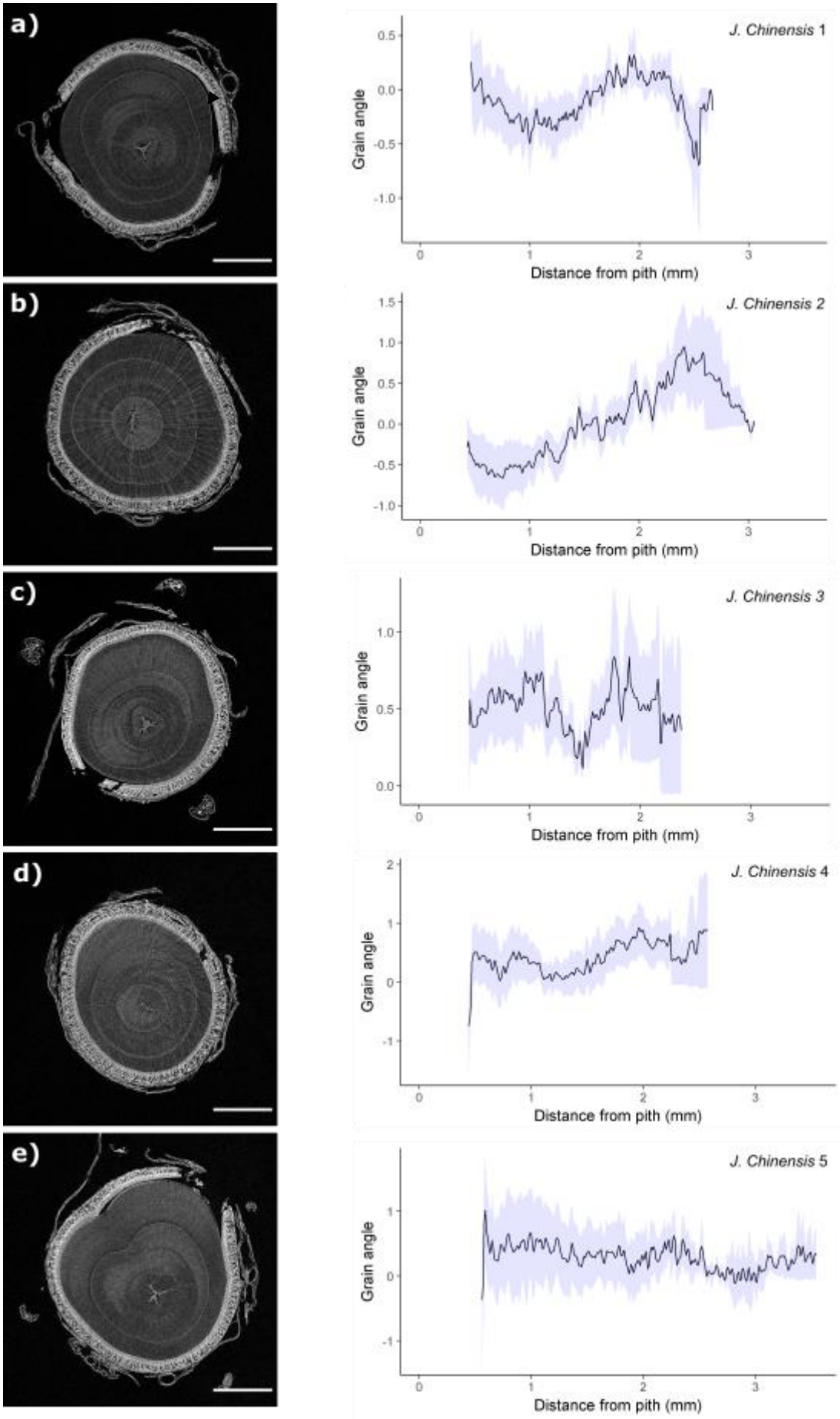
a)
b)
c)
d)
e)
J. Chinensis 1
J. Chinensis 2
J. Chinensis 3
J. Chinensis 4
J. Chinensis 5
Grain angle
Distance from pith (mm)

Figure 2.8

Analysis of five Chinese juniper (*J. Chinensis*) trees allows identification of intraspecies grain trends. Scale bar equals 2mm. Negative grain angle values denote left-handed grain angles; positive grain angle values denote right-handed grain angles. The solid black line in each graph represents the measured grain angle, whereas the light blue area shows the standard error of the mean. a)Chinese juniper 1. b) Chinese juniper 2. c) Chinese juniper 3. d) Chinese juniper 4. e) Chinese juniper 5.

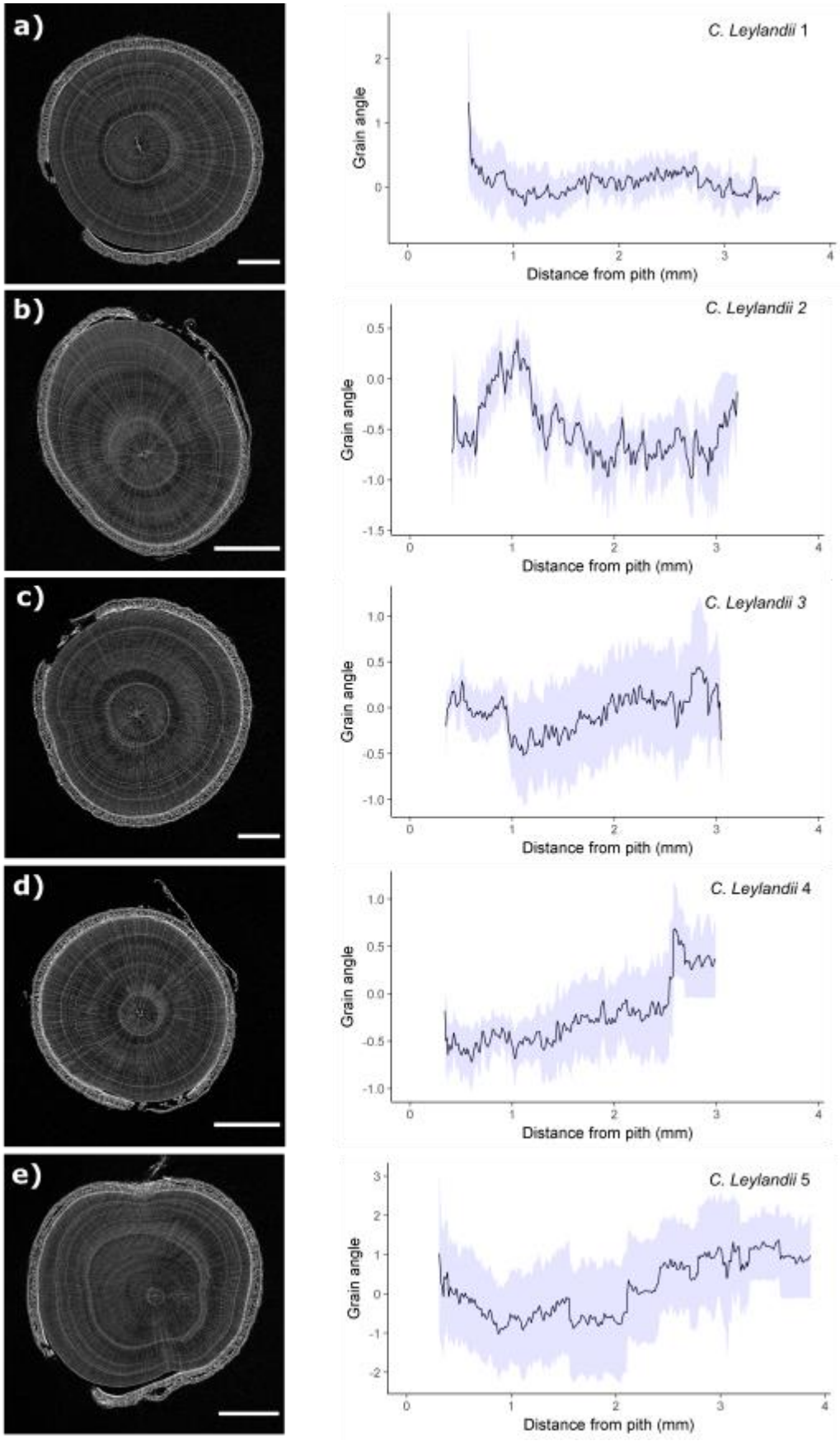
a)
b)
c)
d)
e)
C. Leylandii 1
C. Leylandii 2
C. Leylandii 3
C. Leylandii 4
C. Leylandii 5
Grain angle
Distance from pith (mm)

Figure 2.9

Analysis of five Leyland cypress (*C. leylandii*) trees allows identification of intraspecies grain trends. Scale bar equals 2mm. Negative grain angle values denote left-handed grain angles; positive grain angle values denote right-handed grain angles. The solid black line in each graph represents the measured grain angle, whereas the light blue area shows the standard error of the mean. a) Leyland Cypress 1. b) Leyland cypress 2. c) Leyland cypress 3. d) Leyland cypress 4. e) Leyland cypress 5.

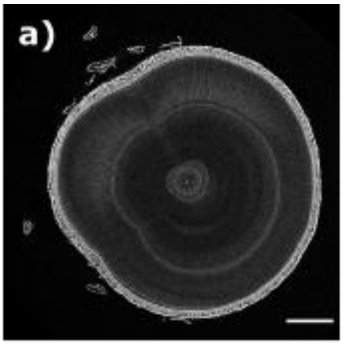
a)

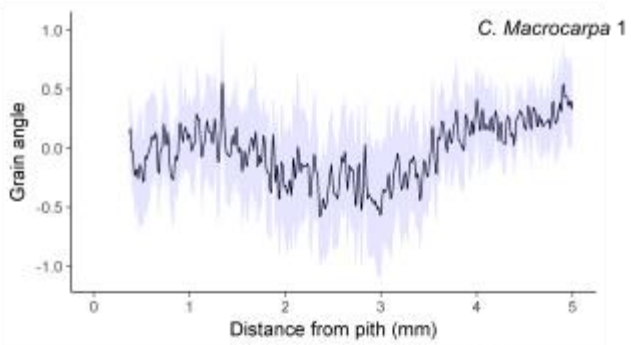
C. Macrocarpa 1
Grain angle
Distance from pith (mm)

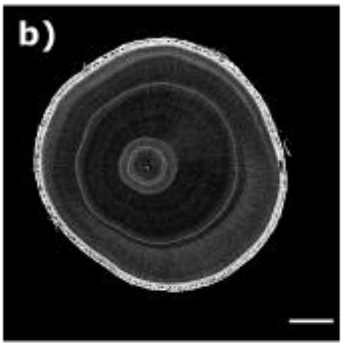
b)

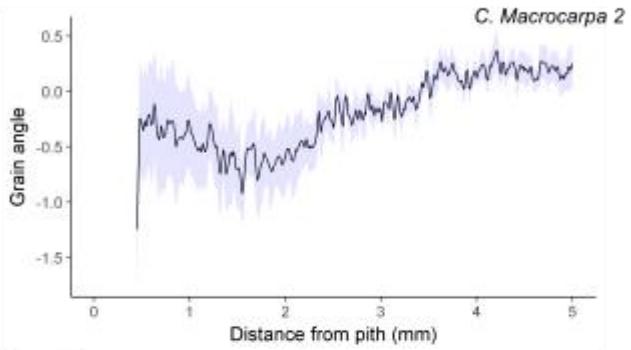
C. Macrocarpa 2
Grain angle
Distance from pith (mm)

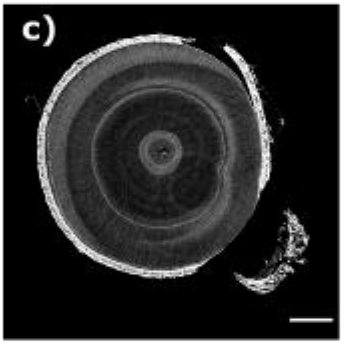
c)

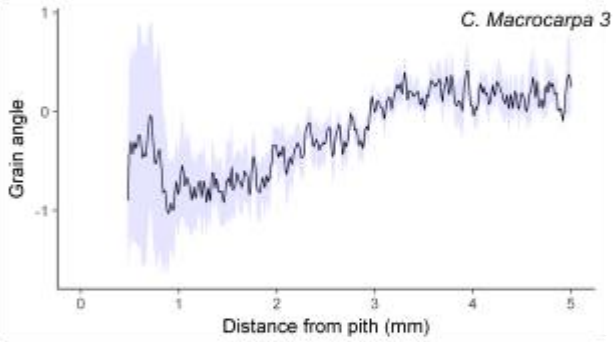
C. Macrocarpa 3
Grain angle
Distance from pith (mm)

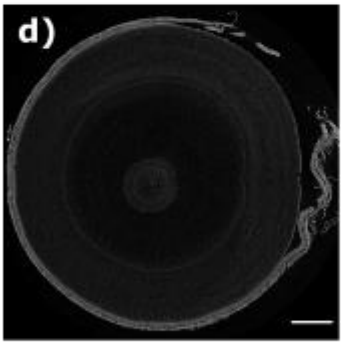
d)

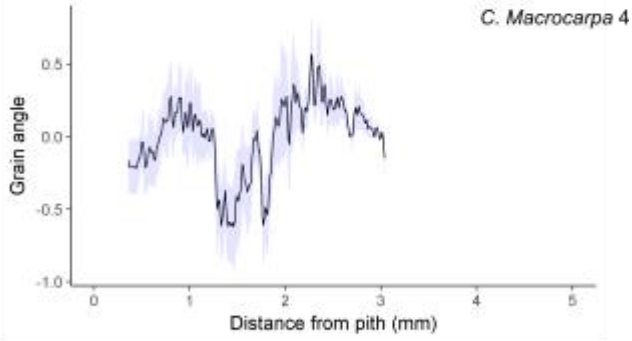
C. Macrocarpa 4
Grain angle
Distance from pith (mm)

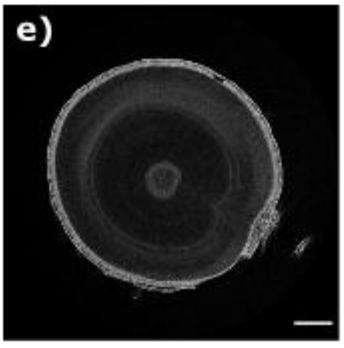
e)

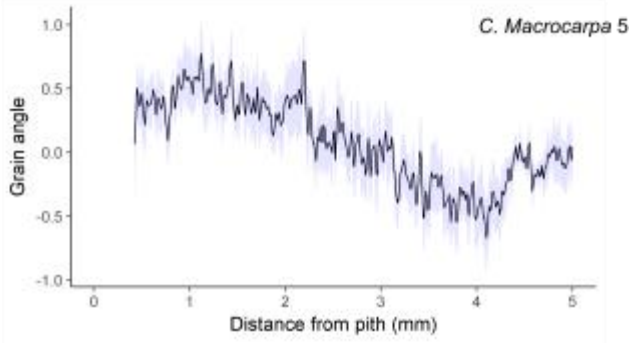
C. Macrocarpa 5
Grain angle
Distance from pith (mm)

Figure 2.10

Monterey cypress

Analysis of five Monterey cypress (*C. macrocarpa*) trees allows identification of intraspecies grain trends. Scale bar equals 2mm. Negative grain angle values denote left-handed grain angles; positive grain angle values denote right-handed grain angles. The solid black line in each graph represents the measured grain angle, whereas the light blue area shows the standard error of the mean. a) Monterey cypress 1. b) Monterey cypress 2. c) Monterey cypress 3. d) Monterey cypress 4. e) Monterey cypress 5.

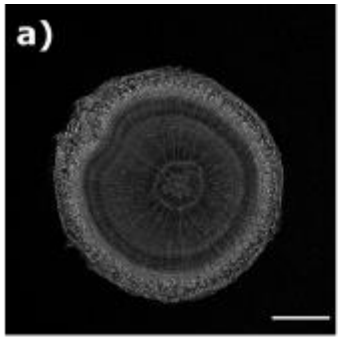
a)

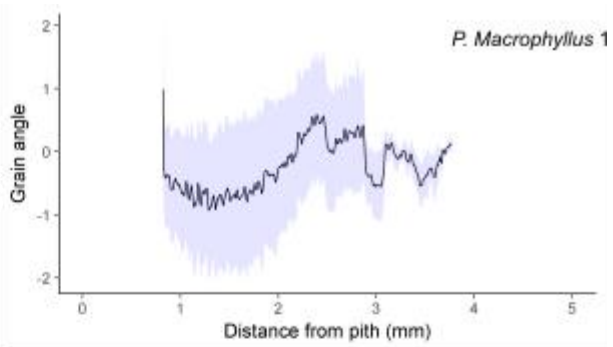
P. Macrophyllus 1
Grain angle
Distance from pith (mm)

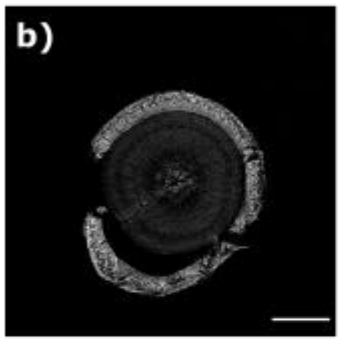
b)

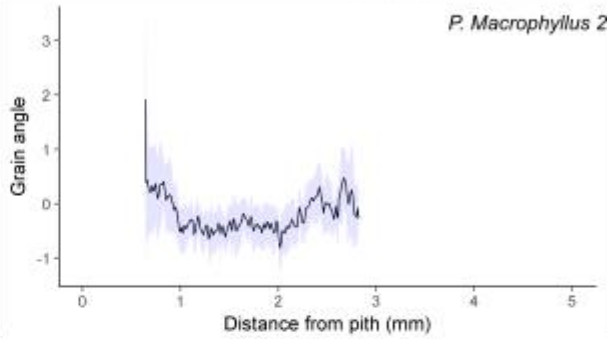
P. Macrophyllus 2
Grain angle
Distance from pith (mm)

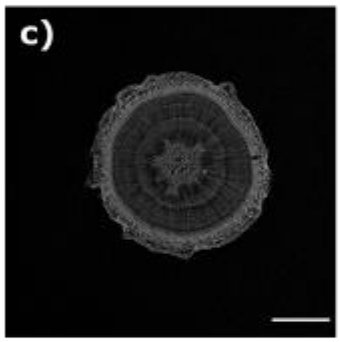
c)

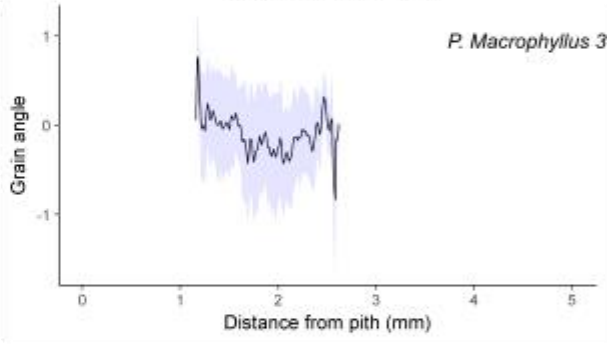
P. Macrophyllus 3
Grain angle
Distance from pith (mm)

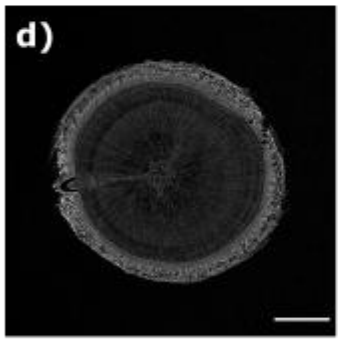
d)

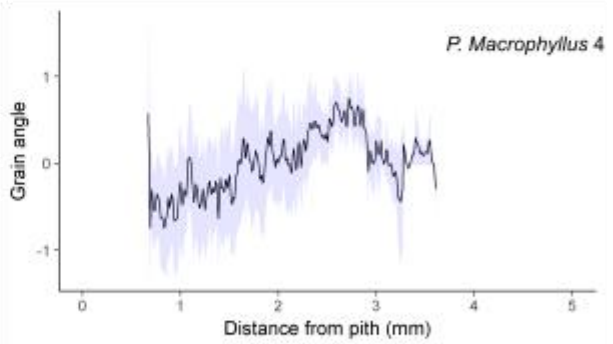
P. Macrophyllus 4
Grain angle
Distance from pith (mm)

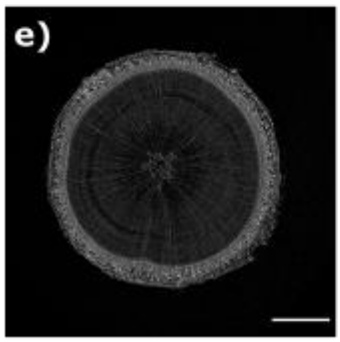
e)

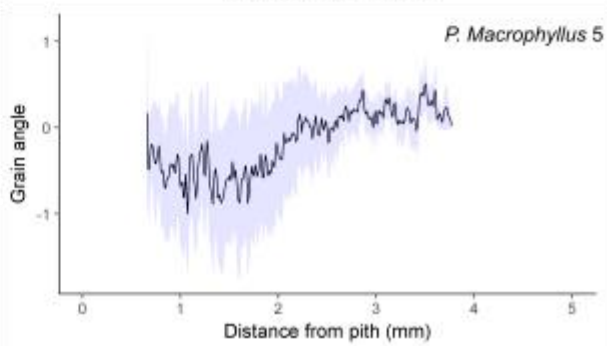
P. Macrophyllus 5
Grain angle
Distance from pith (mm)

Figure 2.11

Buddhist pine

Analysis of five Buddhist pine (*P. Macrophyllus*) trees allows identification of intraspecies grain trends. Scale bar equals 2mm Negative grain angle values denote left-handed grain angles; positive grain angle values denote right-handed grain angles. The solid black line in each graph represents the measured grain angle, whereas the light blue area shows the standard error of the mean. a) Buddhist pine 1. b) Buddhist pine 2. c) Buddhist pine 3. d) Buddhist pine 4. e) Buddhist pine 5.

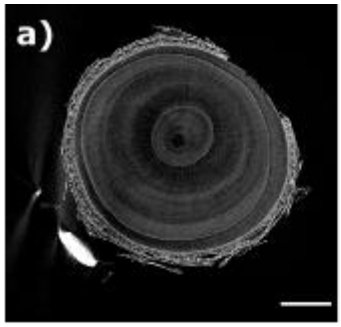
a)

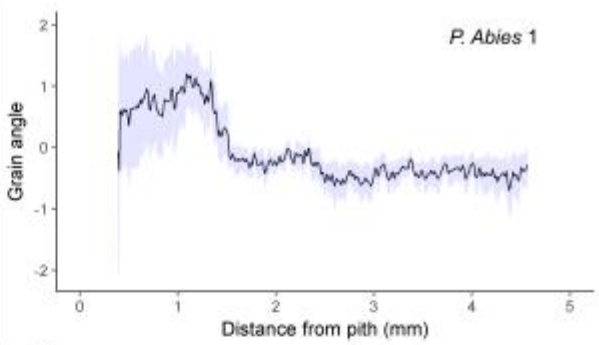
P. Abies 1
Grain angle
Distance from pith (mm)

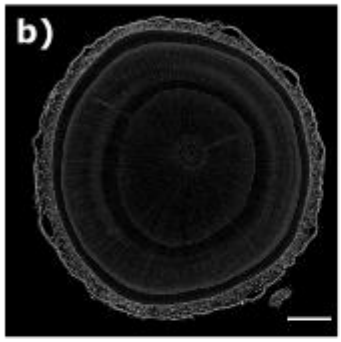
b)

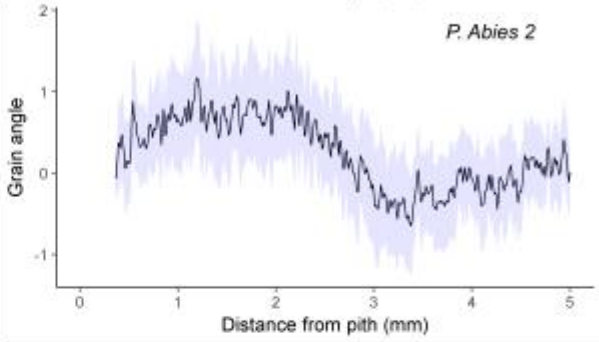
P. Abies 2
Grain angle
Distance from pith (mm)

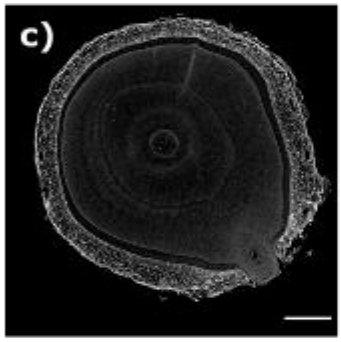
c)

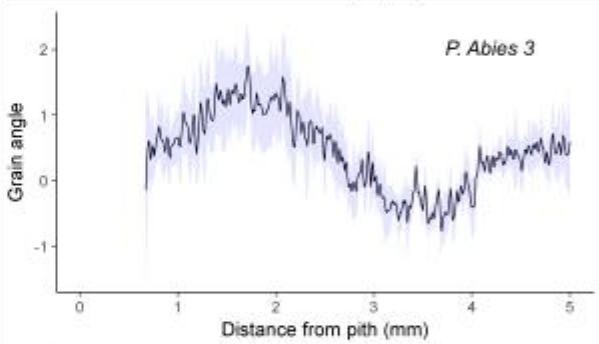
P. Abies 3
Grain angle
Distance from pith (mm)

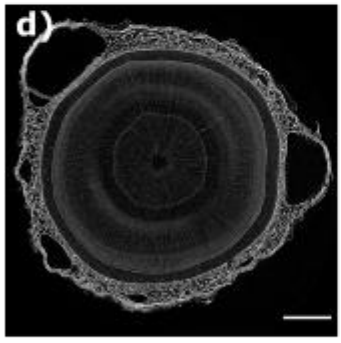
d)

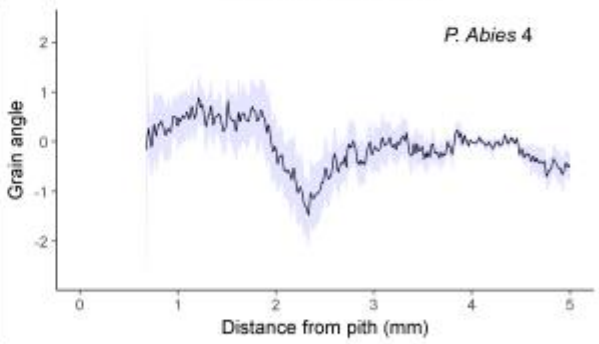
P. Abies 4
Grain angle
Distance from pith (mm)

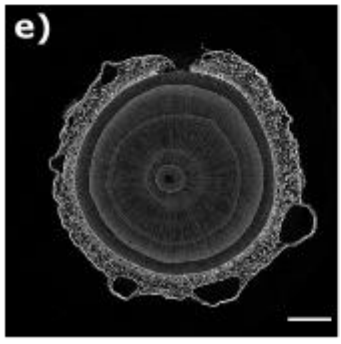
e)

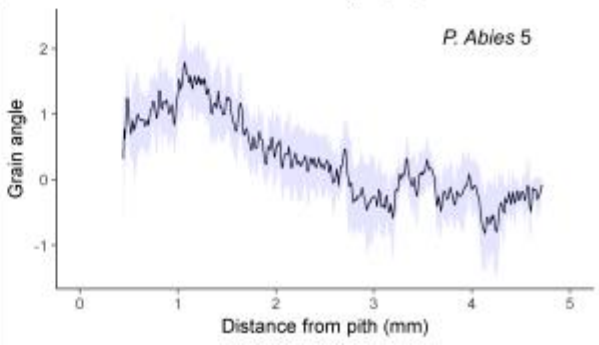
P. Abies 5
Grain angle
Distance from pith (mm)

Figure 2.12

Analysis of five Norway spruce (*P Abies*) trees allows identification of intraspecies grain trends. Scale bar equals 2mm. Negative grain angle values denote left-handed grain angles; positive grain angle values denote right-handed grain angles. The solid black line in each graph represents the measured grain angle, whereas the light blue area shows the standard error of the mean. a) Norway spruce 1. b) Norway spruce 2. c) Norway spruce 3. d) Norway spruce 4. e) Norway spruce 5.

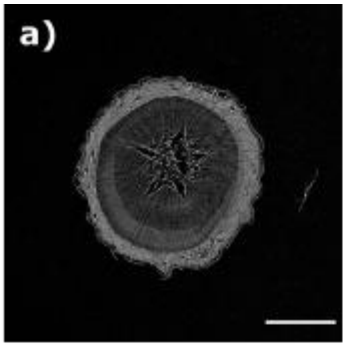
a)

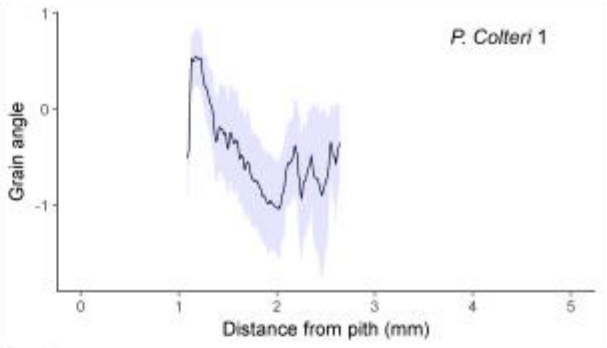
P. Colteri 1
Grain angle
Distance from pith (mm)

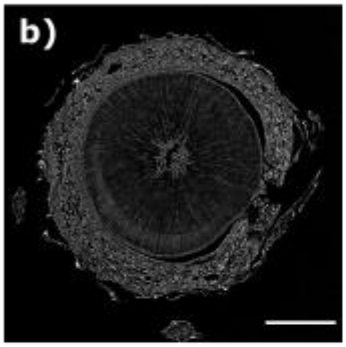
b)

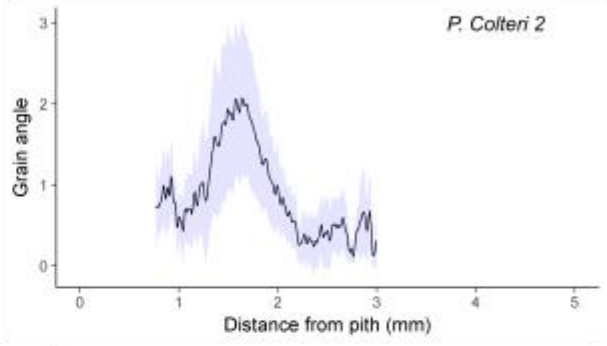
P. Colteri 2
Grain angle
Distance from pith (mm)

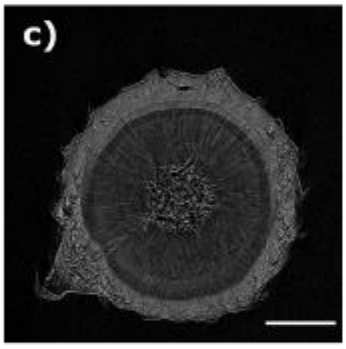
c)

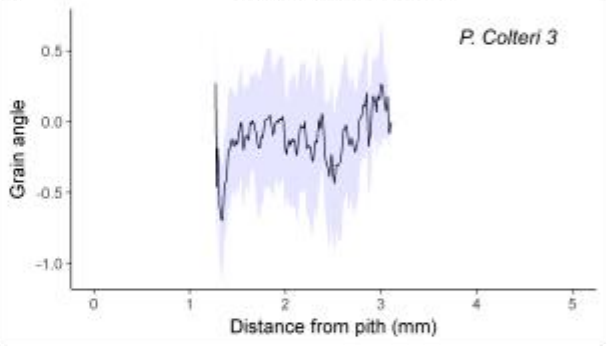
P. Colteri 3
Grain angle
Distance from pith (mm)

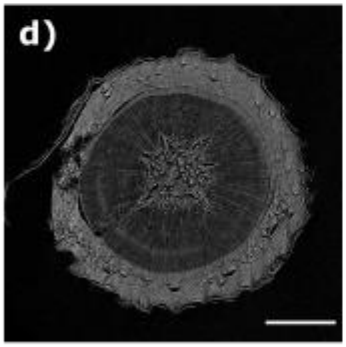
d)

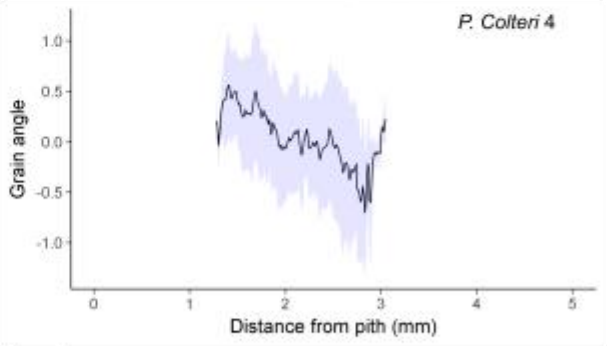
P. Colteri 4
Grain angle
Distance from pith (mm)

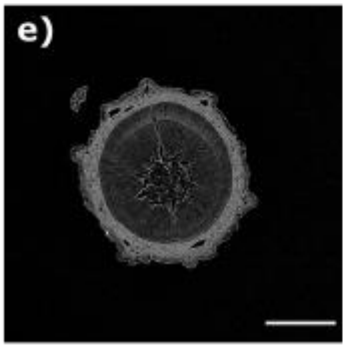
e)

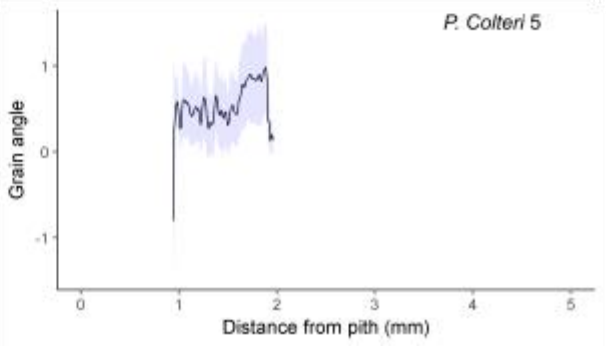
P. Colteri 5
Grain angle
Distance from pith (mm)

Figure 2.13

Analysis of five Coulter pine (*P. Colteri*) trees allows identification of intraspecies grain trends. Scale bar equals 2mm. Negative grain angle values denote left-handed grain angles; positive grain angle values denote right-handed grain angles. The solid black line in each graph represents the measured grain angle, whereas the light blue area shows the standard error of the mean. a) Coulter pine 1. b) Coulter pine 2. c) Coulter pine 3. d) Coulter pine 4. e) Coulter pine 5.

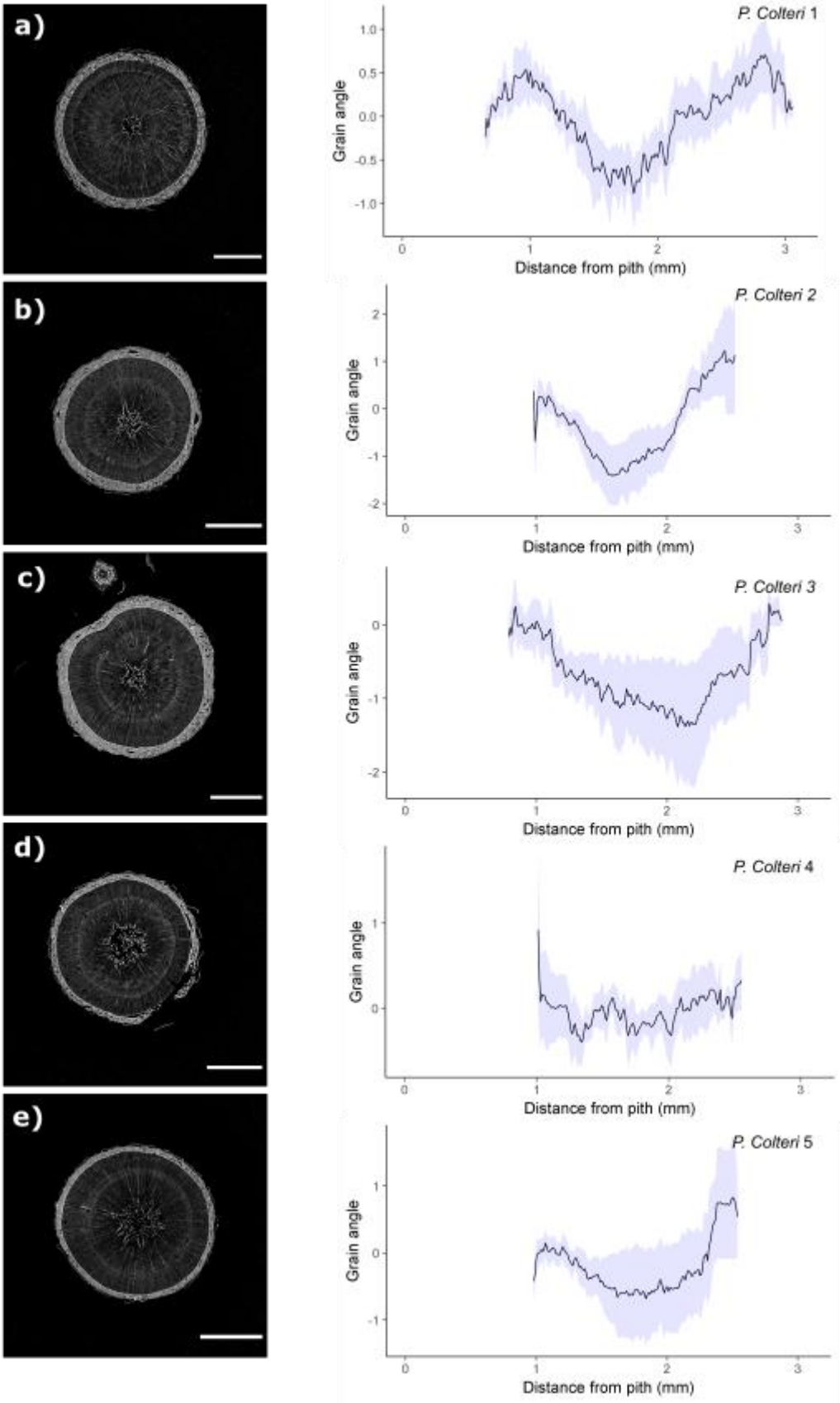
a)
b)
c)
d)
e)
P. Colteri 1
P. Colteri 2
P. Colteri 3
P. Colteri 4
P. Colteri 5
Grain angle
Distance from pith (mm)

Figure 2.14

Analysis of five Maritime pine (*P pinaster*) trees allows identification of intraspecies grain trends. Scale bar equals 2mm. Negative grain angle values denote left-handed grain angles; positive grain angle values denote right-handed grain angles. The solid black line in each graph represents the measured grain angle, whereas the light blue area shows the standard error of the mean. a) Maritime pine 1. b) Maritime pine 2. c) Maritime pine 3. d) Maritime pine 4. e) Maritime pine 5.

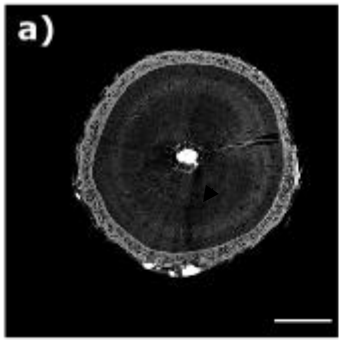
a)

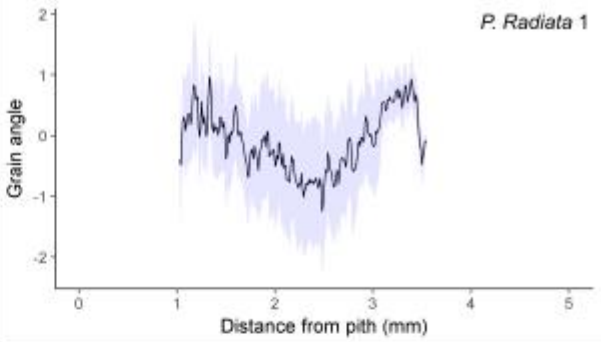
P. Radiata 1
Grain angle
Distance from pith (mm)

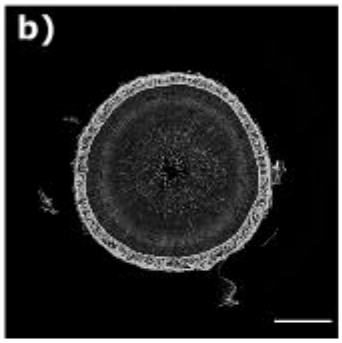
b)

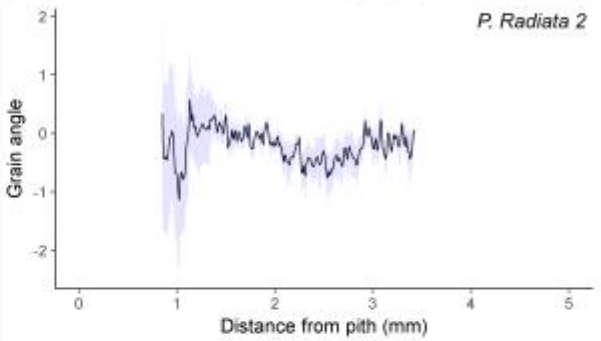
P. Radiata 2
Grain angle
Distance from pith (mm)

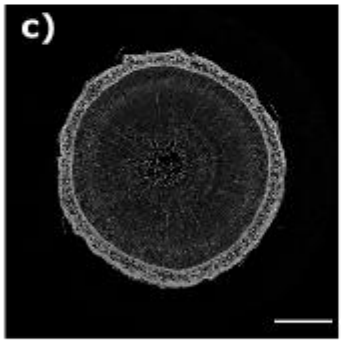
c)

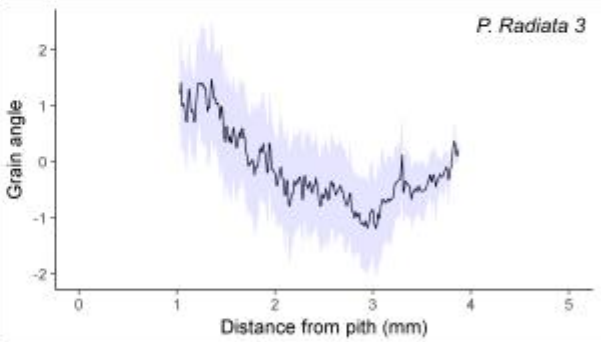
P. Radiata 3
Grain angle
Distance from pith (mm)

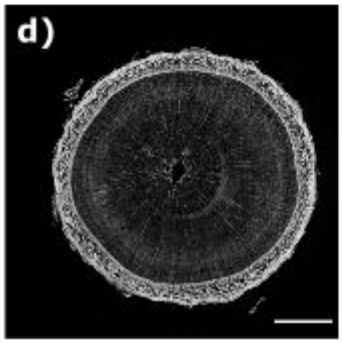
d)

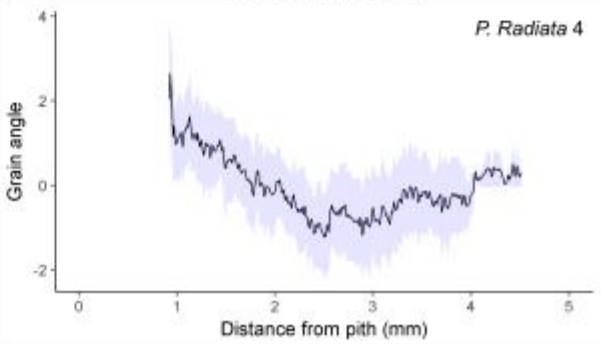
P. Radiata 4
Grain angle
Distance from pith (mm)

Figure 2.15

Analysis of four Radiata pine (*P. radiata*) trees allows identification of intraspecies grain trends. Scale bar equals 2mm. Negative grain angle values denote left-handed grain angles; positive grain angle values denote right-handed grain angles. The solid black line in each graph represents the measured grain angle, whereas the light blue area shows the standard error of the mean. A) Radiata pine 1. b) Radiata pine 2. c) Radiata pine 3. d) Radiata pine 4.

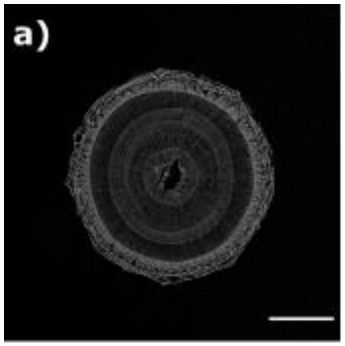
a)

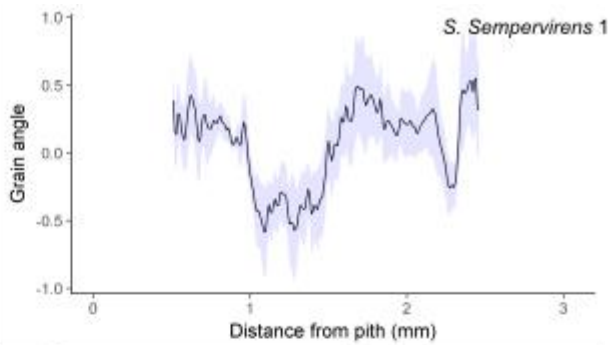
S. Sempervirens 1
Grain angle
Distance from pith (mm)

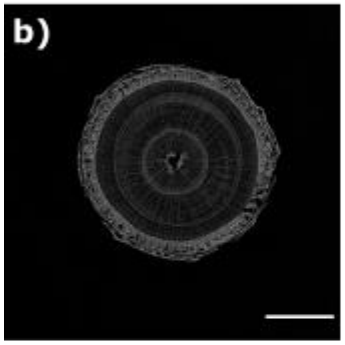
b)

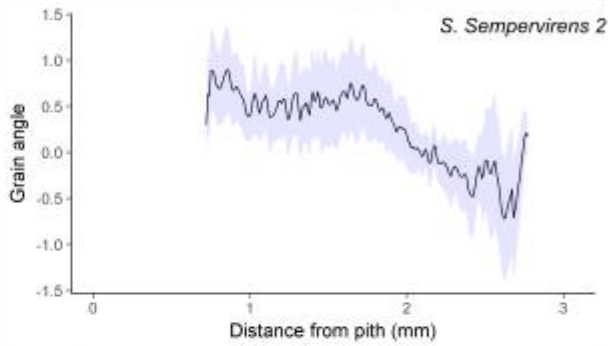
S. Sempervirens 2
Grain angle
Distance from pith (mm)

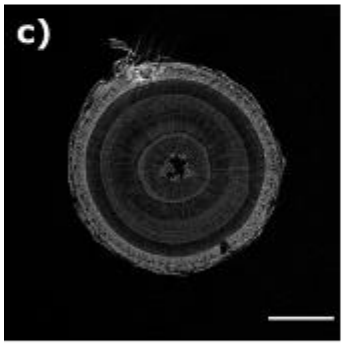
c)

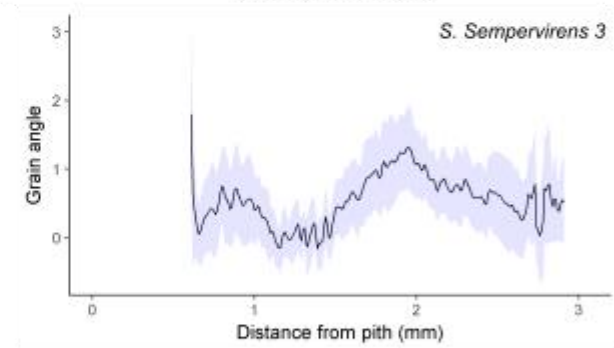
S. Sempervirens 3
Grain angle
Distance from pith (mm)

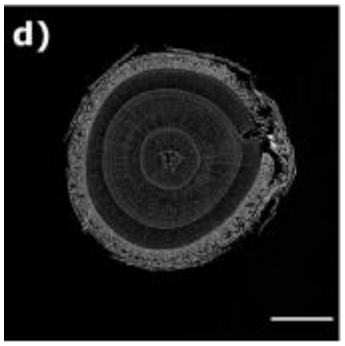
d)

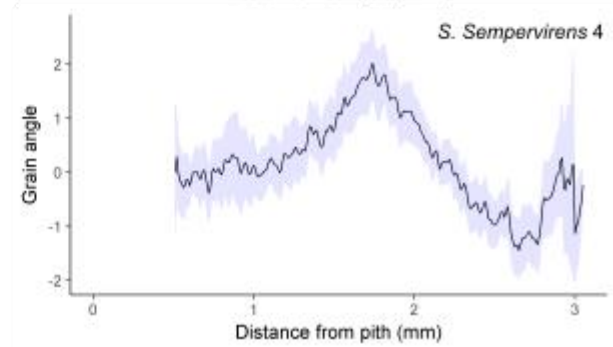
S. Sempervirens 4
Grain angle
Distance from pith (mm)

Figure 2.16

Analysis of four Coast redwood (*S. sempervirens*) trees allows identification of intraspecies grain trends. Scale bar equals 2mm. Negative grain angle values denote left-handed grain angles; positive grain angle values denote right-handed grain angles. The solid black line in each graph represents the measured grain angle, whereas the light blue area shows the standard error of the mean. a) Coast redwood 1. b) Coast redwood 2. c) Coast redwood 3. d) Coast redwood 4.

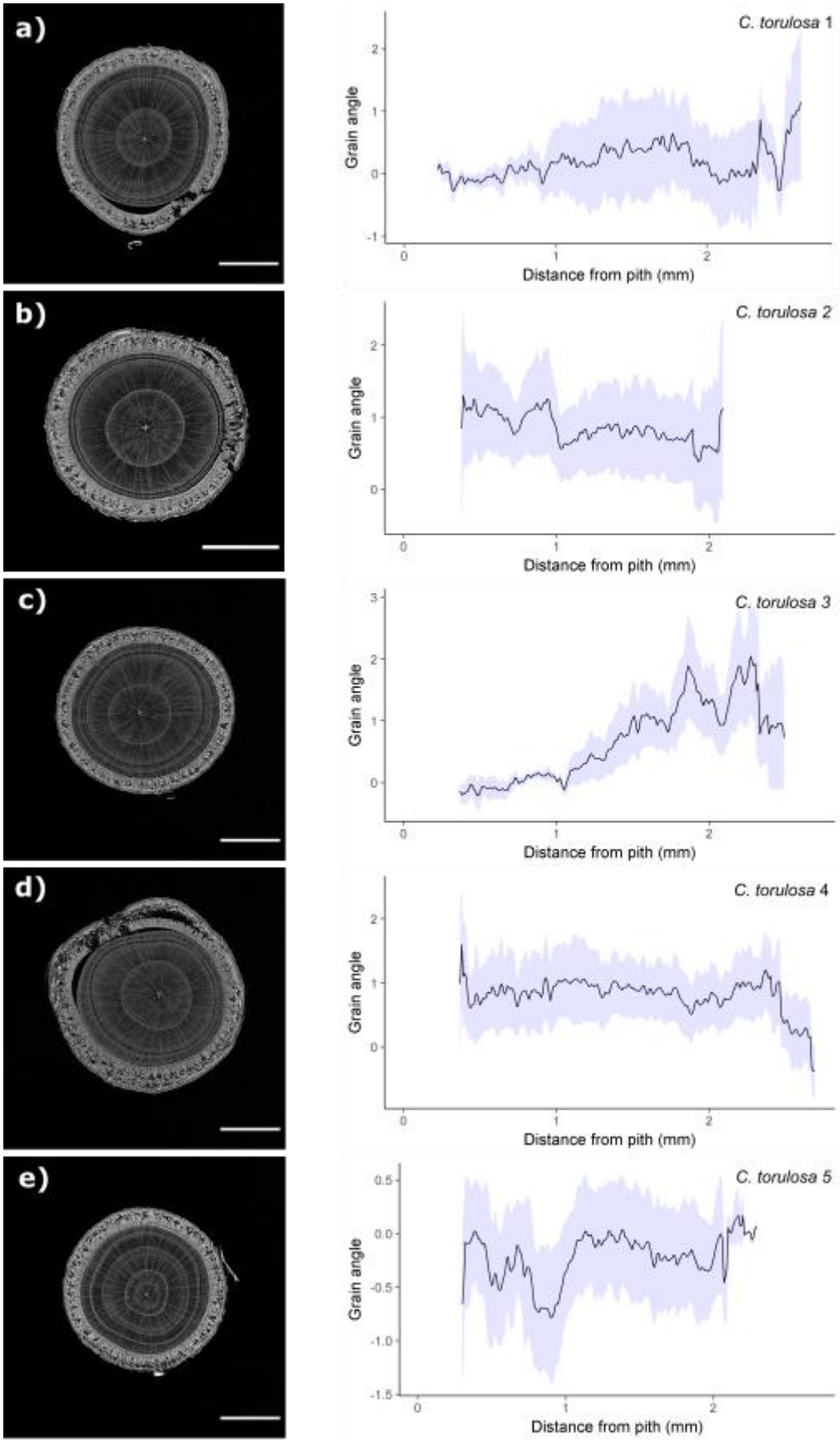
a)
b)
c)
d)
e)
C. torulosa 1
C. torulosa 2
C. torulosa 3
C. torulosa 4
C. torulosa 5
Grain angle
Distance from pith (mm)

Figure 2.17

Analysis of five Himalayan cypress (*C. torulosa*) trees allows identification of intraspecies grain trends. Scale bar equals 2mm. Negative grain angle values denote left-handed grain angles; positive grain angle values denote right-handed grain angles. The solid black line in each graph represents the measured grain angle, whereas the light blue area shows the standard error of the mean. a) Himalayan cypress 1. b) Himalayan cypress 2. c) Himalayan cypress 3. d) Himalayan cypress 4. e) Himalayan cypress 5.

2.3.3 X-ray microtomography of Southern Hemisphere gymnosperms

2.3.3.1 General trends in the grain patterns of New Zealand gymnosperms

As discussed in section 2.1, there has been little scrutiny of grain development and grain pattern formation in New Zealand native timber species. The grain patterns analysed in Ohkura (1958) were the only reference that could be found, and any other studies conducted on New Zealand native gymnosperms lacked grain information (table 2.3).

Of the eight species analysed, only Kauri (figure 2.18a) exhibited the right-handed twist predicted by Skatter and Kucera (1998). Of the remaining species; rimu (figure 2.18f), tōtara (figure 2.18g) and halls tōtara (figure 2.18h) all had left-handed spirality and the remainder were straight grained.

Table 2.3 Grain observations in southern gymnosperms

Common Name	Latin Name	Pattern (measured)[1]	Pattern (literature)[1]	Reference
Kauri	*Agathis australis*	RH	RH	(Ohkura, 1958)
Kahikatea	*Podocarpus dacrydiodes*	O	O	(Ohkura, 1958)
Miro	*Prumnopitys ferrugineus*	O		
Mātai	*Prumnopitys taxifolia*	O	LH	(Ohkura, 1958)
Pāhautea	*Libocedrus bidwillii*	O		
Rimu	*Dacrydium cupressium*	LH	LH	(Ohkura, 1958)
Tōtara	*Podocarpus tōtara*	LH	LH	(Ohkura, 1958)
Halls Tōtara	*Podocarpus hallii*	LH		

[1] Grain direction: L=left-handed, R=right-handed, O=straight grained

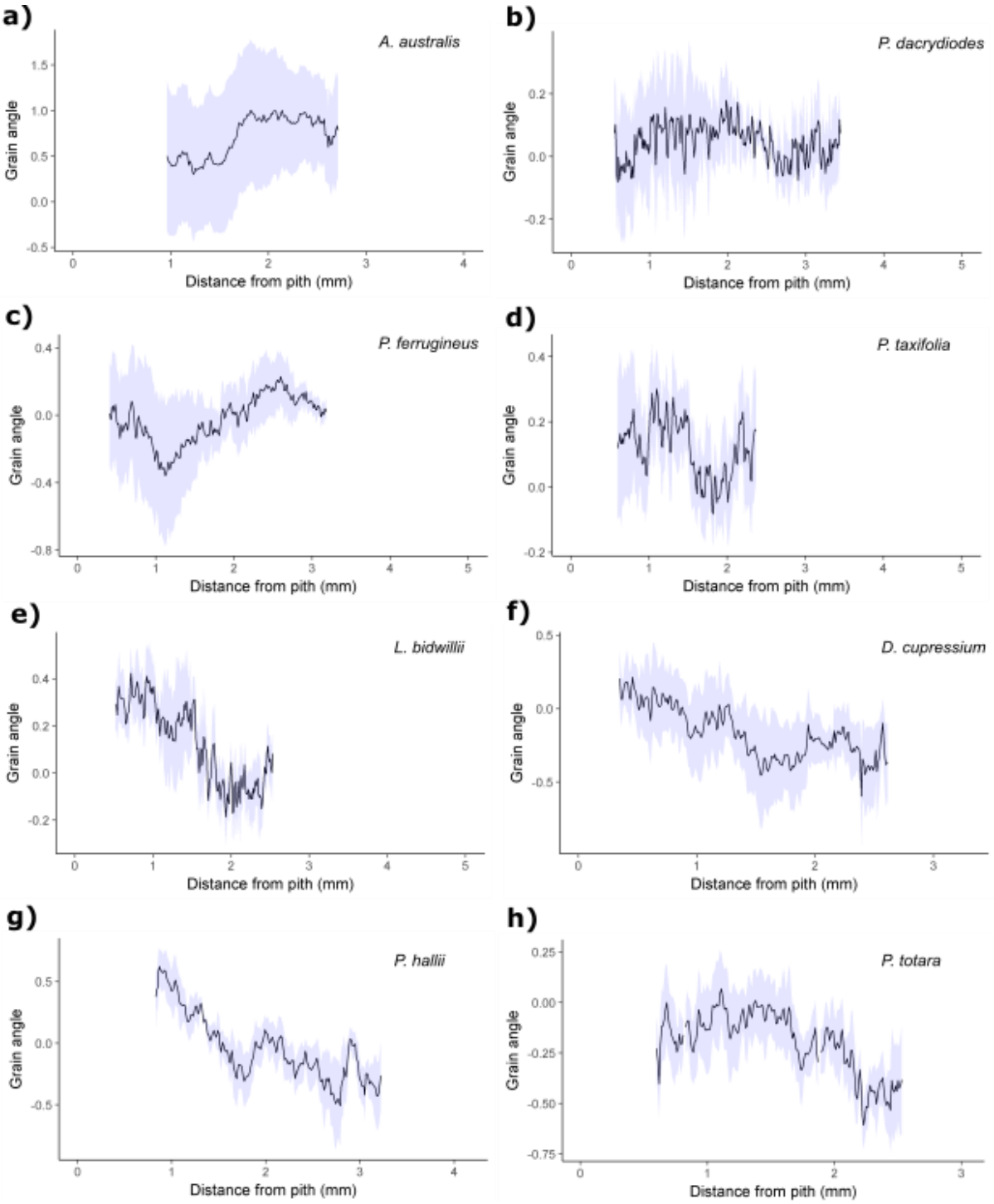

Figure 2.18: Average grain pattern for the eight southern hemisphere gymnosperms analysed with X-ray microtomography.

2.3.3.2 Intraspecies phenotypic variation of grain angle

As the trees utilised for this study were wild type and therefore of unknown genetic stock, it is expected that there will be a high degree of intraspecies variability in the grain patterns observed.

Kauri (Agathis australis)

The nine Kauri trees analysed showed a predominantly right-handed grain pattern (figure 2.18). Tree 1 (figure 2.18a) and tree 3 (figure 2.18c) both had a similar grain pattern, with initial straight grain that shifted to become increasingly left-handed. The grain reached a maximum left-handed angle of 1.27° at 1.43 mm in tree1 and 1.3° at 1.22 mm in tree 3 and then shifted to become increasingly right-handed. A maximum right-handed grain angle of 1.4° was reached at 2.96 mm in tree 1 and 1.78° was reached at 2.69 mm in tree 3. Tree 2 (figure 2.18b) and tree 4 (figure 2.18d) both had initial right-handed grain with a maximum angle of 3.23° at 0.63 mm in tree 2 and 1.3° at 0.56 mm in tree 4. The grain direction then reversed in both samples, becoming weakly left-handed in tree 2 (0.41° left-handed at 2.88 mm) and straight grained in tree 4. Tree 6 (figure 2.18f) showed a more severe version of this trend, with an initial right-handed angle of 4.22° at 0.87 mm that decreased towards 0° at the edge of the sample. Tree 5 (figure 2.18e) and tree 9 (figure 2.18j) both had initial left-handed grain, with grain angles of 2.12° at 0.61 mm for tree 5 and 1.47° at 0.72 mm for tree 9. The grain angle then decreased in both trees, becoming straight grained at 3.67 mm in tree 5 and becoming weakly right-handed in tree 9, with a maximum right-handed grain angle of 0.93° at 3.8 mm. Tree 7 had an initial right-handed grain angle of 1.27° at 0.96 mm, which then increased, reaching a maximum right-handed grain angle of 3.72° at 2.76 mm.

Kahikatea (Podocarpus dacrydiodes)

The five kahikatea trees analysed showed moderate variation in grain patterns (Figure 2.19). Tree 1 (figure 2.19a) and tree 4 (figure 2.19d) both were straight grained, with fluctuations in grain angle ≤ 0.5°. Tree 2 (figure 2.19b) had initial straight grain that became weakly left-handed, reaching a maximum left-handed angle of 0.72° at 1.5 mm. The grain then reversed direction, becoming weakly right-handed with a

maximum grain angle of 0.57° at 3.16 mm. Tree 3 (figure 2.19c) had right-handed grain initially develop, reaching a maximum angle of 0.85° at 1.1 mm. The grain angle then decreased and became straight-grained. Tree 5 (figure 2.19e) had initial weak left-handed grain, with a maximum left-handed angle of 0.91° at 0.64 mm. The grain angle then rapidly switched to become straight grained for the remainder of the section.

Matai

There are two distinct groupings of grain patterns in the nine Matai trees analysed, and this appeared to correlate to the location the trees were sourced from. Trees 1-5 were purchased from Southern Woods (Canterbury, NZ), whereas trees 6-9 were purchased from Taupo Natives (Kumara, West Coast, NZ). Tree 1 (figure 2.20a), tree 2 (figure 2.20b) and tree 3 (figure 2.20c) all have a similar growth pattern with minor variations. Tree 1 was initially straight grained and then shifts to become right-handed, reaching a maximum angle of 0.98°at 2.35 mm. The grain then fluctuates between straight grained (<0.5°) and weakly right-handed (0.5 – 0.81°) for the remainder of the sample. Tree 2 had weak initial left-handed grain, with a maximum angle of 0.62° at 0.86 mm. The grain then became right-handed, reached a maximum angle of 1.1° at 2.65 mm, and then shifted back to left-handed, with a maximum left-handed angle of 0.67° at 4.07 mm from the pith. Tree 3 also had initial weak left-handed grain, with a maximum angle of 1.04° at 0.38 mm from the pith. The angle then shifted to right-handed, reaching a maximum of 0.64° at 1.36 mm, and then decreased, becoming straight grained at 2.18 mm. Tree 4 (figure 2.20d) had straight grain throughout the sample. Tree 5 (figure 2.20e) was smaller than the other samples analysed, but followed a similar pattern to trees 2 and 3, with an initial weak left-handed grain angle of 0.64° at 0.22 mm. The grain then shifted to become weakly right-handed, with a maximum grain angle of 0.67° at 2.25 mm from the pith.

A distinct pattern, opposite to the LH – RH – LH pattern described above, was observed in trees 6-9. Tree 6 (figure 2.20f) and tree 8 (figure 2.20h) had initial right-handed grain with maximum angles of 0.82° at 0.19 mm in tree 6 and 0.67° at 0.47 mm in tree 8. The grain direction then reversed and reached a maximum left-handed angle of 0.5° at 1.55 mm in tree 6 and 0.56° at 2.76 mm in tree 8. Tree 7 (figure 2.20g) followed a modification of this pattern, with initial straight grain changing to a weak

right-handed pattern, reaching a maximum angle of 0.65° at 1.32 mm. The grain then switched direction, becoming left-handed and reaching a maximum angle of 0.63° at 1.71 mm. A final change in grain direction could then be observed after this point, with the tree developing straight grain throughout the remainder of the stem. Tree 9 (figure 2.20i) rapidly developed right-handed grain, reaching a maximum grain angle of 1.22° at 0.64 mm. A steady decrease in the grain angle then occurred over the next 1 mm of growth and the section developed straight grain.

Miro (Prumnopitys ferrugineus)

As observed in matai, two distinct groupings of grain patterns could be observed in the six miro trees analysed. However, these trees were purchased from a single nursery, Taupo Natives (Kumara, West Coast, NZ). Tree 1 (figure 2.21a) and tree 3 (figure 2.21c) both had initial right-handed grain, with a right-handed angle of 1.1° at 0.37 mm for tree 1 and 1.04 at 0.76 mm for tree 3. The grain angle then decreased in both trees with tree 1 forming consistent straight grain, and tree 3 developing left-handed grain ≤0.4°, which is therefore classified as straight grain. Tree 5 (figure 2.21e) followed a similar pattern to tree 1 and tree 3, with an initial right-handed grain angle of 1.03°at 0.92 mm from the pith. The grain direction then reversed, reaching a maximum left-handed grain angle of 0.60° at 2.24 mm from the pith. Following this the grain angle decreased, with the wood becoming straight grained towards the cambium.

Tree 2 (figure 2.21b), tree 4 (figure 2.21d) and tree 6 (figure 2.21f) all had initial left-handed grain develop, reaching a maximum angle of 1.01° at 1.07 mm in tree 2, 1.17° at 1.14 mm in tree 4 and 1.59° at 1.19 mm in tree 6. The grain direction then reversed, becoming straight grained in tree 2 and tree 4, and switching to right-handed in tree 6. A maximum right-handed angle of 1.02° was reached at 2.41 mm in tree 6.

Pahutea (Libocedrus bidwillii)

There was minor variation in the 6 pahutea trees analysed (figure 2.22). Tree 2 (figure 2.22b), tree 3 (figure 2.22c) and tree 5 (figure 2.22e) all had straight grain with minor fluctuations in grain angle and direction ≤0.4°. Tree 1 (figure 2.22b) had initial right-handed grain develop, reaching a maximum of 1.24° 1.3 mm. The grain then reversed direction reaching a maximum left-handed angle of 0.54° at 1.86 mm and then became

straight-grained for the remainder of the tree section. Tree 4 (figure 2.22d) had initial right-handed grain with a maximum angle of 0.77° at 0.91 mm. The grain then changed direction, becoming left-handed and reaching a maximum left-handed angle of 0.83° at 2.36 mm. Tree 4 then developed straight grain in the remaining 2 mm of growth. Tree 6 was initially straight grained and then developed a left-handed twist, reaching a maximum angle of 0.62 mm at 1.32 mm. The tree then returned to the straight grained form after 1.61 mm from the pith

Rimu (Dacrydium cupressium)

There was some variation between the five rimu trees analysed (figure 2.23). Tree 1 (figure 2.23a) had primarily straight grain with fluctuations in grain angle and direction ≤0.5°. Tree 2 (figure 2.23b) had initial left-handed grain develop, with a maximum left-handed angle of 1.05° at 0.61 mm from the pith. The grain direction then reversed, reaching a maximum right-handed angle of 0.58° at 2.58 mm from the pith. Tree 3 (figure 2.23c) had initial right-handed grain develop, with a maximum angle of 1.13° at 1.02 mm. A sharp reversal in grain direction was observed, with the grain reaching a maximum left-handed angle of 1.12° at 1.88 mm, and then remaining left-handed in the remainder of the section. Tree 4 (figure 2.23d) had initial straight grain, followed by a sharp change to left-handed grain, reaching a maximum angle of 0.69° at 1.02 mm. The grain then sharply switched back to straight grained for the remainder of the section. Tree 5 (figure 2.23e) had a gradual shift from initial straight grain to left-handed, reaching a maximum left-handed angle of 1.77° at 1.55 mm. The remainder of the tree 5 section had fluctuating left-handed grain ≥0.5°, with the angle increasing to 1.55° at 2.52 mm from the pith.

Tōtara (Podocarpus tōtara)

There was a low degree of variability between the four tōtara trees analysed (figure 2.23). Tree 1 (figure 2.23a) had straight grain with minor fluctuations in grain angle ±0.4°. Tree 2 (figure 2.23b) had consistent weak left-handed grain throughout the stem section, with a maximum angle of 1.05° at 2.6 mm from the pith. Tree 3 (figure 2.23c) also had consistent weak left-handed grain throughout the stem section, with a maximum left-handed angle of 0.91° at 2.26 mm. Tree 4 (figure 2.23d) had initial

straight grain that changed to left-handed after 2 mm of growth, reaching a maximum left-handed grain angle of 1.26°at 2.75 mm.

Halls Tōtara (Podocarpus hallii)

There was little variation between the four Halls tōtara trees analysed (figure 2.24). Tree 1 (figure 2.24a) had initial right-handed grain with a grain angle of 0.84° at 0.67 mm which then reversed, reaching a maximum left-handed grain angle of 0.98° at 3.05 mm from the pith. Tree 2 (figure 2.24b) and tree 4 (figure 2.24d) had a similar pattern, with an initial right-handed grain angle of 1.52° at 0.66 mm for tree 2, and 0.84° at 0.64 mm for tree 4. The grain then reversed direction, reaching a left-handed grain angle of1.3° at 3.18 mm in tree 2, and becoming straight grained in tree 4. Tree 3 (figure 2.24c) was straight grained, with minor fluctuations in grain angle ≤0.4°.

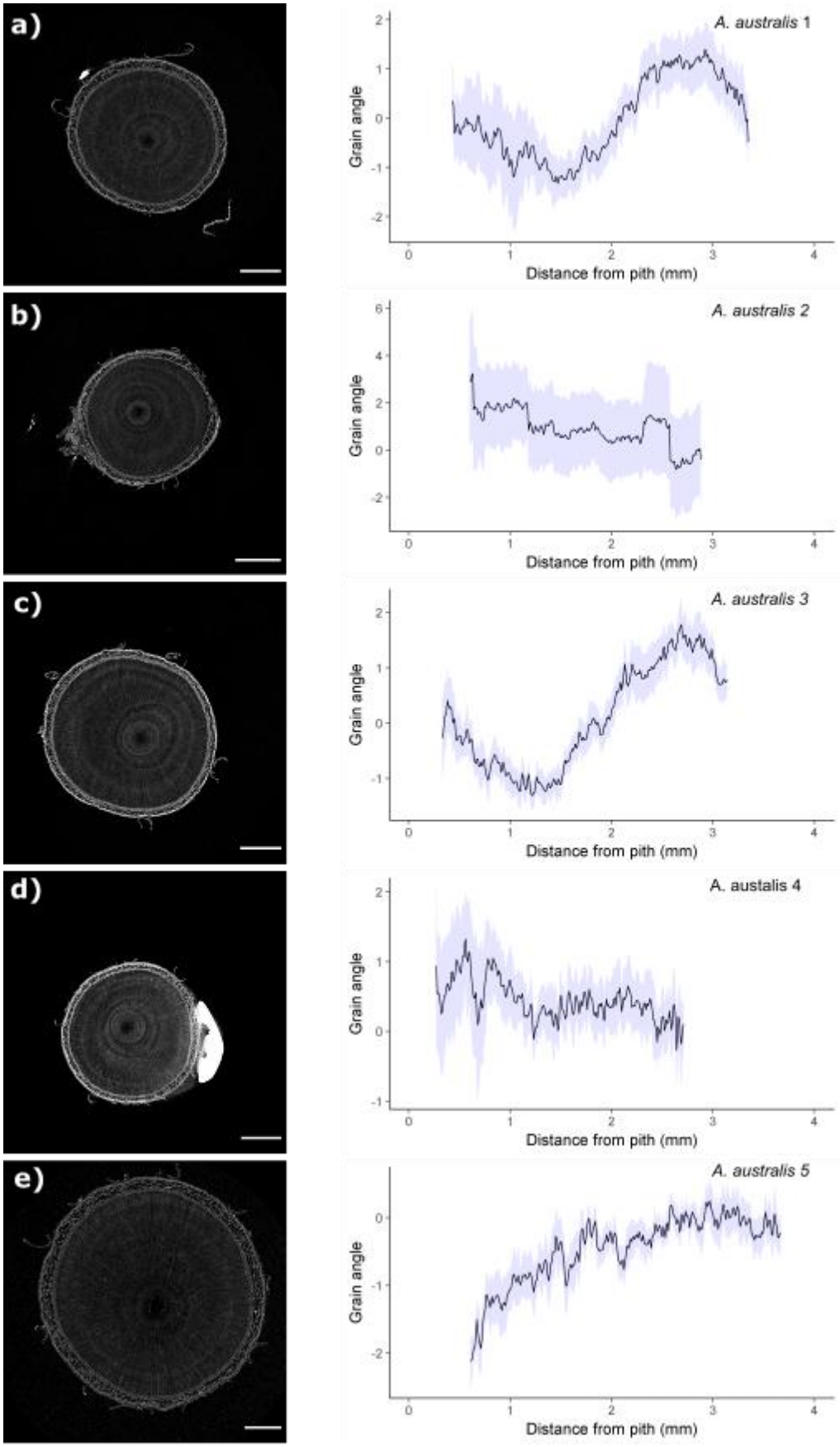
a)
b)
c)
d)
e)
A. australis 1
A. australis 2
A. australis 3
A. austalis 4
A. australis 5
Grain angle
Distance from pith (mm)

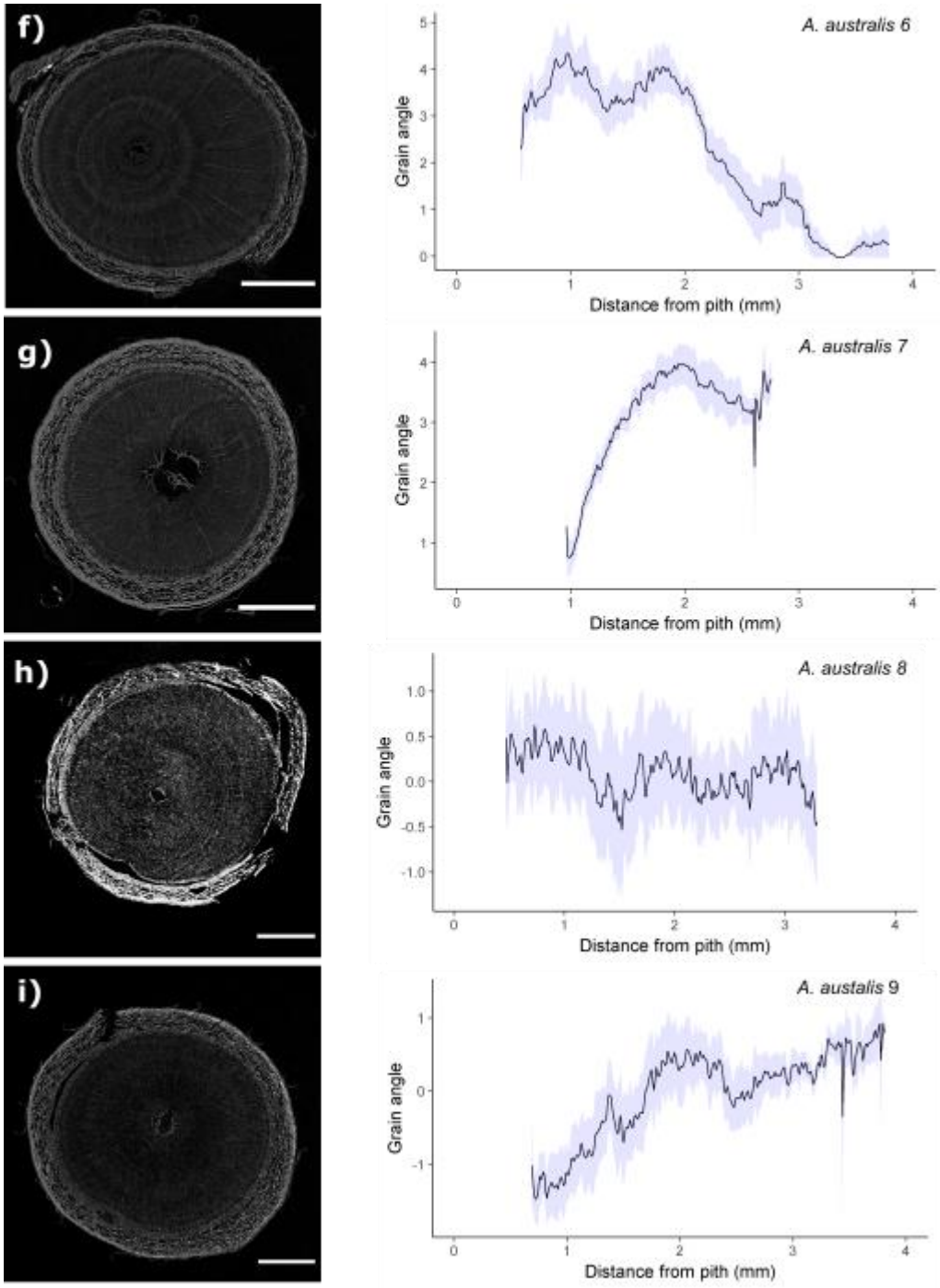

Figure 2.19 Kauri (Agathis australis)

Analysis of nine Kauri (A. *australis*) trees allows identification of intraspecies grain trends. Scale bar equals 2mm. Negative grain angle values denote left-handed grain angles; positive grain angle values denote right-handed grain angles. The solid black line in each graph represents the measured grain angle, whereas the light blue area shows the standard error of the mean. a) Kauri 1. b) Kauri 2. c) Kauri 3. d) Kauri 4. e) Kauri 5. f) Kauri 6. g) Kauri 7. h) Kauri 8. i) Kauri 9.

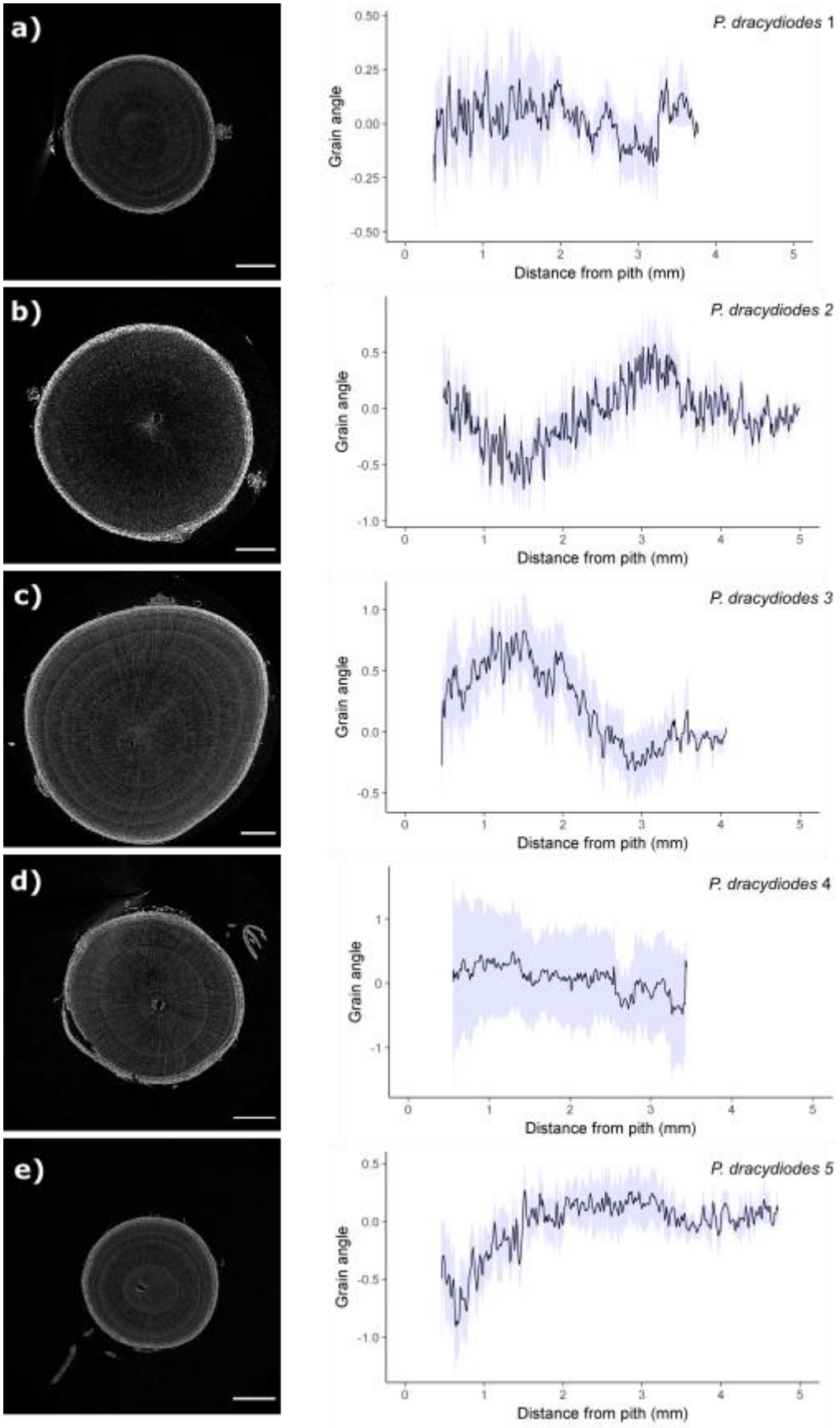
a)
b)
c)
d)
e)
P. dracydiodes 1
P. dracydiodes 2
P. dracydiodes 3
P. dracydiodes 4
P. dracydiodes 5
Grain angle
Distance from pith (mm)

Figure 2.20 Kahikatea (Dacrycarpus dacryoides)

Analysis of five Kahikatea (D. *dacryoides*) trees allows identification of intraspecies grain trends. Scale bar equals 2mm. Negative grain angle values denote left-handed grain angles; positive grain angle values denote right-handed grain angles. The solid black line in each graph represents the measured grain angle, whereas the light blue area shows the standard error of the mean. a) Kahikatea 1. b) Kahikatea 2. c) Kahikatea 3. d) Kahikatea 4. e) Kahikatea 5.

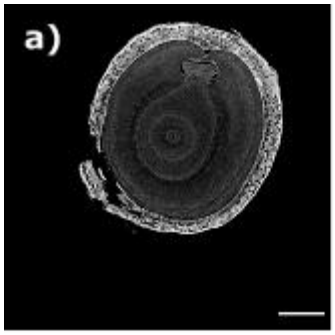
a)

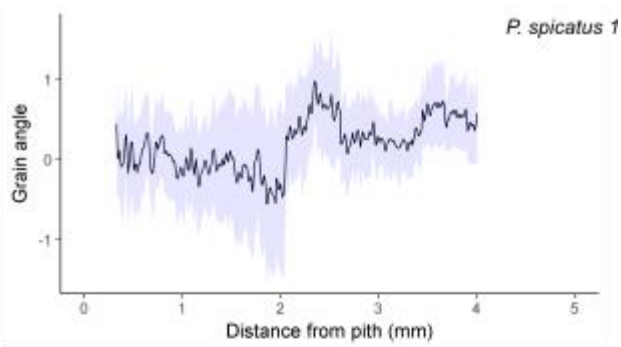
P. spicatus 1
Grain angle
Distance from pith (mm)

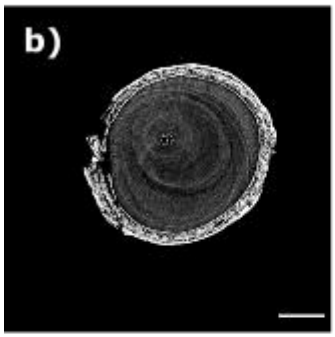
b)

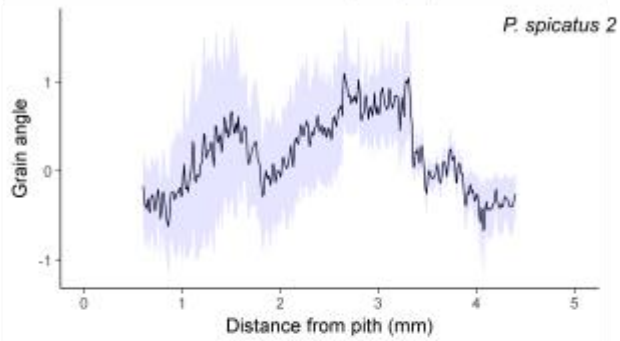
P. spicatus 2
Grain angle
Distance from pith (mm)

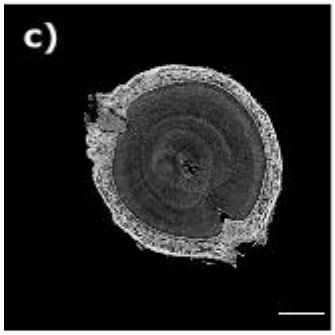
c)

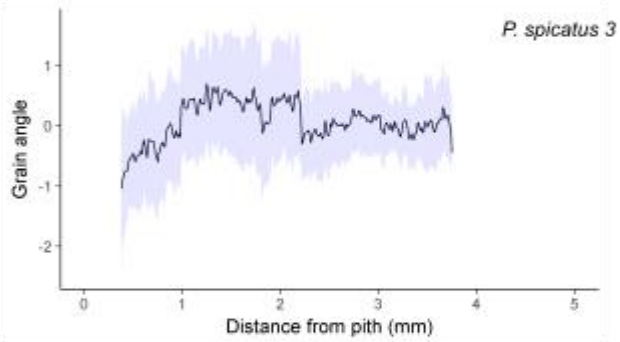
P. spicatus 3
Grain angle
Distance from pith (mm)

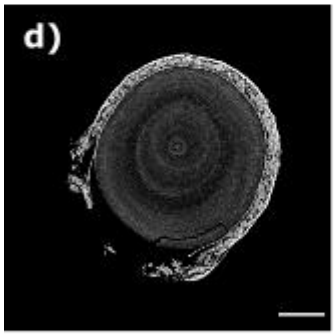
d)

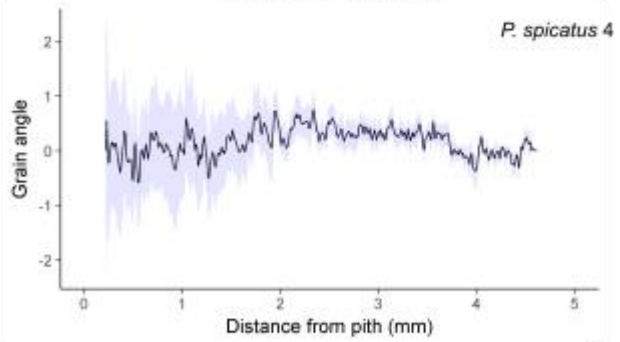
P. spicatus 4
Grain angle
Distance from pith (mm)

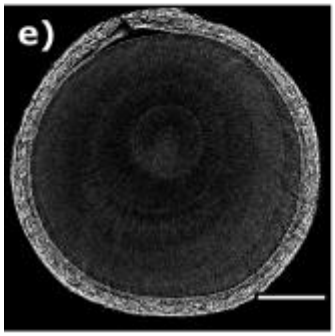
e)

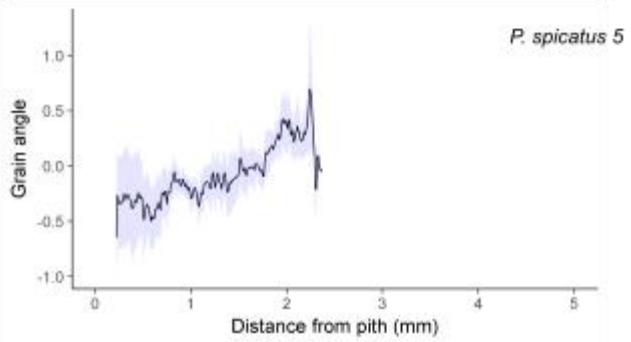
P. spicatus 5
Grain angle
Distance from pith (mm)

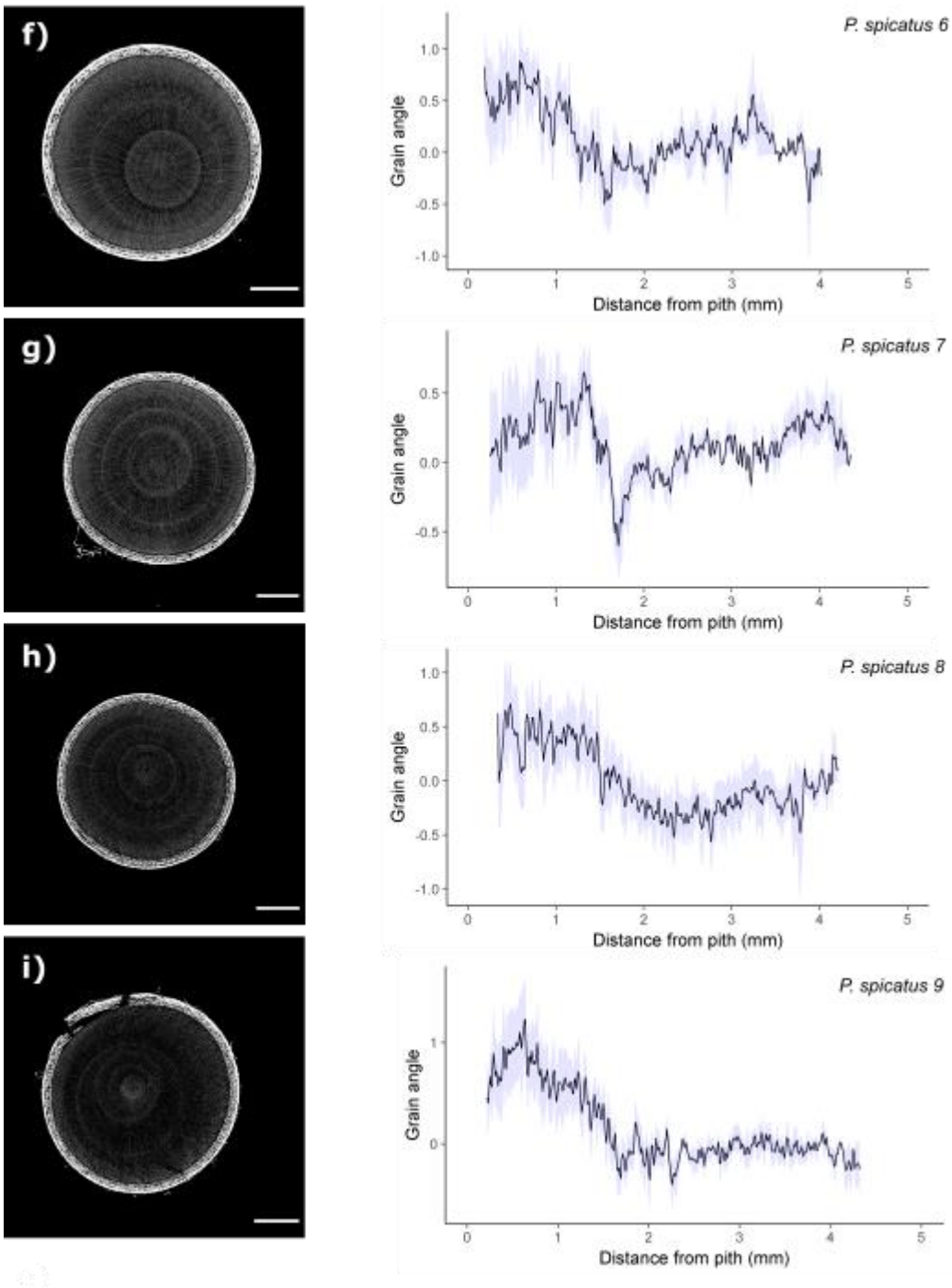

Figure 2.21 Matai (Prumnopitys taxifolia)

Analysis of nine Matai (P*. taxifolia*) trees allows identification of intraspecies grain trends. Scale bar equals 2mm. Negative grain angle values denote left-handed grain angles; positive grain angle values denote right-handed grain angles. The solid black line in each graph represents the measured grain angle, whereas the light blue area shows the standard error of the mean. a) Matai 1. b) Matai 2. c) Matai 3. d) Matai 4. e) Matai 5. f) Matai 6. g) Matai 7. h) Matai 8. i) Matai 9.

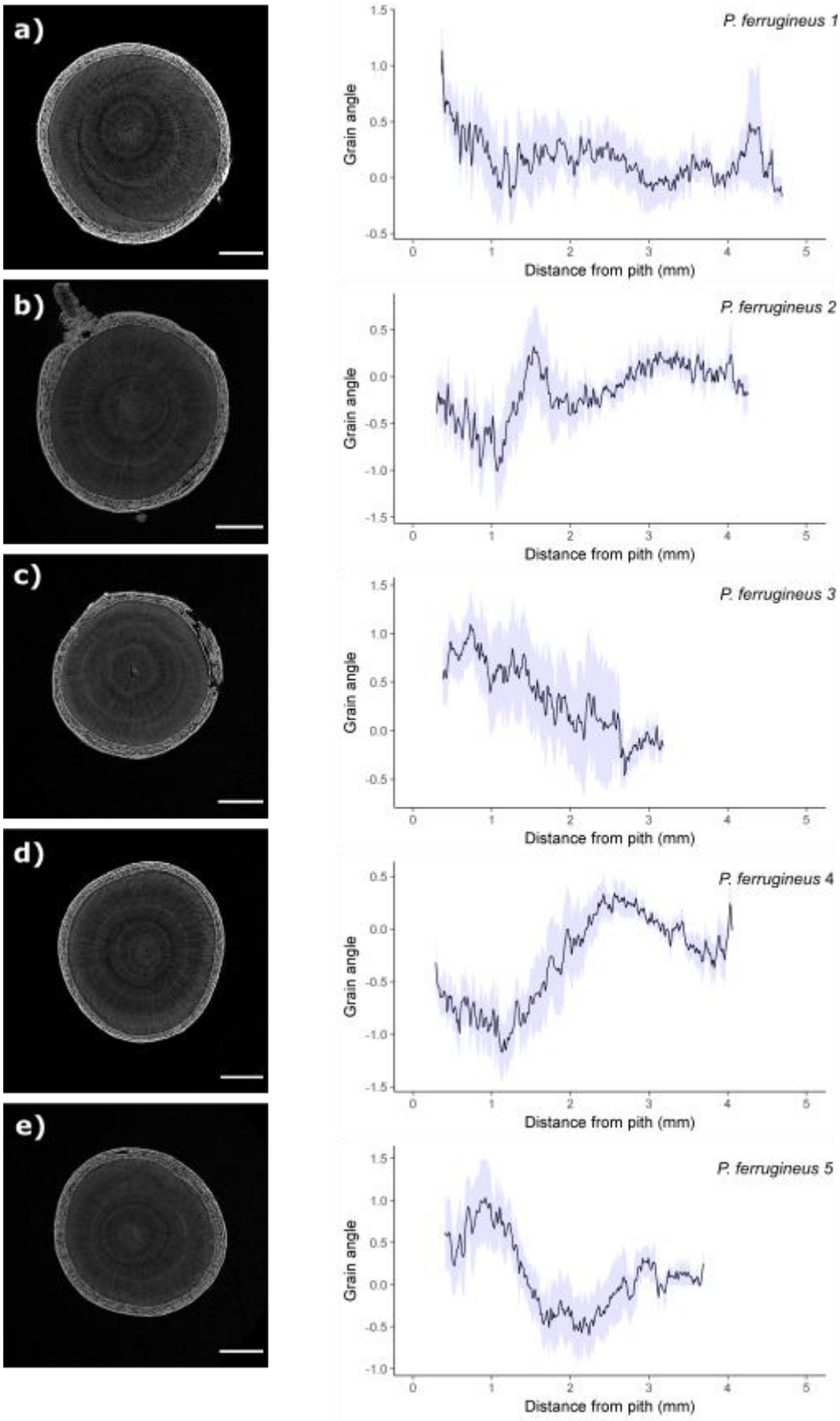
a)
b)
c)
d)
e)
P. ferrugineus 1
P. ferrugineus 2
P. ferrugineus 3
P. ferrugineus 4
P. ferrugineus 5
Grain angle
Distance from pith (mm)

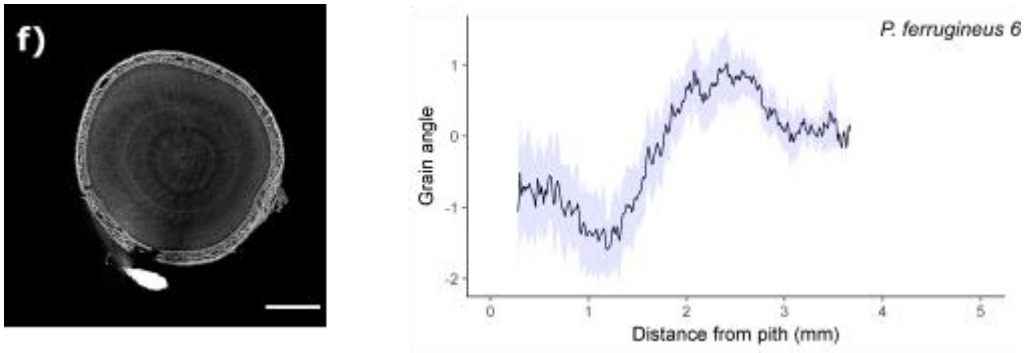

Figure 2.22 Miro (Prumnopitys ferrugineus)

Analysis of six Miro (P*. ferrugineus*) trees allows identification of intraspecies grain trends. Scale bar equals 2mm. Negative grain angle values denote left-handed grain angles; positive grain angle values denote right-handed grain angles. The solid black line in each graph represents the measured grain angle, whereas the light blue area shows the standard error of the mean. a) Miro 1. b) Miro 2. c) Miro 3. d) Miro 4. e) Miro 5. f) Miro 6.

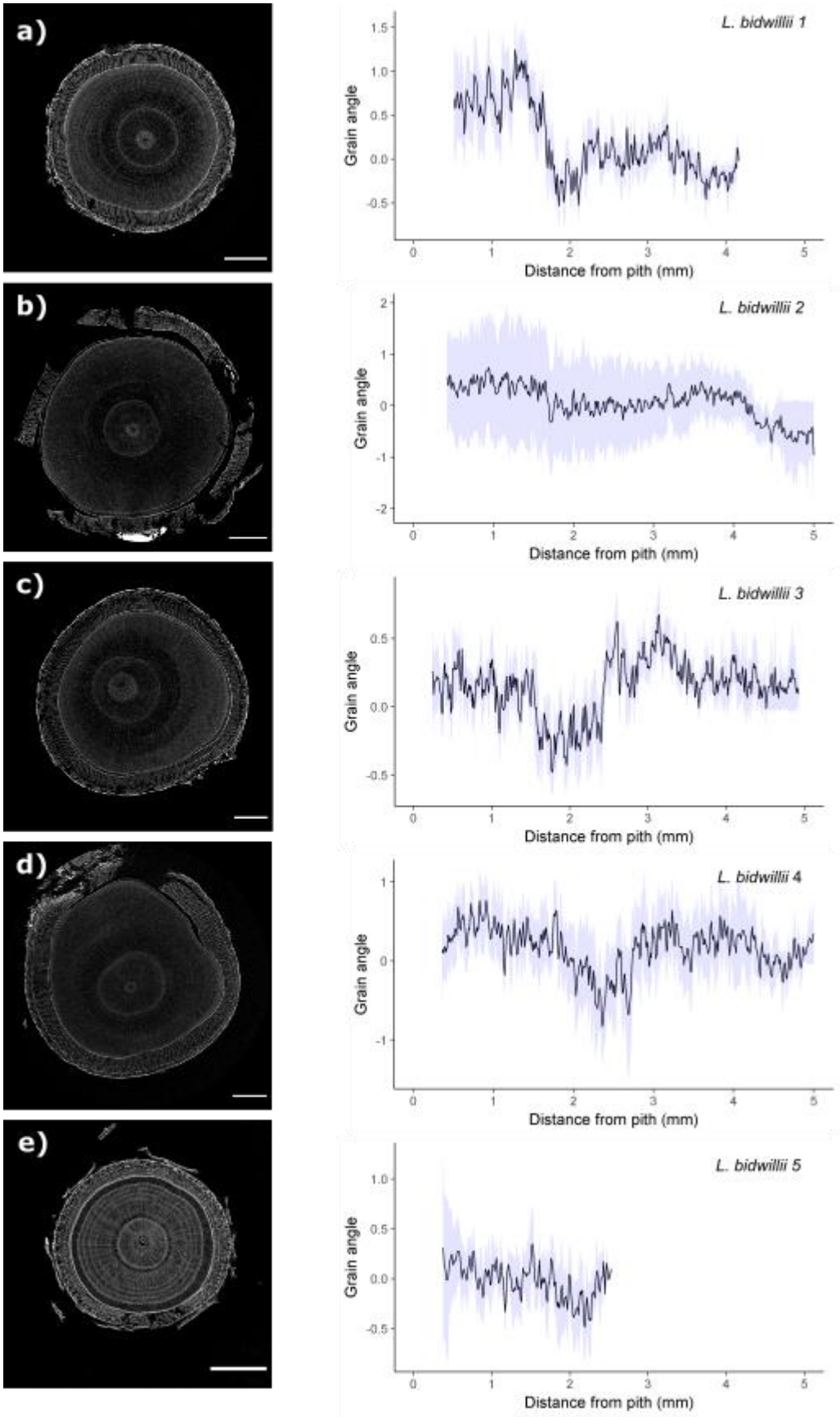
a)
b)
c)
d)
e)
L. bidwillii 1
L. bidwillii 2
L. bidwillii 3
L. bidwillii 4
L. bidwillii 5
Grain angle
Distance from pith (mm)

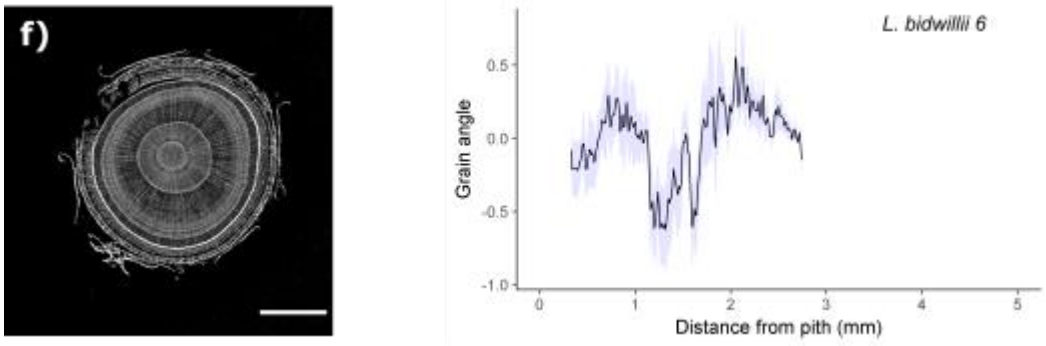

Figure 2.23 Pahutea (Libocedrus bidwillii)

Analysis of five Pahutea (L*. bidwillii*) trees allows identification of intraspecies grain trends. Scale bar equals 2mm. Negative grain angle values denote left-handed grain angles; positive grain angle values denote right-handed grain angles. The solid black line in each graph represents the measured grain angle, whereas the light blue area shows the standard error of the mean. a) Pahutea 1. b) Pahutea 2. c) Pahutea 3. d) Pahutea 4. e) Pahutea 5. f) Pahutea 6.

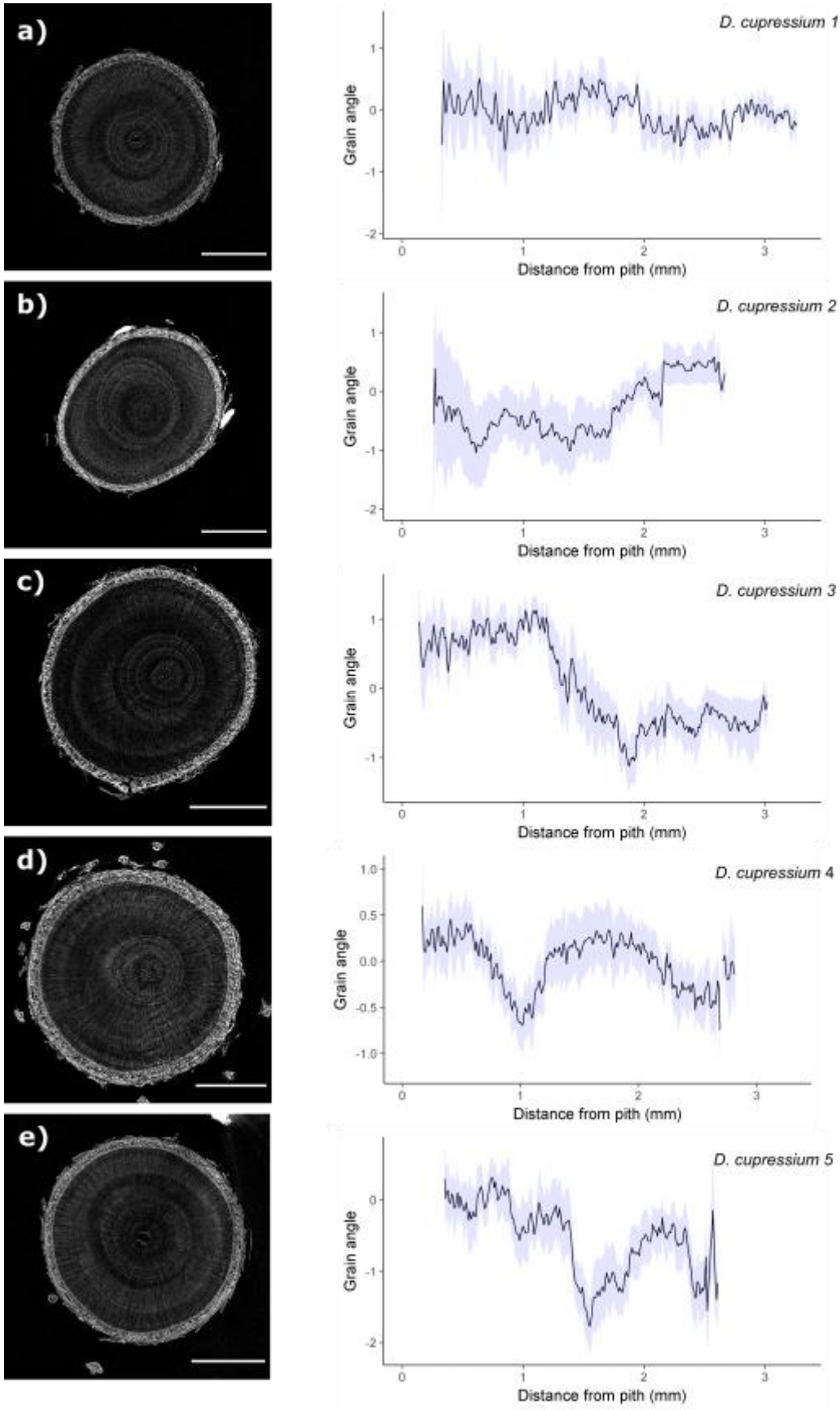
a)
b)
c)
d)
e)
D. cupressium 1
D. cupressium 2
D. cupressium 3
D. cupressium 4
D. cupressium 5
Grain angle
Distance from pith (mm)

Figure 2.24 Rimu (Dacrydium cupressinum)

Analysis of five Rimu (D*. cupressinum*) trees allows identification of intraspecies grain trends. Scale bar equals 2mm. Negative grain angle values denote left-handed grain angles; positive grain angle values denote right-handed grain angles. The solid black line in each graph represents the measured grain angle, whereas the light blue area shows the standard error of the mean. a) Rimu 1. b) Rimu 2. c) Rimu 3. d) Rimu 4. e) Rimu 5.

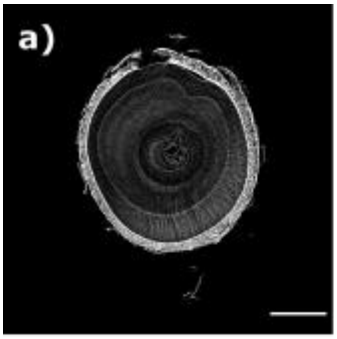
a)

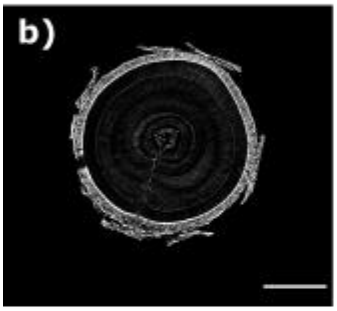
b)

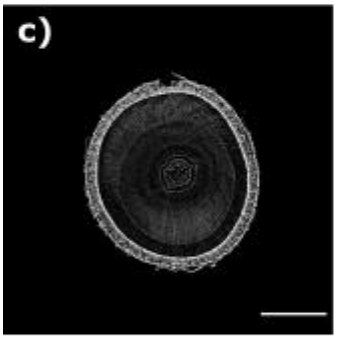
c)

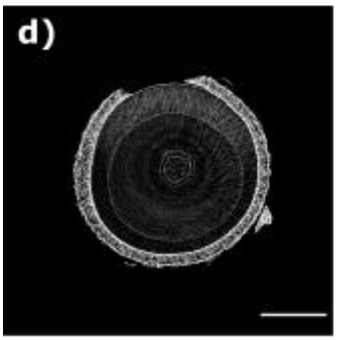
d)

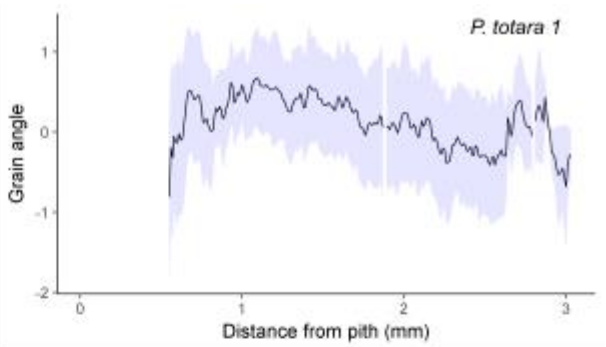
P. totara 1
Grain angle
Distance from pith (mm)

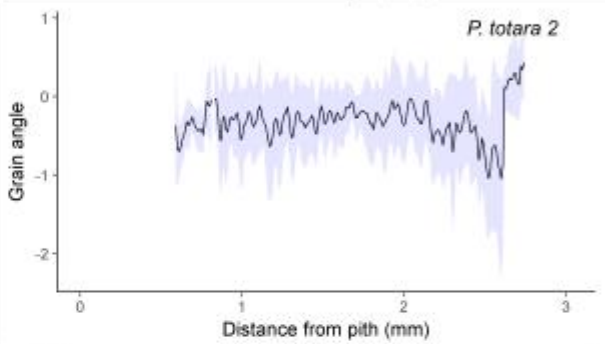
P. totara 2
Grain angle
Distance from pith (mm)

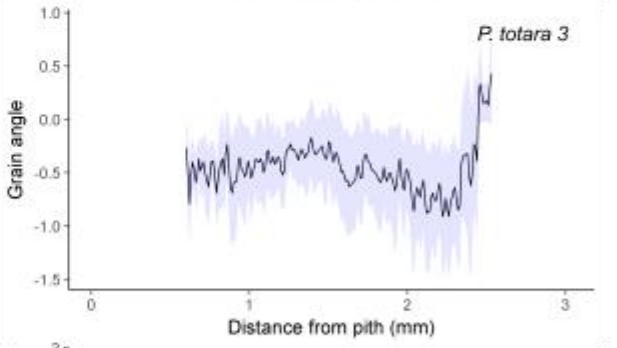
P. totara 3
Grain angle
Distance from pith (mm)

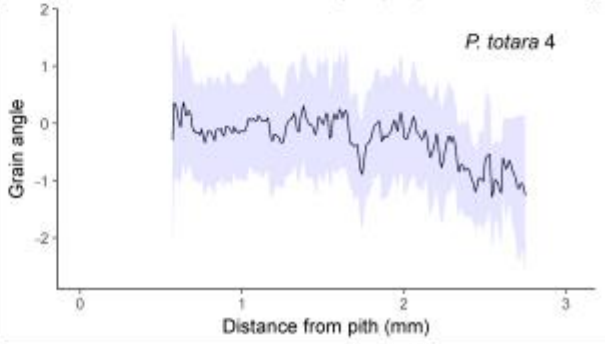
P. totara 4
Grain angle
Distance from pith (mm)

Figure 2.25 Tōtara (Podocarpus totara)

Analysis of four Tōtara (P*. totara*) trees allows identification of intraspecies grain trends. Scale bar equals 2mm. Negative grain angle values denote left-handed grain angles; positive grain angle values denote right-handed grain angles. The solid black line in each graph represents the measured grain angle, whereas the light blue area shows the standard error of the mean. a) Tōtara 1. b) Tōtara 2. c) Tōtara 3. d) Tōtara 4.

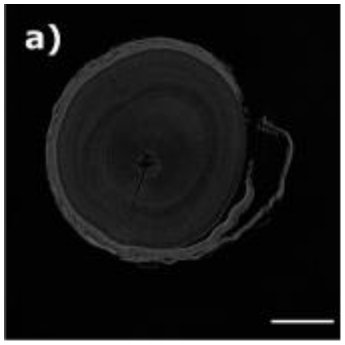
a)

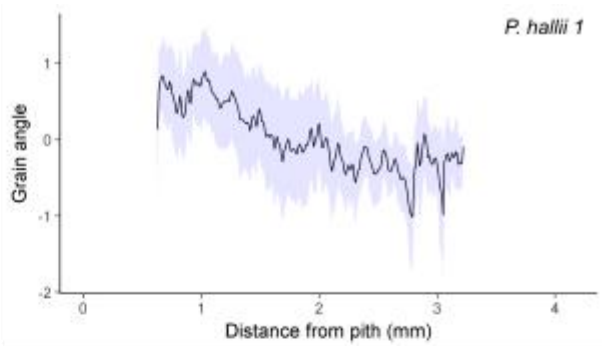
P. hallii 1
Grain angle
Distance from pith (mm)

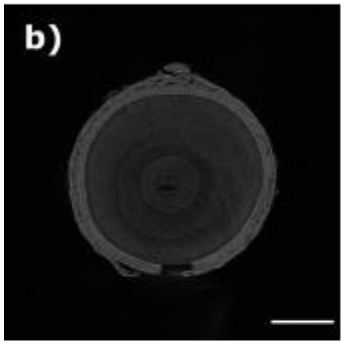
b)

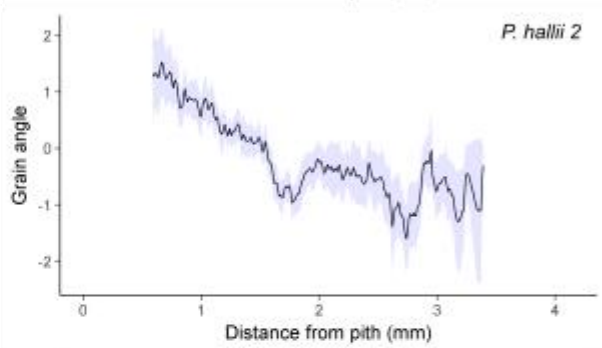
P. hallii 2
Grain angle
Distance from pith (mm)

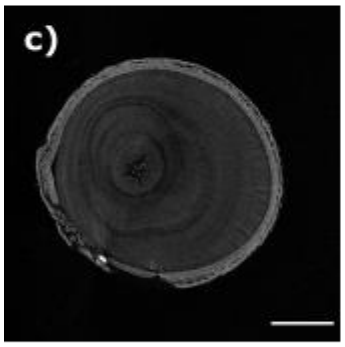
c)

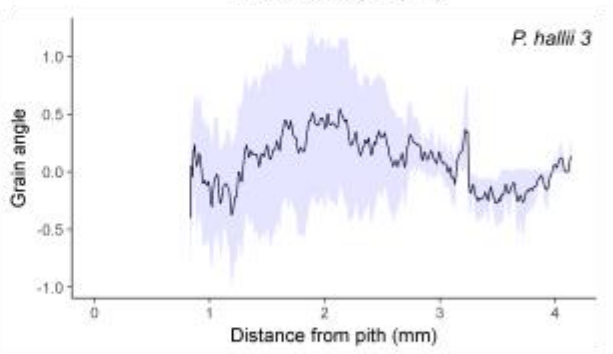
P. hallii 3
Grain angle
Distance from pith (mm)

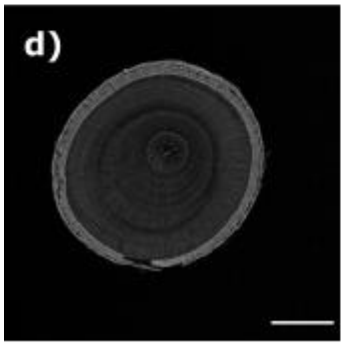
d)

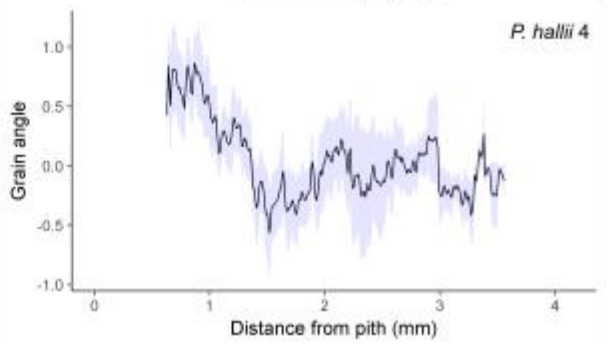
P. hallii 4
Grain angle
Distance from pith (mm)

Figure 2.26 Halls tōtara (Podocarpus hallii)

Analysis of four Halls tōtara (P*. hallii*) trees allows identification of intraspecies grain trends. Scale bar equals 2mm. Negative grain angle values denote left-handed grain angles; positive grain angle values denote right-handed grain angles. The solid black line in each graph represents the measured grain angle, whereas the light blue area shows the standard error of the mean. a) Halls tōtara 1. b) Halls tōtara 2. c) Halls tōtara 3. d) Halls tōtara 4.

2.4 Discussion

2.4.1 The suitability of X-ray microtomography for grain analysis

The analysis conducted with X-ray microtomography provided a suitable alternative to serial sectioning approaches, as young trees could be imaged at cellular resolution in their entirety, with very little sample preparation required. The single limitation of this technique is the inverse relationship between sample dimensions and imaging resolution. To accommodate larger samples, the stub is moved further away from the detector, resulting in greater X-ray scattering and a reduction in resolution. Therefore, it is only possible to image whole stem samples that are less than 2 cm in diameter without resolution degrading to the point where individual cells can't be distinguished, limiting analyses of wood grain to trees that are only 1-2 years old.

An alternative methodology that would allow for the investigation of spiral grain in older trees would be the use of tree core samples. Tree coring allows for the removal of a 5-7mm cross section of the trunk of living trees and is widely utilised to study forest ecology and xylem development (Dickson et al., 2016; Li & Altaner, 2017). The process can be repeated up to four times per tree and, providing care is taken to ensure sterile conditions, causes minimal damage to the tree (Norton, 1998).

2.4.2 Hemispherical trends in tree twisting

Analysis of the fourteen northern hemisphere species selected showed similar grain patterns to those stated in the literature, with radiata pine, maritime pine and european larch having initial left-handed spirality as stated. Coulter pine, deodar cedar, Leyland cypress, Monterey cypress, coast redwood, Chinese juniper and buddhist pine were reasonably straight grained, with overall grain angles less than 0.5° of spirality. While Chinese juniper (Jacot, 1931) is reported as having left-handed spirality, and coast redwood (Ohkura, 1958) and buddhist pine (Ohkura, 1958) as right-handed spirality, no information is given in which ring this develops, and it is therefore possible that the trees utilised in this study were too young. Silver fir had a distinctive right-handed to left-handed pattern, however, no literature information could be found about the grain patterns in this species. Norway spruce was the only northern hemisphere species analysed that had a reversal of the expected L-R pattern and showed a R-L pattern

instead. This pattern was also present in all the individual trees analysed (figure 2.12) and warrants further investigation.

Out of the southern hemisphere gymnosperms analysed, kauri was the only species to exhibit the right-handed spirality predicted by Skatter and Kucera (1998). Rimu, tōtara and Halls tōtara all had left-handed spiral grain and numerous other southern hemisphere trees analysed by Ohkura (1958) also showed preference for the L-R pattern.

There is a discrepancy in the grain direction of the mātai trees, with trees from the eastern coast of New Zealand (Southern woods purchased) showing a L-R-L pattern, and trees from the western coast of New Zealand (Taupo Natives purchased) showing a R-L-R pattern. This leads some validity to the theory that spiral grain directionality is driven by the predominant wind direction. However, without knowing the genetic provenance of the two populations of mātai utilised, no conclusions can be drawn.

2.4.3 Limitations of this study

The initiation of spiral grain, while occasionally observed in the xylem adjacent to the pith (Cown et al., 1991; Gapare et al., 2007; Thomas & Collings, 2017; Young, 1999), often occurs near the end of the first two years of growth (Harris, 1989; Ohkura, 1958). Therefore, the first 2-5mm of growth will often exhibit a straight-grained form. As none of the samples analysed exceeded 5 mm in diameter, there is a strong possibility that the trees defined as straight grained in this thesis were simply too young to develop spiral grain. This is most likely the case with coast redwood, Chinese juniper, and buddhist pine, as the literature values state that these trees have right-handed, left-handed, and right-handed spiral grain respectively, but the averaged grain pattern for these trees is straight grain.

Another significant limitation in this study, as mentioned above, is that the tree utilised were commercial nursery stock of unknown genetic provenance. It was presumed, given the layout of each nursey, that the trees grown together were subject to the same environmental conditions, however, to more robustly analyse the role of prevailing wind directions on spiral grain initiation and development future experiments should ensure greater control over these factors.

2.5 Conclusion

The work conducted in this chapter has provided a case for the utilisation of X-ray microtomography in the analysis of spiral grain, providing cellular resolution over significantly larger tissue areas than previously possible. While the current methodology is limited to young trees (1-2 years), the use of tree cores would allow for significantly older trees to be analysed.

While none of the work completed in this chapter sufficiently proves, or disproves the theory that there is a hemispherical difference in spiral grain direction, or that spiral grain directionality is driven by prevailing wind directions, it shows that the causes of spiral grain are complex and require a multifaceted approach to understand.

Chapter 3 Trends in interlocked grain formation in *Eucalyptus bosistoana*

3.1 Introduction

The work in this chapter focuses on the characterisation of interlocked grain in *Eucalyptus bosistoana* and investigates the link between interlocked grain pattern and stem twist, and the heritability of interlocked grain. Using a collection of 4,033 samples from 81 families, measurements of stem warping were made after drying. This data was then compared to a subset of samples for which interlocked grain measurements were made via stem splitting. To allow for high sample throughput, a new method was developed, in which split stem sections were imaged and analysed in ImageJ. This method was verified through X-ray microtomography of a further subsection of samples, with these experiments showing that while the splitting method often overstated the grain angles, there was a high fidelity with respect to the grain pattern Taken together, these experiments demonstrated that wood splitting methodologies can be utilised as a valuable tool for rapidly characterising patterns of interlocked grain in large sample sets.

3.1.1 Eucalyptus forestry trials in New Zealand

Industry and societies drive towards products with a lower environmental impact, greater durability and sustainability has led to interest in the development of naturally durable timber resources in New Zealand. The New Zealand Dryland Forests Initiative (NDZFI), a consortium between the Marlborough Research Centre Trust, Proseed NZ Ltd, the New Zealand School of Forestry (University of Canterbury) and Vineyard Timbers Ltd, has been tasked with investigating multiple *Eucalyptus* species to determine which timber would be suitable for structural purposes, and then to improve the genetic resources available. The advantages of *Eucalyptus* timber over radiata pine are numerous (see section 1.3.1) and this timber might be utilised as vineyard posts, cross arms for electricity networks, sleepers for railway networks and urban landscaping, wharf timbers, decking and other applications where natural durability is required (Van Ballekom & Millen, 2017). To this end, NZDFI has selected three *Eucalyptus* species (*E. bosistoana*, *E. globoidea* and *E. quadrangulata)* following trials with over 20 species to determine their suitability to the New Zealand climate (Van Ballekom & Millen, 2017). From these three species, the initial focus has been on *E. bosistoana* as this species provides a Class 1

durable timber (Australian Standard, AS5604-2005) with exceptionally high stiffness and strength (Bootle, 1983).

E. bosistoana seedlings were planted at a tree nursey in Woodville, New Zealand in Feb 2015, and harvested when they were 2 years old. This Woodville Trial consisted of 4032 seedlings from 81 families (common mother tree, unknown father(s)) of *E. bosistoana* and trees were planted in family blocked of eight individuals, with blocks replicated 2-3 times depending on availability. The aim of this trial is to assess the wood properties within matriarchal families to identify those suitable for future breeding trials (Davies & Altaner, 2017). The properties measured in these trees included, volumetric shrinkage, acoustic velocity, density, moisture content and modulus of elasticity.

As these families comprise of individuals that are half- and full- siblings, as well as 'selfed' individuals, a high degree of genetic variation within families is therefore possible. This trial has specifically used families of plants, rather than clonal populations. Such clonal populations are established through vegetative propagation of a single individual and therefore have a little-to-no genetic diversity. Thus, to ensure that the 'best' individuals are selected to form a clonal population, it is imperative to maintain enough genetic diversity in the initial stages of a trial. For this reason, early screening involves selection from families (Roberds et al., 1990). Additionally, by analysing traits that are conserved within families, the inheritance of phenotypes can be analysed (Wray & Visscher, 2008). The heritability of interlocked and spiral grain is discussed further in section 4.1.3.

3.1.2 Impacts of interlocked grain on wood properties

Interlocked grain (also known as wavy grain) occurs when there are periodic oscillations in the direction of grain away from the vertical axis of the tree. These changes in grain have an impact on timber strength and shrinkage. The effect on timber strength is generally detrimental, with interlocked grain correlating to a decrease in elasticity and an increase in the likelihood of sudden failure under bending stress (Weddell, 1961) and shear stress (Hernández & Almeida, 2007). However, the grain oscillations of interlocked grain also make timber less susceptible to splitting and results in a greater resistance to general wear. This is advantageous

for certain heavy usage applications such as wharf construction and industrial decking (Harris, 1989; Koehler, 1949).

The grain oscillations of interlocked grain also correspond to changes in the cellulose microfibril angle. As cellulose microfibrils are chiral, they will refract the light at a set angle. Changes to the orientation of the microfibrils will therefore change the angle of light refraction. This results in a beautiful striped pattern in interlocked wood and this is highly prized for decorative solid timber applications and wood veneers (Harris, 1989; Skolmen, 1963).

All timber will undergo a degree of volumetric shrinkage upon drying in the radial, axial and tangential directions. This shrinkage occurs due to loss of water from the cell wall, allowing for tighter packing of the cell wall contents. The majority of volumetric shrinkage, can therefore, be accounted for in the radial and tangential directions in straight grained timber, as the lumen size and length do not change (Spear & Walker, 2006). However, when the cell axis is offset from the stem axis by spiral grain, this results in an increased anisotropy in shrinkage direction which can be observed as a twist in dried timber. Interlocked grain complicates this further: the amplitude of the spiral, the periodicity of the switch and variations across the stem will all effect shrinkage and complex patterns can develop on drying (Chauhan et al., 2006; Harris, 1989). It is, therefore, of significant interest to characterise warping patterns that arise from a variety of interlocked grain patterns.

3.1.3 Interlocked grain in Eucalyptus

Eucalyptus species, like many other angiosperms, have the tendency to develop interlocked grain (Lausberg et al., 1995; Wessels et al., 2016). Angiosperms commonly exhibit interlocked grain with a higher frequency than spiral grain (Harris, 1989). Interlocked grain is incredibly common in tropical angiosperms including *Eucalyptus* species and can form with such severity that the wood becomes impossible to split (Zobel & Jett, 2012). *Eucalyptus bosistoana* has been shown to exhibit interlocked grain and therefore will be utilised to investigate the correlation between board warping and interlocked grain (Bootle, 1983).

3.1.4 Heritability of interlocked grain

As discussed in section 1.55, the heritability of certain traits within a species is influenced by both environmental and genetic factors and can be utilised to predict the phenotypic variation within a population

Furthermore, as timber shrinkage is both a product of grain angle and the periodicity of grain changes, this suggests that warping cannot solely be controlled through genetic means. However, no studies have been conducted on the heritability of warping with respect to interlocked grain. Thus, this possibility will be investigated in this chapter.

3.1.5 Quantification of interlocked grain

While the oscillating nature of interlocked grain complicates grain analysis, existing methodologies utilised in the investigation of spiral grain have been used to quantify interlocked grain. The most commonly utilised methods for interlocked grain investigation are microscopic observations, wood splitting and near-infrared spectroscopy (NIR). The last technique utilises non-destructive methods whereas the first two methods are classified as destructive. Non-destructive methods allow the sample to analysed in its entirety; therefore, the sample can be utilised for further testing. Destructive methodologies, however, generally requires extensive sample preparation and results in permanent alterations to the sample. Therefore, destructive methodologies limit the number of analyses that can be conducted on one sample and include more time-consuming approaches, like serial sectioning.

3.1.5.1 Destructive techniques

The most commonly utilised methods for wood grain analysis include radial splitting where the stem section is split through the pith. The force propagated by the chisel will switch to following the grain pattern in the first 1 cm, and the splitting pattern on the opposite face of the stem section will therefore match the wood grain in the stem (Harris, 1989). Measurement of the grain pattern is then conducted either by transcription of the splitting pattern onto graph paper (Webb, 1969) or imaging of the crack (Hernández & Almeida, 2007; Thinley et al., 2005). By measuring the deviation from the original splitting line, the grain angle can be calculated. This method

provides lower resolution than serial sectioning approaches and NIR spectroscopy and is, therefore, favoured for high throughput analyses. A limiting factor of this splitting technique is that all measurements are relative to the defined vertical axis. Therefore, if the pith is not aligned with the stem axis, or the stem section is not cut at right angles to the stem axis, accuracy of the measurements will decrease. This can be accounted for by measuring splitting along perpendicular axes, and by averaging the values from the opposite sides (Harris, 1989).

Scribing methodologies are also commonly utilised to assess spiral grain in wood planks or on the stem itself. It involves inserting a sharp point into the wood, which, when pulled, will indicate the direction of grain with a scratch mark (Koehler, 1960). This method only elucidates the grain angle along the longitudinal plane scribed and to analyse more complex grain patterns a significant number of lines would, therefore, need to be scribed.

3.1.5.2 Non-destructive techniques

Near-infrared (NIR) spectroscopy is a non-destructive technique utilised to measure a variety of wood properties. In NIR a sample is illuminated with a broad spectrum of infrared light (800-2500 nm). This light is differentially absorbed depending on the chemical bonds in the sample and compared to spectra from reference samples with a known chemical composition. Measurement of the absorption wavelengths can provide extensive information about the chemical structure of the sample, but is heavily reliant on the accuracy of the reference samples selected (Baillères et al., 2002).

Gindl and Teischinger (2007), however, reported that NIR could also be utilised to measure grain angle in boards. This methodology, however, has a low sensitivity, with a root mean squared error (RMSE) of 6°, meaning that the reference model utilised could only predict grain angle with ±6° of certainty. Additionally, as the interplay between grain angle, periodicity of grain oscillations and board warping is not understood, NIR is only suited to broad classifications of interlocked grain.

Several other non-destructive methods have been developed, and these use various forms of X-ray imaging; soft X-ray microscopy, computed tomography and X-ray microtomography. There has been some success in utilising soft X-rays to analyse

grain patterns in *Acacia mangium* (black or hickory wattle) (Ogata et al., 2003). Soft X-ray microscopy is a technique where a sample is exposed to X-rays between 2.34 – 4.44 nm and the resulting transmitted X-rays are recorded by a detector. The short wavelength of soft X-rays allows for imaging of structures greater than 30nm and, therefore, provides superior resolution to light-based imaging systems. Analysis of a disk of *A. mangium* with soft X-ray by Ogata et al. (2003), detected vessel angles and the abrupt changes in grain angle characteristic of interlocked gain. Moreover, measurements made with X-ray analysis matched conventional splitting data.

An alternative approach to investigate grain is to use X-ray computed tomography (CT). CT consists of multiple X-ray images being taken at differing angles to produce a cross-sectional composite. This allows a cross-sectional view of the sample, without sectioning. Sepúlveda (2001) scanned *Picea abies* stems with CT and found that the grain angle observed through this technique correlated with measurements collected from destructive wood splitting experiments (r= 0.81). However, this methodology is a low-resolution technique (one pixel = 10mm) and therefore any small fluctuations in grain angle would not be detected. Additionally, the images produced by CT fail to show the cellular structure of the sample and therefore, the effects of cellular organisation on wood grain were not measured.

As discussed in section 2.1.3, X-ray microtomography can also be utilised for the non-destructive analysis of wood samples. This methodology has been used for grain analyses, including investigations of interlocked grain in *Khaya* spp. (African mahogany) and *Artocaprus hirsutus* (jungle jack) (Collings et al, in preparation) and spiral grain in radiata pine (Thomas & Collings, 2017). Furthermore, the work conducted in chapter 2 shows that this technique can determine the spiral grain angle and pattern in a large stem section (1-2cm in diameter). Thus, it can be a valuable tool for the characterisation of more complex grain patterns like interlocked and wavy grain.

Increased resolution in X-ray microtomography is achieved by bringing the sample closer to the camera, and further away from the X-ray source. Larger samples will therefore be imaged at a lower resolution and therefore higher contrast is needed within the sample to visualise the cell wall. This can be achieved either through

heavy metal staining (as discussed in Chapter 2), or through drying. Due to the size of the samples utilised in this study, heavy metal staining would have been impractical and therefore dried samples were used. To ensure that no structural changes resulted from this, the samples will need to be dried over multiple days and then stored in a humidity controlled room until their moisture content has stabilised (Davies & Altaner, 2017).

3.1.6 Board warping and interlocked grain

A small number of studies have been conducted investigating the link between spiral grain and board warping (Mishiro & Booker, 1988; Shelly et al., 2007; Shelly & Simpson, 2000). Shelly and Simpson (2000) discovered a strong positive correlation between spiral grain and board warping ($p = 0.001$). Mishiro & Booker (1988) also discovered a positive relationship between spiral grain and board twisting, but suggested that other factors, such as longitudinal shrinkage, might contribute to this observation.

While it has been acknowledged that the presence of interlocked grain causes board warping (Hernández & Almeida, 2007; Weddell, 1961), no studies have attempted to quantify the relationship between interlocked grain patterns and board warping. By understanding the relationship between interlocked grain and board warping it will be possible to select for interlocked grain patterns that have a minimal effect on end use parameters.

3.1.7 Aims in this Chapter

The work conducted in this chapter aims to further the understanding of interlocked grain effects on other wood properties through the development of a high throughput splitting methodology. The relationship between interlocked grain and board warping will also be investigated utilising the wood splitting methodology developed. And a high-level analysis of intra-familial trends in interlocked grain will be conducted.

3.2 Methodology

3.2.1 Collection of material

The material collected for this chapter was sourced through the Woodville trial, which was based at Murrays Nursery, Woodville near (location) in the North Island of New Zealand. Seedlings were planted in Feb 2015 and harvested at 2 y in Sept/Oct 2017. The trees were assessed prior harvest to ensure growth and good form. The tops were then removed and discarded, with the bottom 50 cm selected for harvest. The samples were then labelled, bundled and packed in ice for transport to the University of Canterbury, ensuring that they arrived with minimal degradation. All samples were processed within 1 week of arrival.

3.2.2 Measurement of warp in dried Eucalyptus bosistoana stem halves

Samples for warping analysis were processed by debarking one end of the sample and then making a longitudinal split with a bandsaw. The two stem halves were then cut off the larger sample at ~150 mm and the opposite end of the sample reserved for further analysis. The mass and volume of the stem halves was recorded, and they were then dried at 103°C for 48 h to amplify drying defects (Altaner, 2017). Following this, the stem halves were placed in a climate-controlled room (for ~3 weeks) at 20°C and 65% relative humidity. This allowed the moisture content within the halves to reach equilibrium and therefore ensured that no further sample shrinkage or warping would occur (Davies & Altaner, 2017).

Wood warping measurements were conducted with the Bubble Level Android app (version 3.23, NixGames) on a cell phone (Xperia Z5 Compact, Sony). Once calibrated, this app utilises the internal accelerometer sensor to determine the angle at which the phone is held. The app was calibrated by holding the phone vertically against the edge of the measurement rig. This measurement was then set as 0° and all warping angles were therefore measured relative to this. The butt end of the sample was then placed so that the radial face was flat against the vertical section of the measurement rig and the edge of the cell phone was placed along the radial face of the free end (Figure 3.1). This gave the degrees of deflection caused by volumetric shrinkage upon drying.

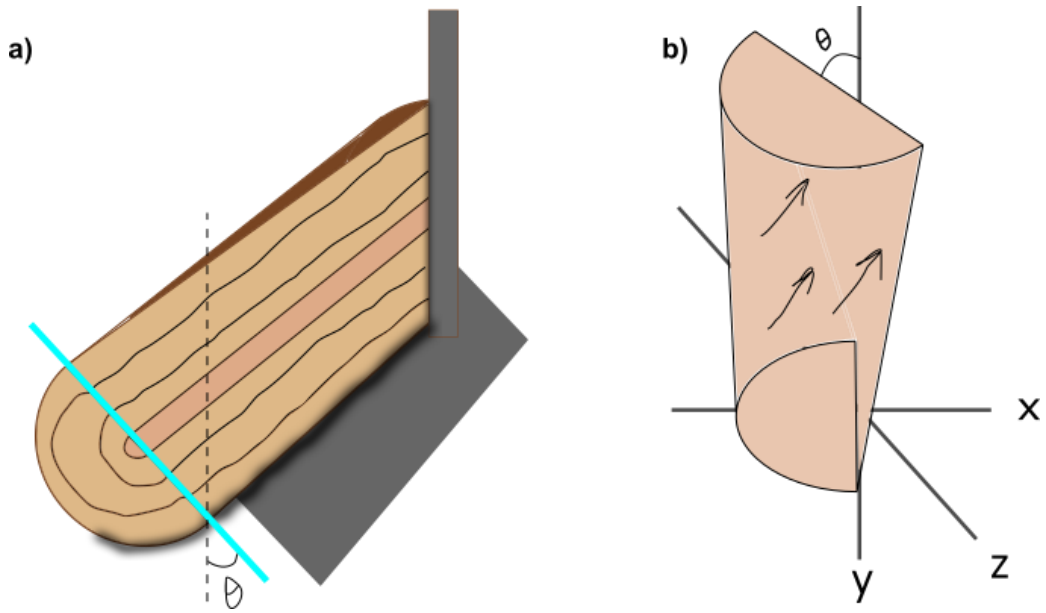

Figure 3.1: Warping angle measurements

- **a)** Each piece of wood was placed with one end flat against the 90° surface and the opposite end measured with the bubble level app
- **b)** the vertical plane is treated as zero therefore a right-handed twist will give a negative value (bottom).

Multiple measurements were taken on one piece of wood by different people using the same phone and with different phones to account for equipment variation. Values obtained were concurrent within ±0.1°between individuals and showed no variation between cell phones. These values will be compared to grain angles obtained from split samples to determine the effect that grain patterns and overall grain angle has on dried “board” warping measurements.

3.2.3 Splitting of Eucalyptus samples

Samples processed for splitting were whole, cross-sectional wood discs that were 4 cm thick and that had been cut from the non-peeled end of a subsection of samples from the Woodville trial. This subsection was created by randomly selecting 90 samples from the larger trial, ensuring that each family contained at least four individuals. The wood discs were then kiln dried at 103ºC (~48 h) and stored in a

temperature-controlled room at 20°C. While this temperature was chosen to amplify drying defects, no warping or uneven shrinkage was observed in the discs.

Prior to splitting, the wood discs were trimmed to 2 cm thickness with a bandsaw to ensure that the cross-sectional faces remained 90° to the stem axis. The pith of each disc was then marked using a white paint pen so that it could be identified during image analysis. Using a hammer and a chisel that was wider than the wood disc, the disc was then split. The splitting pattern followed the path of the chisel for ~1 cm before switching to follow the grain pattern (Ohkura, 1958). Samples that did not have the cross-sectional faces square to the stem axis resulted in a splitting pattern that did not pass through the pith on the opposite face and these samples were discarded. Some samples split poorly, loosing wood splinters from the fracture which confounded splitting analysis, and these samples were discarded from further analyses.

3.2.4 Quantification of splitting pattern

Following splitting, the two halves of the wood discs were placed together on a flatbed scanner (Epson Perfection V700 Photo, Auckland, New Zealand), and scanned using reflected light in 24-bit colour and at 266 dpi and saved as TIFF images without compression or scale changes.

Image scans were optimised in several ways. Multiple discs were scanned at the same time. To ensure that the two halves were aligned with respect to each other, they were held together with elastic hair ties (The Warehouse, Riccarton, New Zealand). Further, the orientation of the chisel mark was horizontally aligned to graduations along the edge of the scanner, ensuring that each disc was placed in a horizontal orientation (Figure 3.a).

To quantify the split wood samples and interlocked grain, the scanned images, as collected above, were opened in ImageJ and turned into a binary image that contained only the crack using an imageJ macro (Appendix 1). The centre of the pith was selected and the x- and y-axis points defined as XPith and YPith values respectively. These values were then imported into R-studio and subtracted from the crack coordinates to give distance from the pith. The y-axis crack coordinate values

were then converted to an angle (given in degrees) to obtain the angle of twist in each section of the stem (appendix 2).

3.2.5 uCT measurements and calculations

Four samples were selected based on the splitting and warping analyses. Two of the samples selected exhibited a strong left-handed warp, one a strong right-handed warp and the fourth, a weak left-handed warp. Due to the symmetry of the two halves, only one half was selected. There is an inverse relationship between sample size and image resolution, and it was necessary to further split these samples into quarters, resulting in some loss of material. The original split edge was marked to ensure that the grain was measured in the same orientation as that of the grain pattern observed through the splitting test.

The samples were analysed using a Bruker µCT Skyscan 1172 machine, and a similar protocol followed to that discussed in chapter 3. As the samples had already been dried in a humidity-controlled room (see section 3.2.3), it was unnecessary to place them through the ethanol series mentioned in section 2.2.2.

Processing varied from chapter 3 as only a quarter of each round was imaged at a time, therefore instead of measuring the grain across four strips, as discussed in section 2.2.2, the grain was measured along the original split edge and perpendicular to the original edge. This resulted in two measurements at right-angles, therefore allowing for the correction of off axis effects through measurement of the radial offset angle with the directionality algorithm, as discussed in section 2.2.2.

3.3 Results

In these experiments, three different techniques have been used to assess interlocked grain. The lowest resolution technique, measurements of warping, had the highest throughput and minimal costs whereas the highest resolution method, X-ray microtomography, had the lowest throughout (several hours per sample for imaging and processing) and involved some considerable expense (~NZ$100 per sample). Thus, while all 4032 trees could be assessed by warping measurements,

only 4 were assessed by X-ray microtomography. It was, therefore, necessary to validate the different experimental methods, and most notably compare the high-throughput low-resolution warping measurements and low-throughout high-resolution tomography observations with a more standard approach for measuring interlocked grain, the use of wood splitting.

While the protocols for measuring grain in X-ray microtomography images were described in a previous chapter (see section2.2.2), protocols for calculating grain angles from split wood discs required development. Therefore, the development of these protocols in first reported in this chapter, followed by a comparison of the 4 trees through all analytical methods.

3.3.1 Development of a protocol to determine the grain angle from split wood discs

A protocol was developed in ImageJ (version 1.52i) to identify and measure the splitting pattern in wood discs. The main steps of this protocol involved:

1. Manual selection of the centre of the pith using the point selection tool. This gave a reference coordinate for the centre of the sample, and all subsequent calculations of the angle and distance from the pith were based off this coordinate.
2. Isolation and selection of the crack. As the crack is a much darker colour than the rest of the image, it was possible to isolate it by using image thresholding and binarization (Figure 3.2d).
3. Measurement of the crack through selection. The image coordinates of the were selected and exported
4. In R-studio, the measured coordinates were then converted into a distance from the pith centre, and an angle of deflection was calculated.

To achieve these steps, a macro was written in ImageJ (Appendix 1.1). For the first step, the wood disc was selected either using the circle or freehand tools. Wood defects, the background and bark were excluded by this process. The centre of the pith was manually selected, and this value was exported to a .csv file. The value of the pith was then used as the reference point for subsequently converting the coordinates to grain angles.

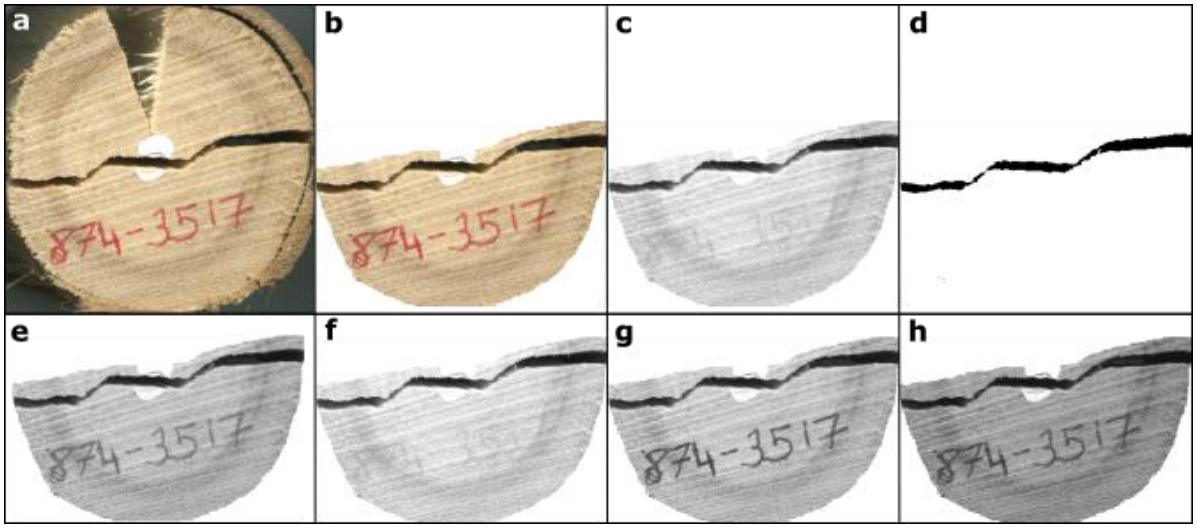

Figure 3.2: Major steps in the image processing of split wood discs.

a) the scanned split disc. An even band of tension wood is present (arrow).

b) manual selection of the crack and deletion to avoid wood defects.

c) conversion to 8-bit image using red channel.

d) thresholding and masking resulting in isolation of the crack.

e) conversion to 8-bit using all channels.

f) conversion to 8-bit using red channel. Note how the red pencil used to mark the sample is no longer prominent. However, there is an increase in contrast between the wood and the crack.

g) conversion to 8-bit using green channel

h) conversion to 8-bit using green channel

The red channel of the RGB colour image was then selected and converted to 8-bit, discarding the blue and green channels (Figure 3.c). This gave the lowest contrast between tension wood and normal wood, homogenizing the disc, and therefore resulting in the highest contrast between the wood and the crack (Figure 3.e-g). A similar channel selection approach in wood disc scans was previously used by (Thomas, 2014), where the blue channel was selected, highlighting the locations of compression wood in radiata pine wood discs. A threshold was then limiting the greyscale values to between 0 and 140. As the crack was significantly darker that the rest of the image, this caused the crack to be isolated. Using the binary image, a mask could be used to select the crack and the coordinates of the pixels within with were exported as a *.csv file, which was then opened in R-Studio (Figure 3.d).

Two protocols were then developed in RStudio (version 1.0.153, RStudio, Boston, MA, USA) to convert the crack coordinates into the grain angle, and to remove values that had been erroneously identified as the crack. The first protocol (Appendix 1.2) utilised batch processing to convert the crack and pith coordinate files generated by the ImageJ macro. The x-axis coordinates were converted into distances from the pith (mm), and the y-axis coordinates converted into the grain angle (°). This was possible as all discs were cut to a length of 20mm and therefore had a uniform height. The second protocol (appendix 1.3) used the dbscan function (Hahsler et al., 2018) to identify density-based clusters which could then be selected. By inputting both the minimum size for a cluster and the distance between the points in the cluster, the crack was separated from other marks identified on the wood disc.

3.3.2 Experimental validation in four trees

Stem sections from four individuals were selected and were analysed through all three methods; measurement of warp in stem halves, splitting of stem cross-sections and X-ray microtomography. This low and limited replicate number was dictated by the financial and time constraints associated with the X-ray microtomography technique. Furthermore, the size of the wood samples meant that to obtain the cellular resolution required in X-ray microtomography, it was necessary to work with partial samples only. Thus, it was not possible to analyse all stem sections utilising this technique, and, therefore, the analysis of the four individuals does not provide

any information on the trends of interlocked grain in *Eucalyptus bosistoana*, but rather shows whether the three methods give concordant results.

The selection of the four samples used for X-ray microtomography was based on the experimental data collected from the warping and splitting experiments. These samples represented two samples that appeared to have left-handed grain based on warping and splitting, one sample that had right-handed grain, and on a single sample that appeared to have weakly left-handed or straight grain.

Analyses demonstrated that there was a good correlation between the X-ray microtomography data and wood splitting data, but there was only a limited correlation between warping and splitting measurements. These comparisons are described in more detail in the following subsections, but first the measurements made on the four trees are presented.

3.3.2.1 Splitting measurements of the four selected trees

Stem sections were split using the method as described in section 4.2.3, with the crack on the opposite face from the chisel mark following the grain pattern. The orientation of the splitting was chosen to maximise symmetry, and to avoid branches, knots and wood defects in the resulting halves. While the split was identical through the two halves, differences in the grain pattern could be observed either side of the pith in some samples. To reflect this non-equivalence, measurements taken from the left of the pith are labelled side C and measurements to the right of the pith side D. The grain patterns observed in most split samples was roughly symmetrical either side of the pith, suggesting that grain angles are relatively constant within each ring of xylem cells.

Sample 130-2988 (figure 3.3a) had an initial left-handed twist with a maximum of 1.99°. This then shifts 2mm from the pith, becoming increasingly right-handed and reaching a maximum of 5.12°. The grain angle then starts decreasing back towards 0°. This second change in grain direction coincides with a growth ring 5cm from the pith. Both sides of the pith closely followed this pattern

Sample 872-2973 (figure 3.3b) shows a disparity between each side of the pith. While both side c and side D initially are straight grained, side C switches to an

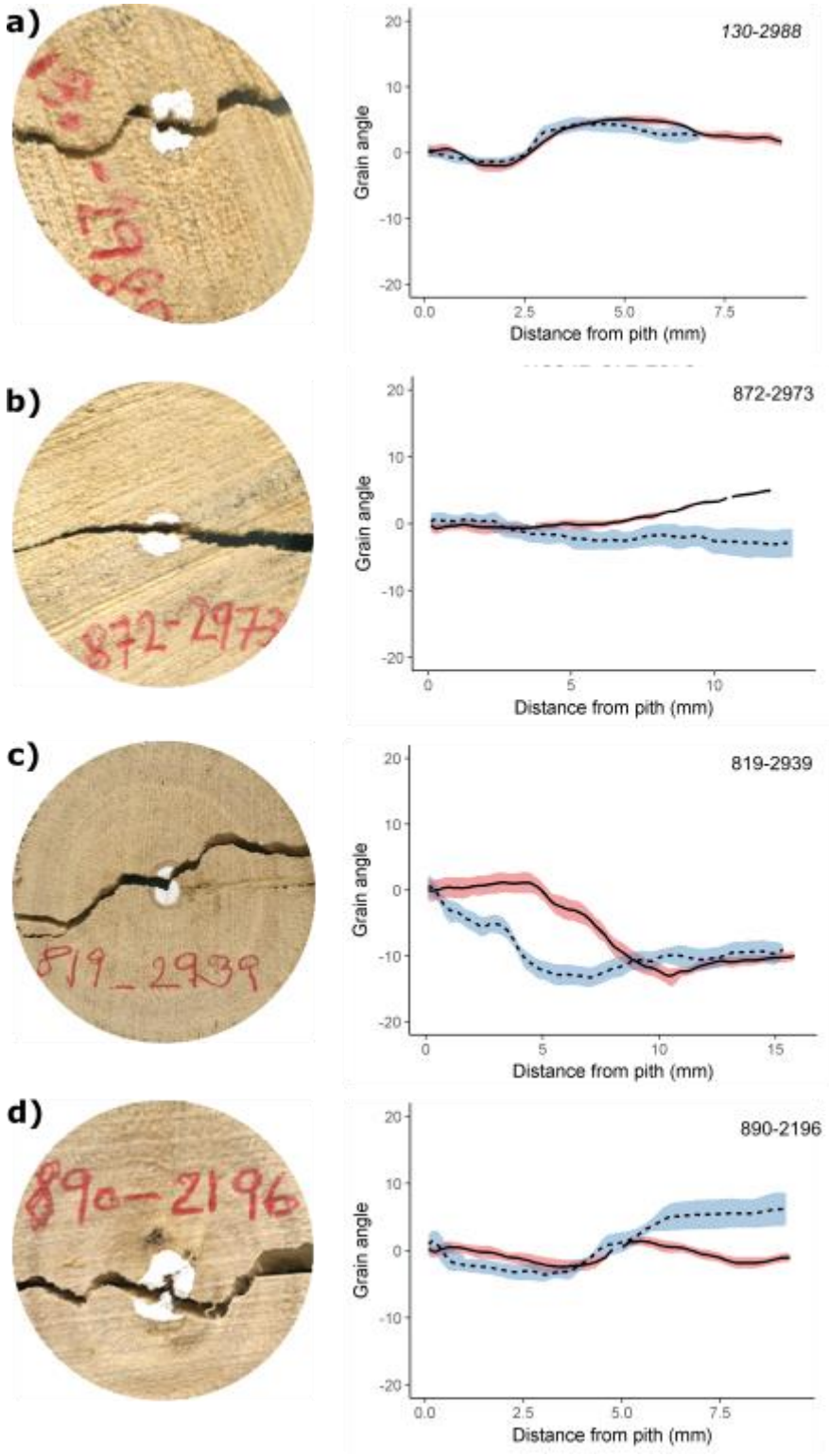

Figure 3.3: Splitting patterns of the four selected trees. **a)** sample 130-2988, **b)** sample 872-2973, **c)** sample 819-2939,

increasingly left-handed grain at 2.8mm from the pith, reaching a maximum of 3.09°. Side D, however, continues as straight-grained until 6mm, where the grain becomes steadily more right-handed, reaching a maximum of 4.96°.

Sample 819-2939 (figure 3.3c) shows the same trend between the two side of the pith, with the grain becoming increasingly left-handed and reaching a maximum of 13.25°. However, there is a delay in spiral grain development between the two sides, with side D immediately developing a left-handed twist, while side C had straight grain for the first 4mm of growth, before switching to left-handed and reaching a maximum left-handed angle of 13.02°. This disparity does not coincide with an observable wood defects in the sample.

Sample 890-2196 (figure 3.3d) had an increasingly left-handed grain angle, reaching a maximum of 3.58° at 3.8mm from the pith. This then reversed to an increasingly right-handed angle on both sides; however, side C reaches a maximum right-handed angle of 1.44° at 5.6mm from the pith before switching to an increasingly left-handed angle. Side D continues to become increasingly right-handed, reaching a maximum of 6.28° at the outside of the sample.

3.3.2.2 Warping measurements of the four selected trees

The interplay between grain patterns and the resultant warping in timber is poorly understood. To explore the link between grain direction and the severity of stem warping that this imparts, stem sections were cut in half and dried, with one half stem being labelled side A and the other side B. The drying process caused anisotropic shrinkage in the stem half, due to differing grain angles and growth stresses. This manifested in a twist (or warping) across the section that was measured by hand as described in section 3.2.2. It is important to note that the orientation of the vertical cut was randomly determined and therefore does not match the orientation of the chisel split in the above measurements. Due to the symmetry of grain angles around the pith, as observed in the splitting tests, this is not considered to be a significant issue.

Sample 130-2988 had a right-handed twist of 6.9° in side A and a weak left-handed twist of 0.9° in side B. This was the only sample of the four that had a right-handed

twist. This twist was accompanied with a longitudinal deflection of 6.85mm, causing the samples to bow.

Sample 872-2973 had a weak left-handed twist in both sides, with side A measuring 3.0° and side B measuring 2.3°. The forestry industry views angles >5° as acceptable for timber production, therefore this individual would be suitable for structural products based on twisting alone. However, there was significant bowing in the sample, with a longitudinal deflection of 11mm.

Sample 819-2939 had a strong left-handed twist in both sides, with side A measuring 5.3° and side B measuring 11.9°. There was only a slight longitudinal deflection of 4.18mm in this sample.

Sample 890-2196 also had a strong left-handed twist in both sides, with side A measuring 9.5° and side B measuring 12.7°. The longitudinal deflection in this sample was 3.86mm, similar to that in sample 819-2939.

3.3.2.3 X-ray microtomography of the four selected trees

The X-ray microtomography technique allows for a cellular approach in grain angle determination and has a significantly higher resolution that warping and splitting methods. However, this technique requires significant processing time and is limited in the size of samples that can be analysed. It is therefore ill-suited for larger analyses. The wood splitting methodology allows for high throughput of samples but produces a wood grain profile of an unknown resolution and accuracy. By comparing the grain profile generated through splitting to the cellular grain angle measurements obtained from X-ray microtomography, the accuracy of the wood splitting method can be determined.

Each of the samples were quartered and one quarter was imaged. The images of the samples were rotated to match the orientation of the splitting images and the grain calculated along the fracture plane caused by the splitting test.

Sample 130-2988 (figure 3.4a) showed an initial left-handed grain, reaching a maximum of -2.38° at 2.33 mm from the pith, before switching to right-handed and reaching a maximum of 10.69 at 6.47 mm from the pith. The grain angle then decreased back towards zero.

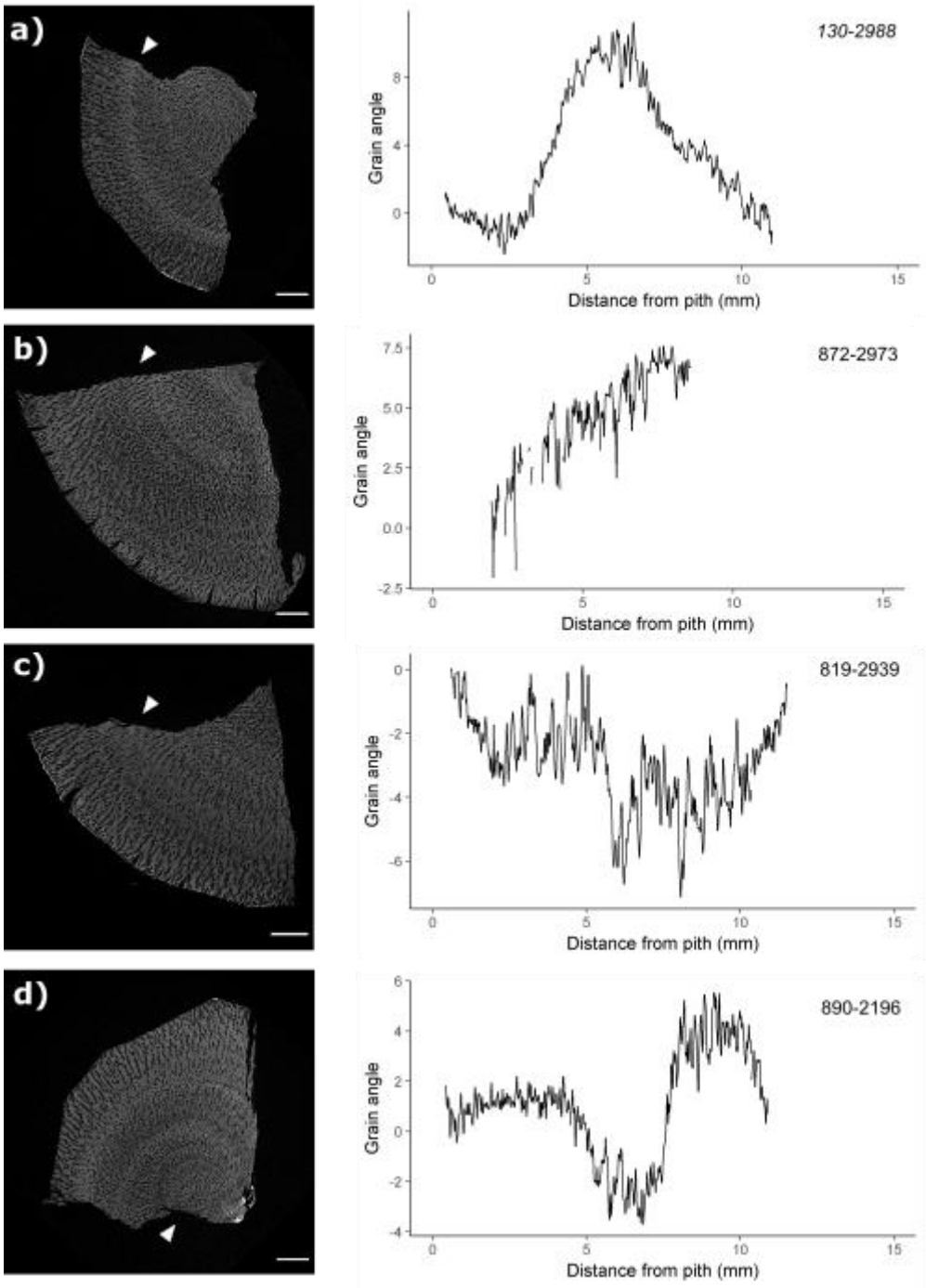

Figure 3.4: X-ray microtomography of the four selected *Eucalyptus bosistoana* samples. Scale bar = 2 mm. Negative grain angles indicate left-handed grain, positive grain angles indicate right-handed grain. Arrow to indicate the side analysed (corresponds with crack in splitting measurements).

Sample 872-2973 (figure 3.4b) had an initial right-handed grain angle of 1.13° at 1.95 mm. The grain angle then continued to increase, reaching a maximum right-handed angle of 7.59° at 7.68 mm.

Sample 819-2939 (figure 3.4c) rapidly develops a left-handed twist within the first 2 mm of growth, reaching 3.84°, stabilising and then increasing again at 6 mm from the pith, where the grain reaches the maximum left-handed angle of 6.73°.

Sample 890-2196 (figure 3.4d) has an initial weak right-handed twist, reaching a maximum of 1.74° at 2.71 mm from the pith. This is then followed by a shift to increasingly left-handed grain angles. Reaching a maximum of 3.48° at 6.71 mm from the pith. The grain angle then finally shifts again, becoming more right-handed and reaching 5.19° at 9.31 mm from the pith.

3.3.2.4 Comparison of the three measurement methods

As mentioned in the above section, sides A and B differ in location from the area denoted side C and D. While this therefore will not allow for direct site comparisons, the symmetry of the grain across the pith in most of the samples demonstrates that grain angles are relatively constant throughout radial cell files. The X-ray microtomography conducted in Chapter 2 also supports this conclusion as there was little variation between the angles measured in the four strips.

The wood warping vales, along with maximum left and right-handed grain angles obtained from the splitting analysis are summarised in table 3.1 for ease on comparison.

Of the four samples selected, 103-2988 was the only one to exhibit a right-handed warping angle (side A = 6.9°). This corresponded to an initial weak left-handed grain angle (side C = 1.99°, side D = 1.36°), changing to a right-handed grain angle (figure 4.3a) after 60% of the total growth.

Sample 872-2973 exhibited a weak left-handed warping angle (Side A = -3.0, side B = -2.3), and showed left-handed twisting on side C and right-handed twisting on side D. The maximum left-handed angle in side D closely matched the maximum right-handed angle in side C.

Sample 819-2939 exhibited a strong left-handed warp (Side A = -5.3, side B = -11.9). This appears to correlate to an increasingly left-handed grain pattern that reaches a maximum of 13° in both side C and side D (figure 4.3c).

Sample 890-2196 also had a strong left-handed warp (Side A = -9.5, side B = -12.7). The grain pattern on both sides shows the grain initially becoming more left-handed, reaching a maximum of 2.43° (side C) and 3.58° (side D), and then becoming more right-handed after 30% of growth (figure 4.3d).

Comparison of the warping and splitting measurements of the four samples showed a weak correlation between the maximum right-handed angle of side C and the side A warping angle ($r^2 = 0.609$). No other significant correlations between the warping angle and the maximum grain angle were observed. The relationship between grain pattern and board warping will be further explored with a larger data set in the following section

Comparison of the X-ray microtomography results to the wood splitting grain patterns showed that these methods both give a similar grain pattern but differ in the magnitude of grain angles given. For samples 130-2988, 872-2973, and 890-2196 the splitting values were 50% of the X-ray tomography values. However, for sample 819-2939, the maximum left-handed angle is double that of the X-ray tomography measurement (13.5° vs 6.73° respectively). The wood splitting method is therefore best utilised to investigate the overall grain pattern present in a sample, rather than measure an absolute grain angle.

Table 3.1. Warping measurements on four selected trees.

Tree ID	Side A warping angle (°) [*1]	Side B warping angle (°)	Difference (°) [*1]	Twist direction	Max LH grain angle (°) Side C [*2]	Max LH grain angle (°) Side D [*2]	Max RH grain angle (°) Side C [*2]	Max RH grain angle (°) Side D [*2]
130-2988	6.9	-0.9	-6.0	RH	1.99	1.36	5.12	4.42
872-2973	-3.0	-2.3	0.7	weak LH	0.75	3.09	4.96	0.63
819-2939	-5.3	-11.9	6.6	LH	13.02	13.25	1.17	0.58
890-2196	-9.5	-12.7	2.9	LH	2.43	3.58	1.44	6.28

[*1] Positive values denote a right-handed (RH) twist while negative values denote a left-handed (LH) twist

[*2] Side C refers to the left of the pith. Side D refers to the right of the pith

3.3.3 Correlation between splitting and warping measurements

The relationship between wood the wood splitting pattern and the warping measurements is more complex than the chosen methods of analysis allowed for. Comparisons between the maximum left-, and right-handed grain angles, and the warping angles showed minimal to no correlation. A weak correlation between the maximum right-handed splitting angle and the wood warping angles can be observed (table 3.2), however more robust mathematical modelling is required to further understanding of this relationship.

Table 3.2: Relationship between splitting and wood warping angles

		Side A warp	Side B warp
Splitting Side C [2]	Max LH [1]	$r^2 = 0.0081$	$r^2 = 0.0017$
	Max RH [1]	$r^2 = 0.14$	$r^2 = 0.18$
Splitting Side D [2]	Max LH [1]	$r^2 = 0.014$	$r^2 = 0.014$
	Max RH [1]	$r^2 = 0.089$	$r^2 = 0.13$

[1] Max LH – maximum left-handed angle, Max RH – maximum right-handed angle

[*2] Side C refers to the left of the pith. Side D refers to the right of the pith

3.3.4 General trends in grain angle as determined by splitting

A subsection of samples consisting of 101 individuals, from 12 families, was randomly selected from the Woodville trial and the wood grain analysed utilising the splitting method described in section 3.2.3. There was no discernible grain pattern specific to *E. bosistoana*, rather the grain patterns differed both between families and within families. Further development of analysis methodologies is required before the heritability of interlocked grain can be investigated. Therefore, the results presented here are a high-level summary only.

Family 20 (figure 3.5) showed two distinct grain patterns. A right-handed twist develops after the first 5cm in individuals 20-2909, 20-3417 and on one half of 20-

3732. Interestingly 20-2599 shows development of a left-handed twist as does the other half of 20-3732.
Family 22 (figure 3.6) was relatively straight grained (interlocked grain angles did not exceed 5°) over first 5cm of the sample and then a gradual left-handed twist begins developing in individuals 22-2671, 22-2981, 22-3230. This is mirrored across the pith and the change occurs around 5cm from the pith.

The interlocked grain direction and severity differs across the pith in all samples from family 31 (figure 3.7) and no unifying grain pattern could be identified. There is a noticeable inflexion point around 5cm in

Family 103 (figure 3.8) had no interlocked grain present and most individuals were relatively straight grained. Tree 103-2827 had strong right-handed spiral grain develop on the left side of the pith.

The grain angle and direction were consistent in family 103 (figure 3.9) with trees 130-2514, 130-2674, 130-2985, 130-2988 and 130-3548 all containing an initial weak left-handed twist that shifts to become right-handed following the first 5 mm of growth.

Individuals from family 823 (figure 3.10) had a predominantly L-R trend. Trees 823-2641 and 823-2808 switch to become increasingly right-handed at 5 mm from the pith. Tree 823-2955 is asymmetric across the pith, with the left side becoming increasingly left-handed and the right-hand side becoming increasingly right-handed. Tree 823-2808 had predominantly straight grain.

Family 846 had no unifying grain pattern (figure 3.11). Tree 846-2525 and tree 846-2595 had straight grain throughout the stem. Trees 846-2840, 846-2908 and 846-2527 had asymmetric divergent grain patterns across the pith. Tree 846-2528 had initial left-handed grain that then reverted to straight grain at 5 mm.

Family 855 (figure 3.12) had a consistent right-handed grain pattern develop in trees 855-2197, 855-1187, 855-2198, 855-2199 and 855-3599. Tree 855-1886 was straight grained throughout the sample.

Family 862 (figure 3.13) had minor variations in the grain patterns of the six trees analysed. Tree 862-1899, 862-1900, 862-2212 and 862-3283 had initial straight grain that briefly changed to right-handed at 5 mm, before returning to the straight

grained form. Tree 862-2209 and 862-2210 had the reverse of the above pattern, with the grain briefly becoming left-hande4d before returning to straight grain.

Family 872 (figure 3.14) had no unifying grain pattern. Tree 872-2973 is predominantly straight grained. Tree 872-2976 develops weak left-handed grain at 5 mm before shifting to increasingly right-handed grain. Tree 872-3728 is asymmetric across the pith, with the left side developing sever left-handed grain and the right side remaining straight grained.

Family 890 (figure 3.15) has a consistent grain pattern, with all individual trees developing right-handed grain 5 mm from the pith.

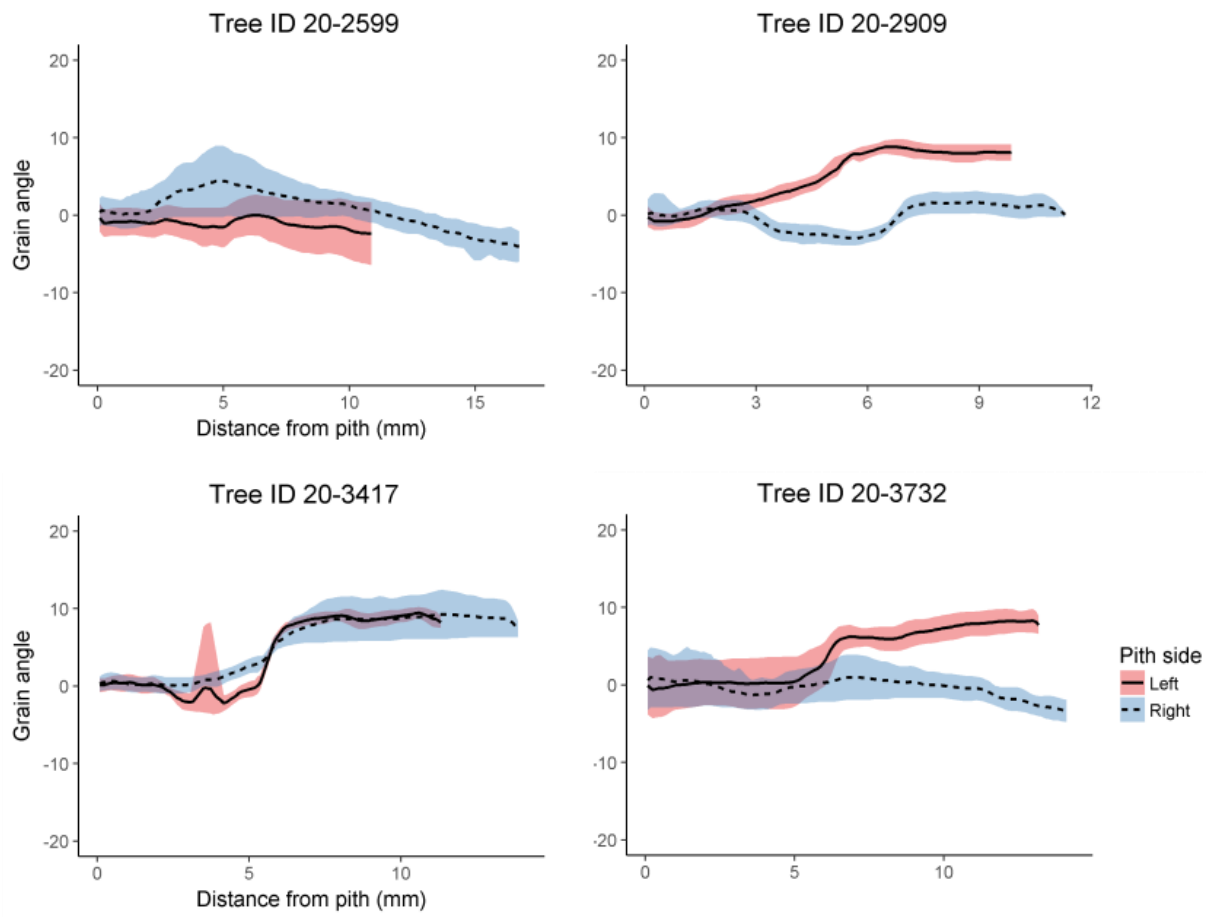

Figure 3.5 Grain splitting patterns for family 20. Negative values denote left-handed grain, positive values denote right-handed grain.

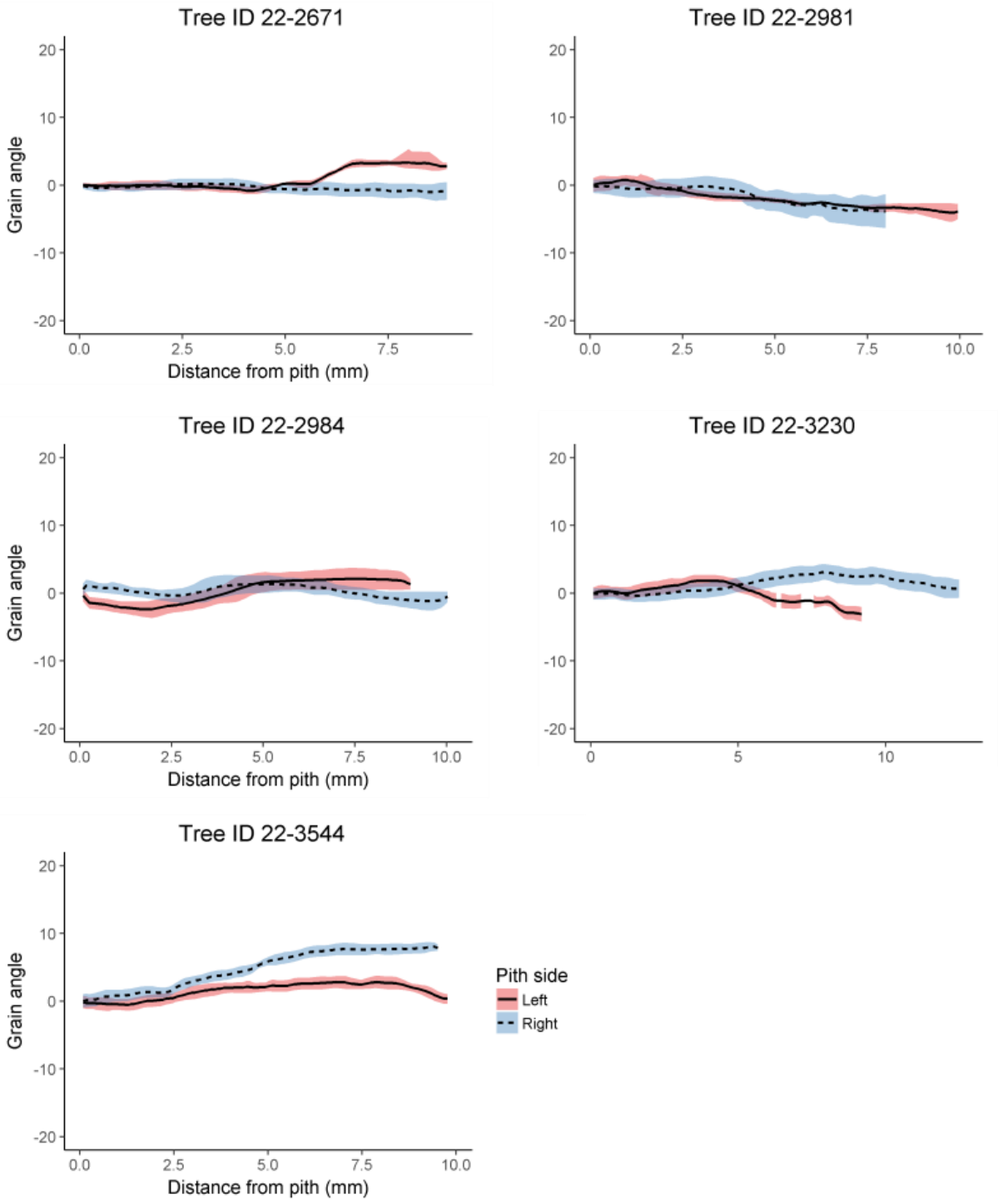

Figure 3.6 Grain splitting patterns for family 22. Negative values denote left-handed grain, positive values denote right-handed grain.

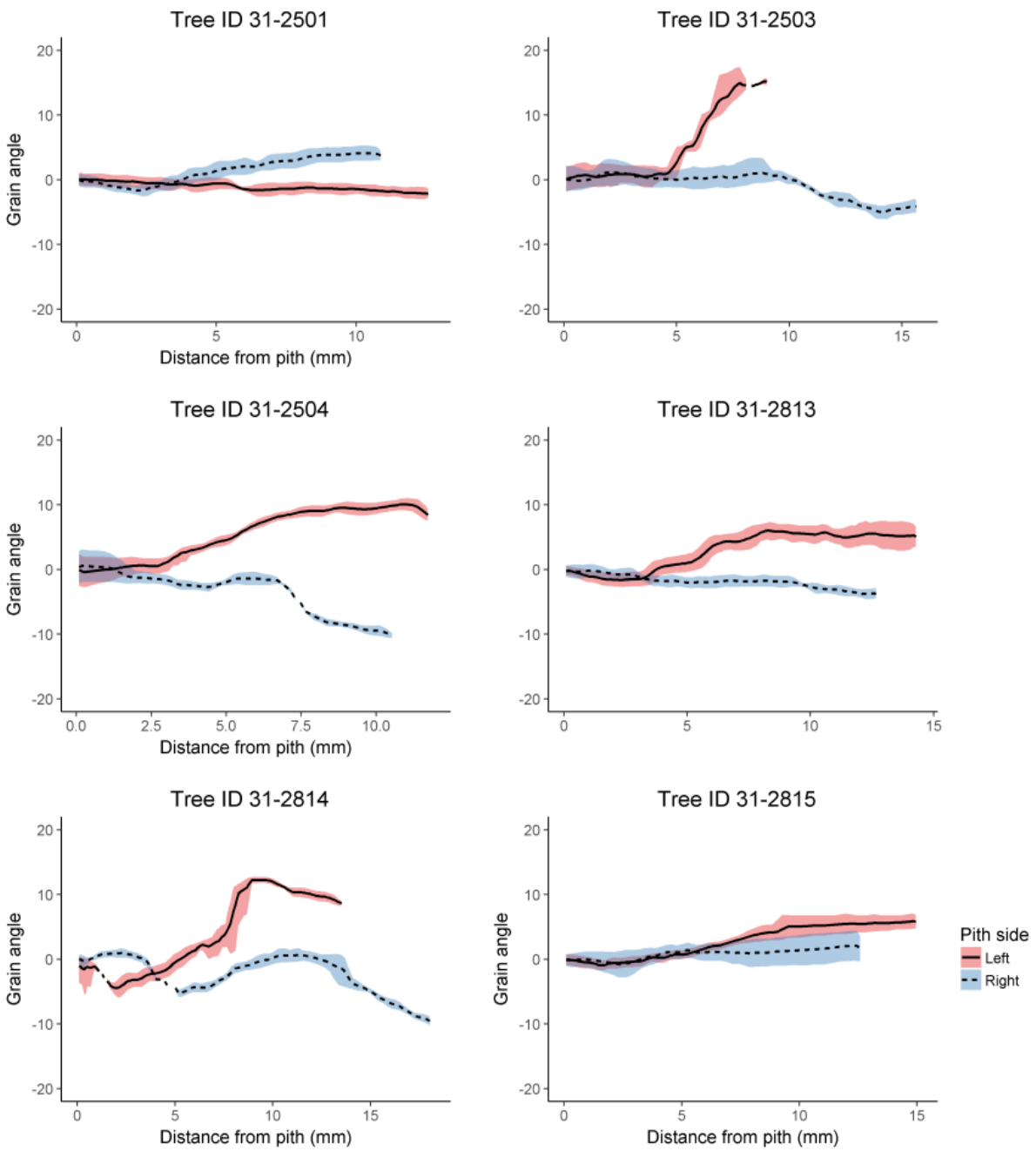

Figure 3.7 Grain splitting patterns for family 31. Negative values denote left-handed grain, positive values denote right-handed grain.

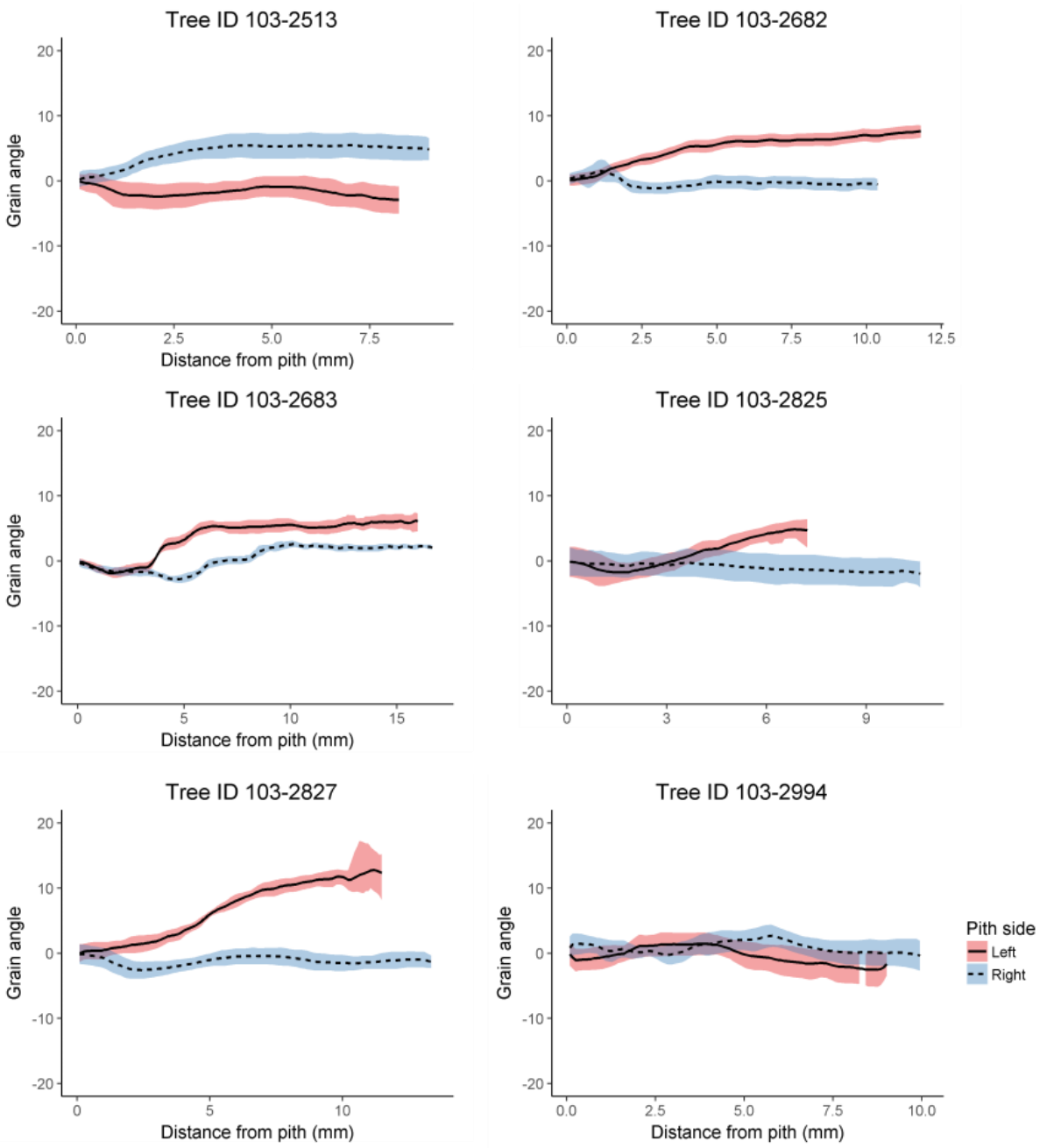

Figure 3.8 Grain splitting patterns for family 103. Negative values denote left-handed grain, positive values denote right-handed grain.

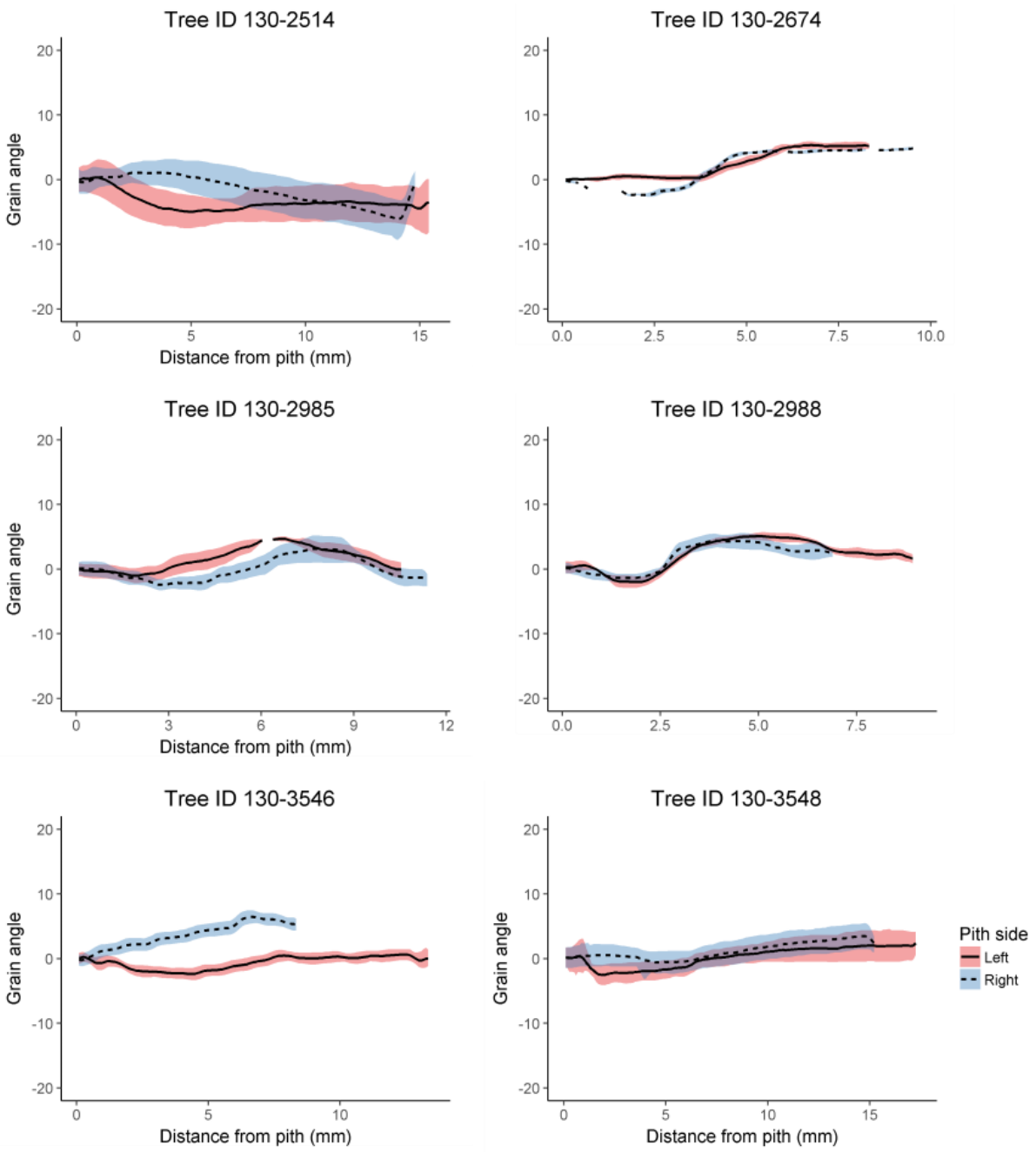

Figure 3.9 Grain splitting patterns for family 130. Negative values denote left-handed grain, positive values denote right-handed grain.

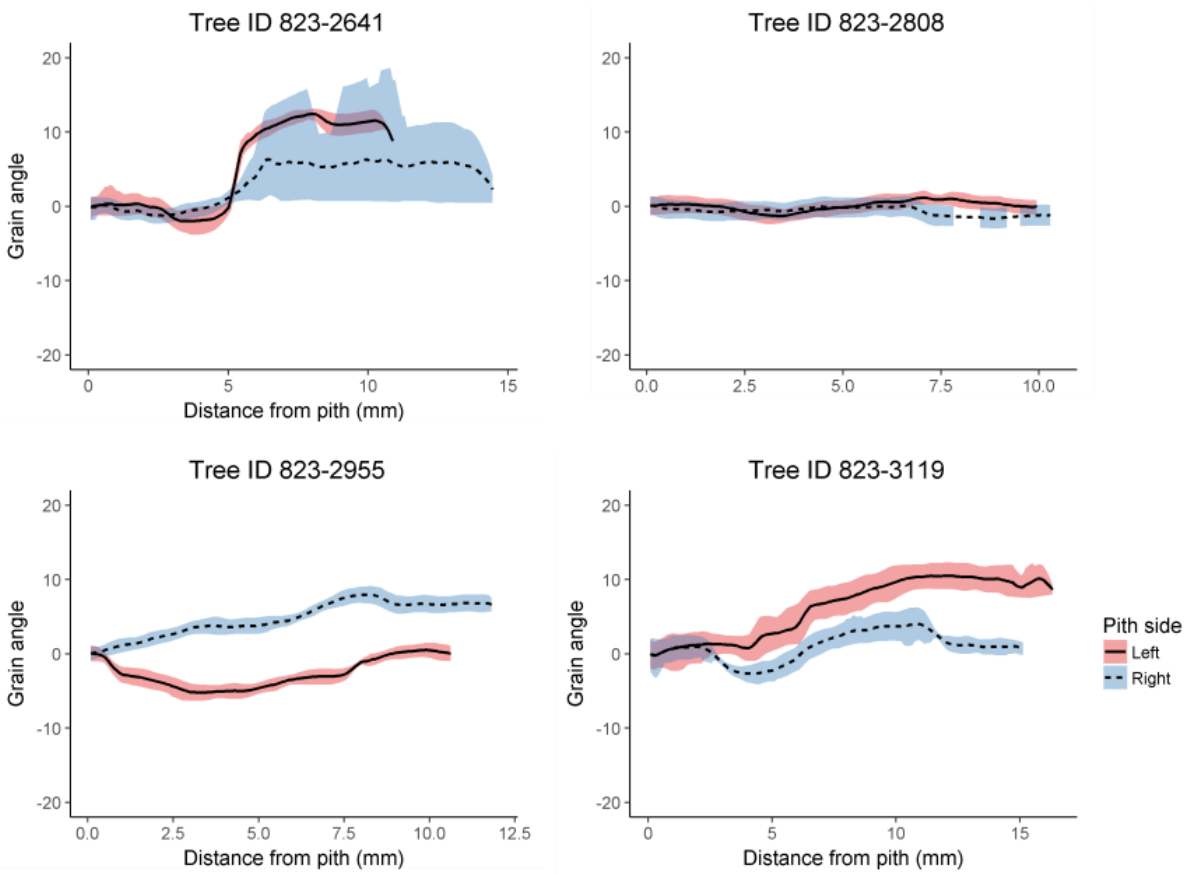

Figure 3.10 Grain splitting patterns for family 823. Negative values denote left-handed grain, positive values denote right-handed grain.

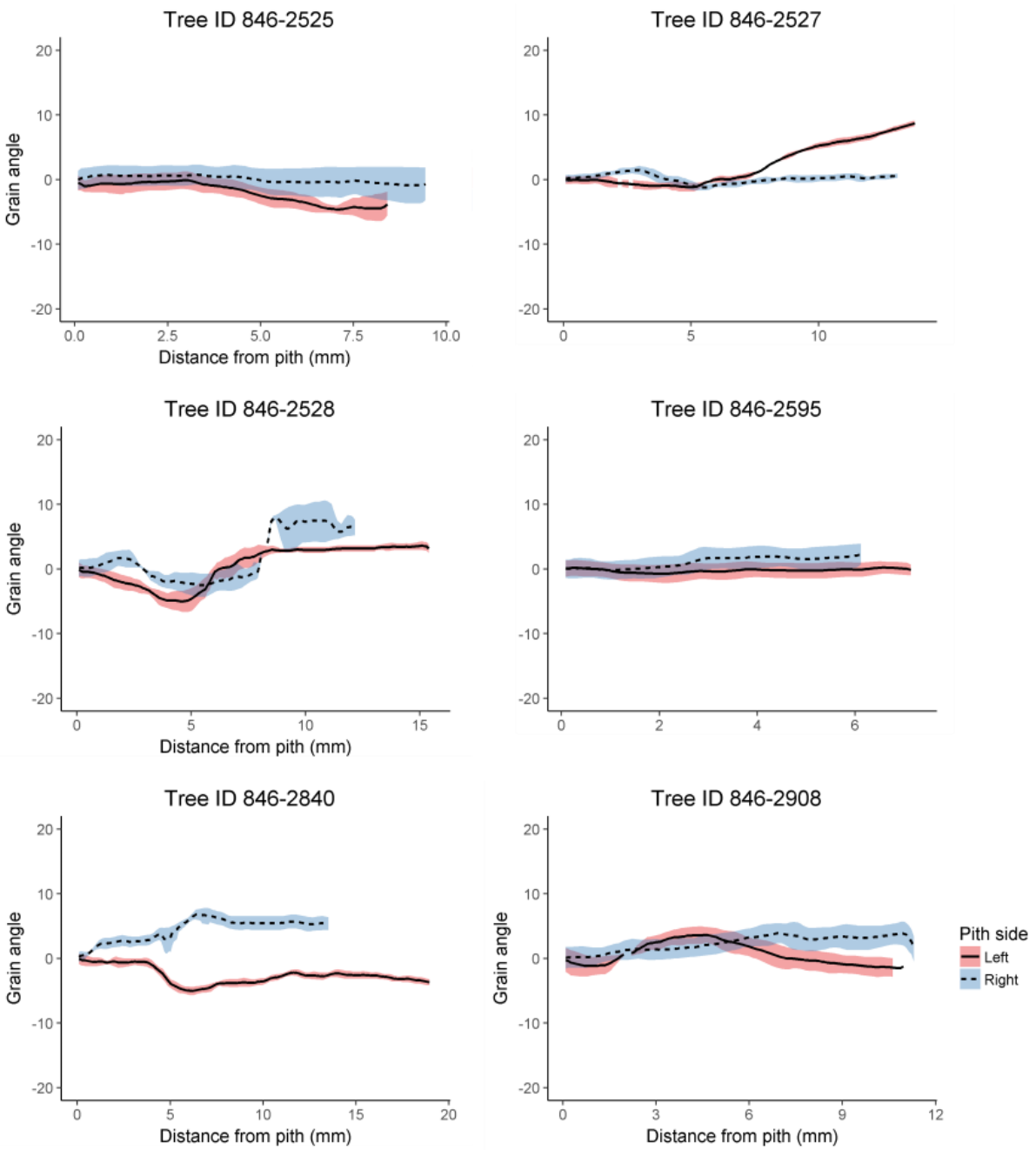

Figure 3.11 Grain splitting patterns for family 846. Negative values denote left-handed grain, positive values denote right-handed grain.

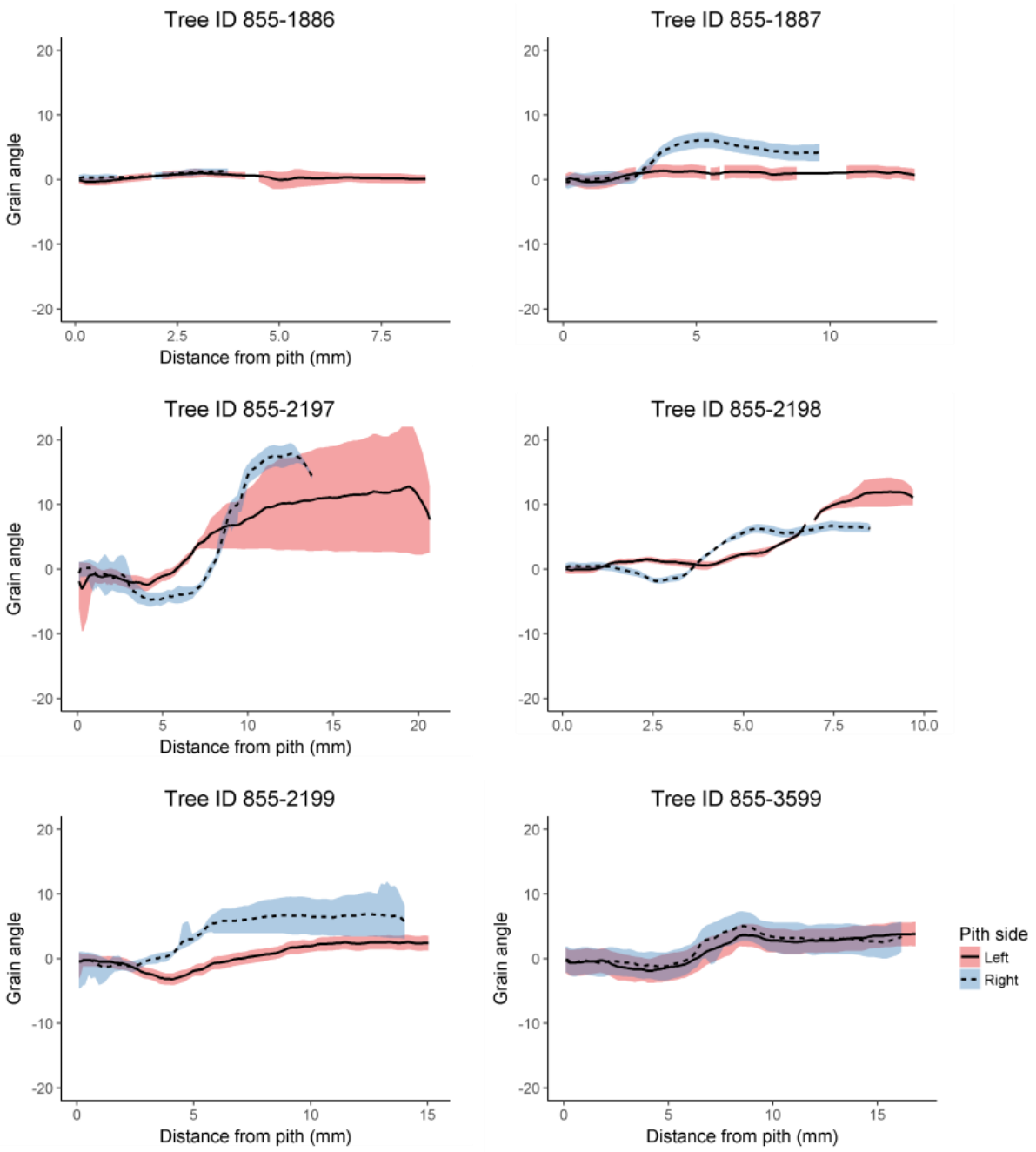

Figure 3.12 Grain splitting patterns for family 855. Negative values denote left-handed grain, positive values denote right-handed grain.

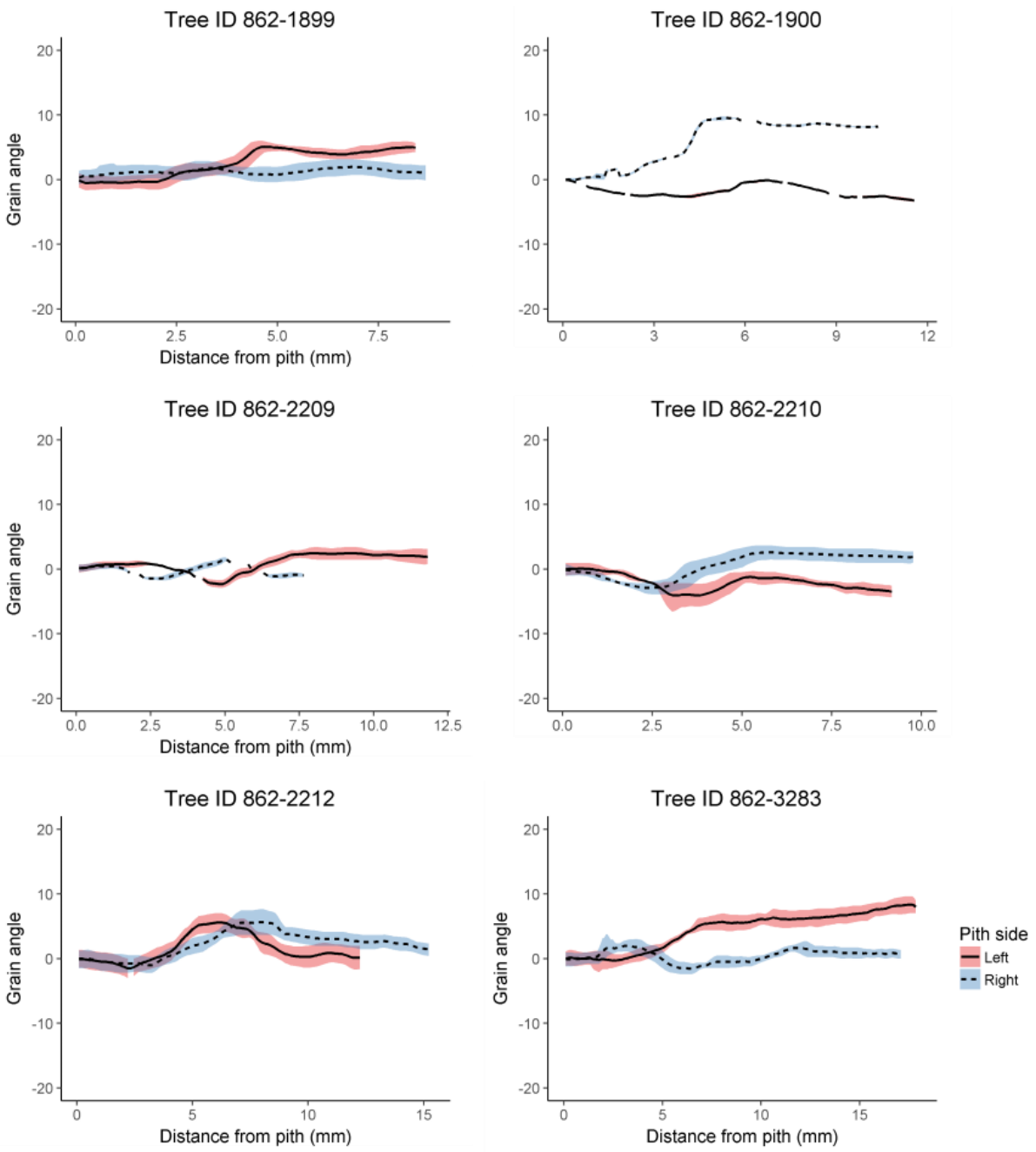

Figure 3.13 Grain splitting patterns for family 862. Negative values denote left-handed grain, positive values denote right-handed grain.

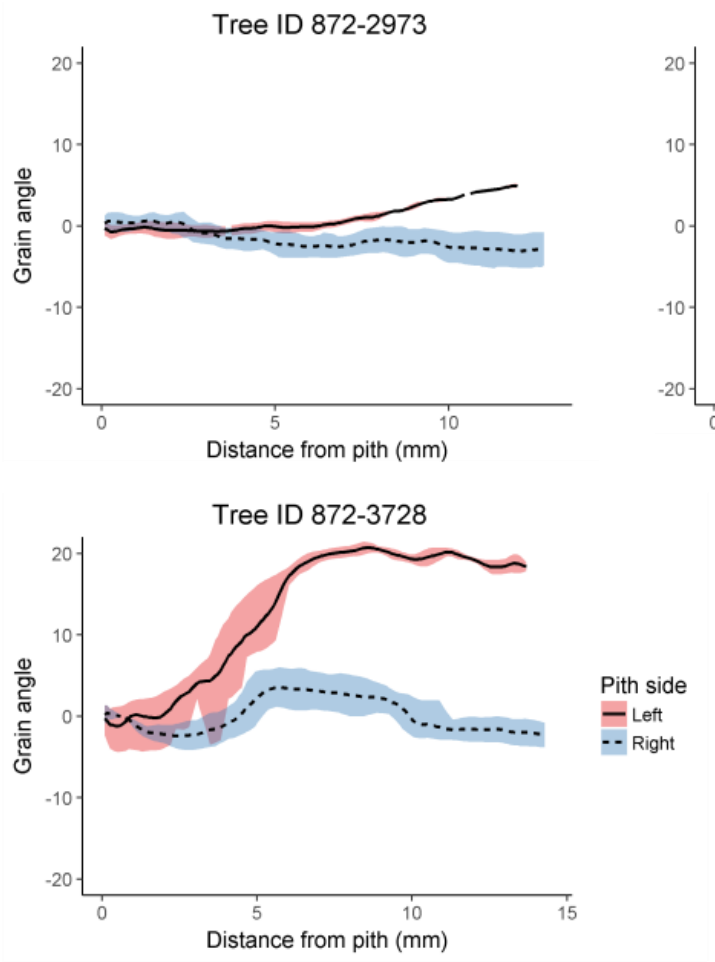

Figure 3.14 Grain splitting patterns for family 872. Negative values denote left-handed grain, positive values denote right-handed grain.

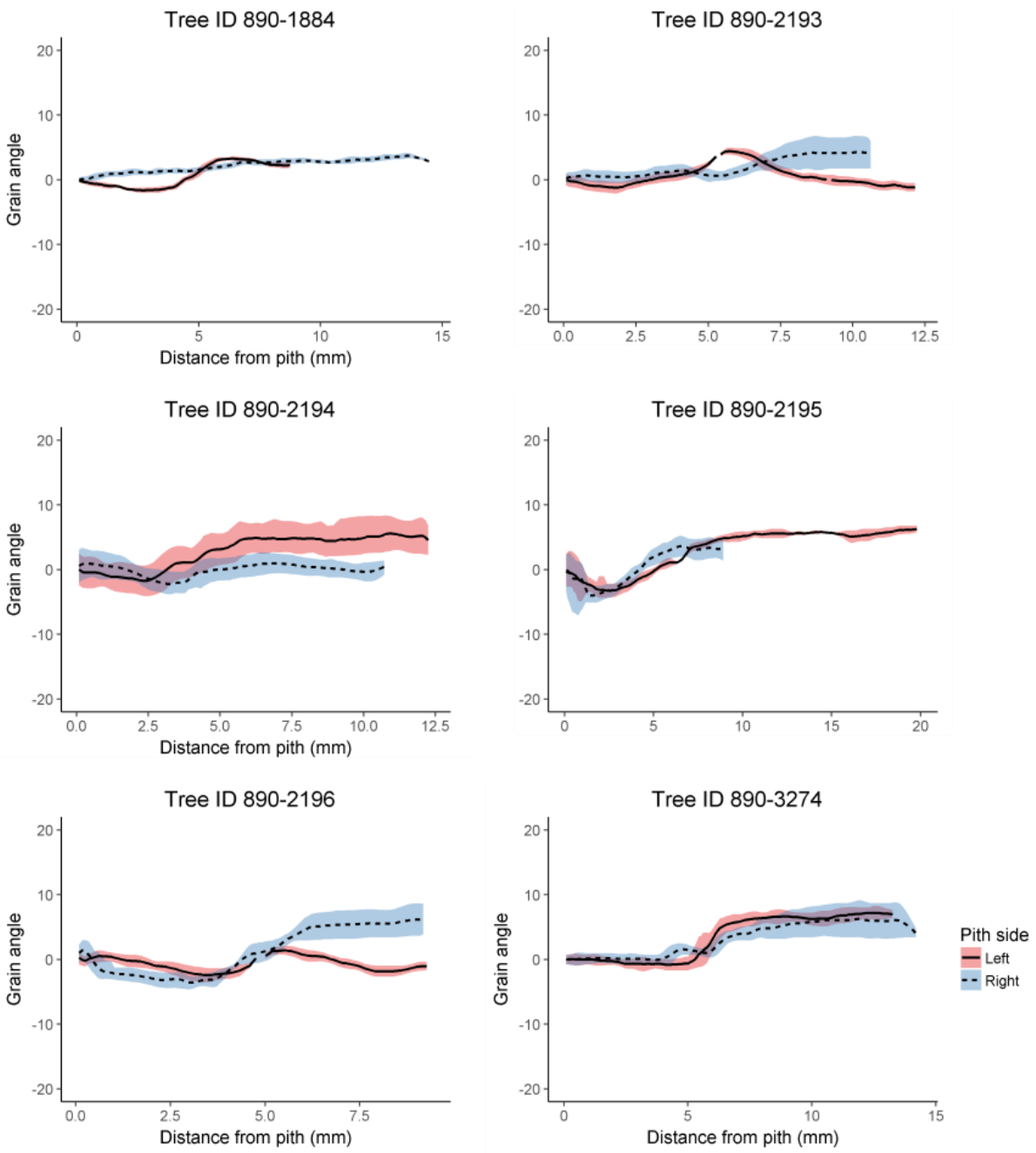

Figure 3.15 Grain splitting patterns for family 846. Negative values denote left-handed grain, positive values denote right-handed grain.

3.4 Discussion

As discussed in section 3.3.2.4, there was a large discrepancy between the grain angles obtained through X-ray microtomography and wood splitting. As the wood splitting measurement has a lower resolution than X-ray microtomography, this is not surprising. However, the grain pattern observed with the wood splitting technique concurred with that obtained through x-ray microtomography. Therefore, the wood splitting technique is useful for initial characterisation of trends in grain patterns and the identification of families of interest for further analysis.

Due to the complexity of interlocked grain, it was not possible, with the analysis methods utilised, to discern the relationship between interlocked grain patterns and the resulting board warping angles measured. Mathematical modelling approaches that take other factors such as volumetric shrinkage, microfibril angle and density, along with the periodicity of interlocked grain oscillations may have more success but were out of the scope of this research.

While some of the *E. bosistoana* families analysed had consistent interlocked grain patterns, suggesting that interlocked grain is heritable (Fan et al., 2013; Thinley et al., 2005). Many had no discernible pattern, suggesting that interlocked grain development is complex process. To further understand the heritability and genetics of interlocked grain, a smaller and more highly controlled study is required. Additional wood properties that may affect interlocked grain formation, such as tension wood formation, should also be considered (Hernández & Almeida, 2007; Weddell, 1961).

3.5 Conclusion

The wood splitting technique utilised in this thesis provides a high throughput method for the analysis of general trends in interlocked grain patterns but is not suitable for in depth analyses investigating the heritability of interlocked grain or the link between interlocked grain patterns and board warping. Furthermore, to fully investigate the link between interlocked grain and board warping, more complex modelling methodologies need to be developed.

Appendix

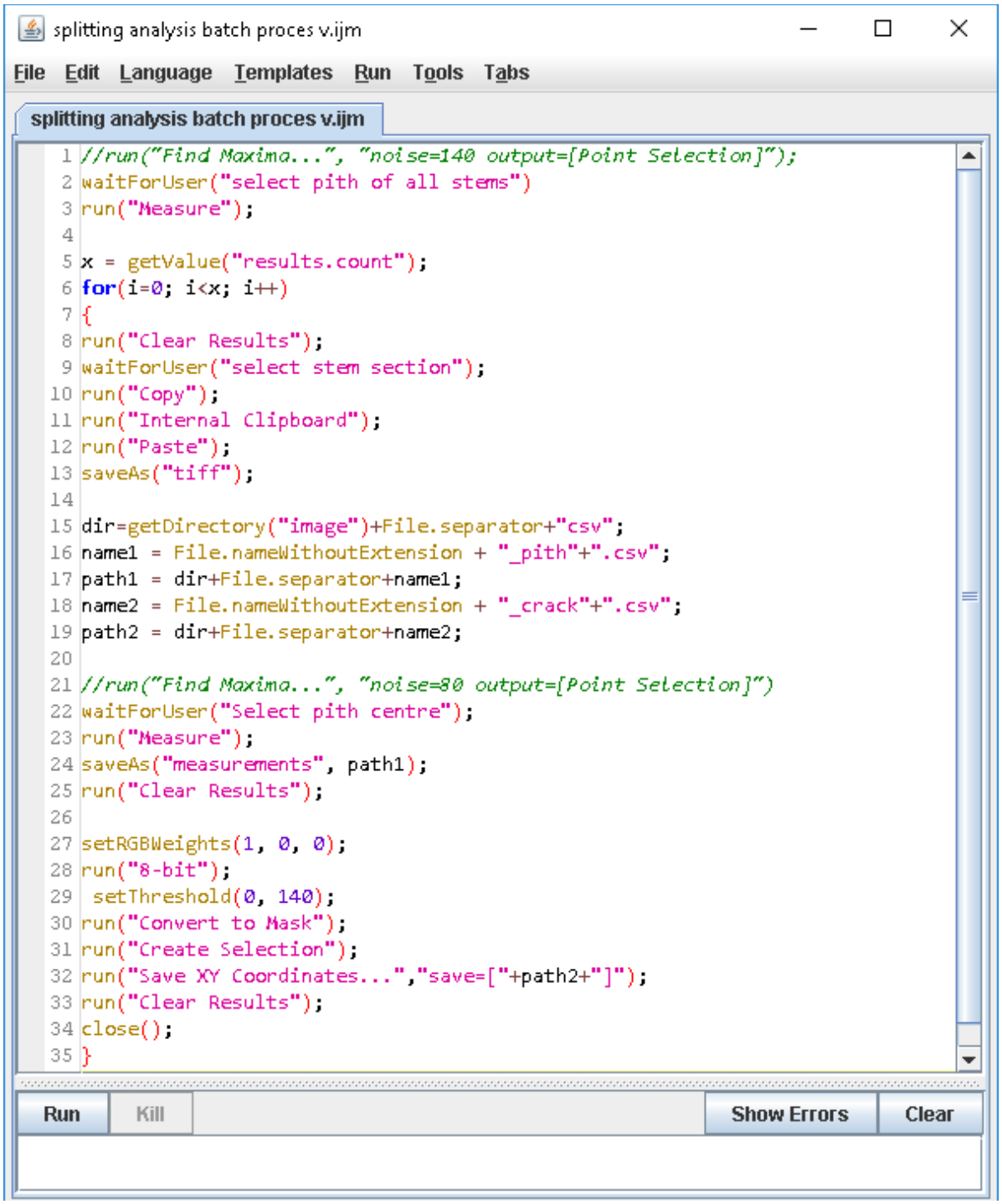

Appendix 1: The macro written in imageJ for the batch processing of split wood discs

```
setwd("C:\\Users\\steph\\Documents\\University\\Thesis\\Wood splitting\\Results\\csv\\")
Pith=list.files(pattern = "*pith.csv")
Crack=list.files(pattern = "*crack.csv")

for (i in 1:length(Pith)){
  PithFile  = paste("C:\\Users\\steph\\Documents\\University\\Thesis\\Wood splitting\\Results\\csv\\",Pith[i], sep="")
  PD<-read.csv(PithFile)[,3:4]
  PD<-cbind(strsplit(Pith[i],"_")[[1]][1],PD)
  colnames(PD)<-c("Sample","XPith","YPith")

  CrackFile = paste("C:\\Users\\steph\\Documents\\University\\Thesis\\Wood splitting\\Results\\csv\\",Crack[i] , sep="")
  CD<-read.csv(CrackFile)[,2:3]
  CD<-cbind(strsplit(Crack[i],"_")[[1]][1],CD)
  colnames(CD)<-c("Sample","XCrack","YCrack")

  data<-cbind(CD,PD)[,-c(4)]

  combname<-paste("C:\\Users\\steph\\Documents\\University\\Thesis\\Wood splitting\\Results\\csv\\comb\\",
            sub("crack.csv","comb.csv",Crack[i]), sep="")
  write.csv(data,combname)}

setwd("C:\\Users\\steph\\Documents\\University\\Thesis\\Wood splitting\\Results\\csv\\comb\\")
Comb=list.files(pattern = "*comb.csv")

rad2deg <- function(rad) {(rad * 180) / (pi)}
deg2rad <- function(deg) {(deg * pi) / (180)}

for (i in Comb){
  File= paste("C:\\Users\\steph\\Documents\\University\\Thesis\\Wood splitting\\Results\\csv\\comb\\", i , sep="")
  FD <-read.csv(File)[,2:6]
  FD2<-FD
  FD2[,2]<-FD[,2]-FD[,4]
  FD2[,3]<-FD[,3]-FD[,5]
  FD2[,2:3]<-FD2[,2:3]*0.085
  FD3<-FD2
  FD3[,3]<-ifelse(FD3[,3]<0,0-FD3[,3],FD3[,3])
  FD3[,3]<-atan(FD3[,3]/20)
  FD4<-FD3
  FD4[,3]<-rad2deg(FD4[,3])
  FD4[,3]<-ifelse(FD2[,3]<0,0-FD4[,3],FD4[,3])
  FD4[,3]<-ifelse(FD2[,2]<0,0-FD4[,3],FD4[,3])

  procname<-paste("C:\\Users\\steph\\Documents\\University\\Thesis\\Wood splitting\\Results\\csv\\comb\\processed\\",
                  sub("comb.csv","proc.csv", i), sep="")
  write.csv(FD4,procname)}
```

Appendix 2: RStudio script to process the crack and pith coordinates exported from ImageJ

```
library(dbscan)
library(readr)
library(tidyverse)
library(dplyr)
library(ggplot2)
library(zoo)
only_Crack<-function(x) {
FD7[FD7[,3] == x,]
}
setwd("C:\\Users\\steph\\Documents\\University\\Thesis\\Wood splitting\\Results\\csv\\comb\\processed")

#-----------------------------------------------------------------
filename <- file.choose()
data <- read.csv(filename, header = TRUE)
name <- basename(filename)

x<- data
FD5<-x      ## rename file
FD5[,4]<-FD5[,4]*-1    ## Ensure LH = negative and RH = positive
FD5<-FD5[,3:4]          ##select data
FD6<-as.matrix(FD5)     ##Convert to numeric matrix
kNNdistplot(FD6, k=40)
abline(h=1.5, col="red",lty=2)
knee<-locator(1)
res<-dbscan(FD6, eps=knee$y,minPts = 20)
pairs(FD6, col= res$cluster + 1L)
FD7<-cbind(FD6, res$cluster)
res

##-------------------------------------------------------------------------------------------
Crack<-only_Crack(1)
Crack1<-data.frame(Crack)
Crack1<-tbl_df(Crack1)
```

Appendix 3: RStudio protocol to remove erroneous points through density-based clustering

References

Albersheim, P. (2011). *Plant cell walls: from chemistry to biology*. New York: Garland Science.

Aloni, R. (1987). Differentiation of vascular tissues. *Annual Review of Plant Physiology and Plant Molecular Biology, 38*, 179-204

Altamura, M. M., Possenti, M., Matteucci, A., Baima, S., Ruberti, I., & Morelli, G. (2001). Development of the vascular system in the inflorescence stem of Arabidopsis. *New Phytologist, 151*, 381-389

Altaner, C. (2017). *SFF grant 407602 - Milestone M-3461: Woodville harvest (Summer 2016/2017)*. Retrieved from http://nzdfi.org.nz/wp-content/uploads/2017/03/Wood-properties_Woodville-harvest_methods.pdf

Azimzadeh, J., Nacry, P., Christodoulidou, A., Drevensek, S., Camilleri, C., Amiour, N., . . . Bouchez, D. (2008). *Arabidopsis* TONNEAU1 proteins are essential for preprophase band formation and interact with centrin. *The Plant Cell, 20*, 2146-2159

Baillères, H., Davrieux, F., & Ham-Pichavant, F. (2002). Near infrared analysis as a tool for rapid screening of some major wood characteristics in a eucalyptus breeding program. *Annals of Forest Science, 59*, 479-490

Balodis, V. (1971). *Twist in seasoned boards from plantation thinnings.* Paper presented at the IUFRO 15 World Congress.

Bannan, M. (1966). Spiral grain and anticlinal divisions in the cambium of conifers. *Canadian Journal of Botany, 44*, 1515-1538

Bannan, M. W. (1968). Anticlinal Divisions and the Organization of Conifer Cambium. *Botanical Gazette, 129*, 107-113

Baskin, T. I. (2001). On the alignment of cellulose microfibrils by cortical microtubules: a review and a model. *Protoplasma, 215*, 150-171

Batish, D. R., Singh, H. P., Kohli, S. K., & Kaur, S. (2008). Eucalyptus essential oil as a natural pesticide. *Forest Ecology and Management, 256*, 2166-2174

Boas, H. (1933). Cross, diagonal and spiral grain in timber *CSIRO Trade Circular* (Vol. 13). Melbourne: Council for Scientific and Industrial Research. Division of Forest Products.

Bootle, K. R. (1983). *Wood in Australia. Types, properties and uses*. Sydney: McGraw-Hill Book Company.

Braun, A. (1854). *Über den schiefen Verlauf der Holzfaser und die dadurch bedingte Drehung der Stämme*. Berlin: Königlichen Akademie der Wissenschaften.

Brodersen, C. R., Lee, E. F., Choat, B., Jansen, S., Phillips, R. J., Shackel, K. A., . . . Matthews, M. A. (2011). Automated analysis of three-dimensional xylem networks using high-resolution computed tomography. *New Phytologist, 191*, 1168-1179

Brodersen, C. R., Roark, L. C., & Pittermann, J. (2012). The physiological implications of primary xylem organization in two ferns. *Plant, Cell & Environment, 35*, 1898-1911

Bubble Level, NixGame, Android App (Version 3.23) Retrieved from https://play.google.com/store/apps/details?id=org.nixgame.bubblelevel

Burdon, R. (2010). Wood properties and genetic improvement of radiata pine. *New Zealand Journal of Forestry, 55*, 22-27

Burdon, R., & Bannister, M. (1973). Provenances of *Pinus radiata*: their early performance and silvicultural potential. *New Zealand Journal of Forestry, 18*, 217-232

Burger, H. (1950). Derwuchs bei der Lärche. *Forstwiss Clb, 69*, 121-125

Butterfield, B. (2006). The structure of wood: form and function *Primary Wood Processing: Principles and Practice* (pp. 1-22). Dordrecht: Springer Netherlands.

Butterfield, B. G., & Meylan, B. A. (1980). *Three-dimensional structure of wood: An ultrastructure approach* (2nd ed.). London: Chapman and Hall Ltd.

Carson, M. J. (1987). *Improving log and wood quality: the role of the radiata pine improvement programme*. Wellington: New Zealand Institue of Foresters.

Chaffey, N., Cholewa, E., Regan, S., & Sundberg, B. (2002). Secondary xylem development in *Arabidopsis*: a model for wood formation. *Physiologia Plantarum, 114*, 594-600

Chaffey, N. J., Barnett, J. R., & Barlow, P. W. (1997). Cortical microtubule involvement in bordered pit formation in secondary xylem vessel elements of *Aesculus hippocastanum* L (Hippocastanaceae): a correlative study using electron microscopy and indirect immunofluorescence microscopy. *Protoplasma, 197*, 64-75

Chan, J. (2012). Microtubule and cellulose microfibril orientation during plant cell and organ growth. *Journal of Microscopy, 247*, 23-32

Chase, J. S. (1911). *Cone-bearing trees of the California mountains*. Chicago: A.C. McClurg & Co.

Chauhan, S., Donnelly, R., Huang, C., Nakada, R., Yafang, Y., & Walker, J. C. F. (2006). Wood quality: multifaceted opportunities *Primary Wood Processing: Principles and Practice* (pp. 159-202). Dordrecht: Springer Netherlands.

Cornelius, J. (1994). Heritabilities and additive genetic coefficients of variation in forest trees. *Canadian Journal of Forest Research, 24*, 372-379

Cosgrove, D. J. (1997). Assembly and enlargement of the primary cell wall in plants. *Annual Review of Cell and Developmental Biology, 13*, 171-201

Cown, D. J., McConchie, D. L., & Young, G. D. (1983). Wood properties of Pinus caribaea var. hondurensis grown in Fiji (pp. 54 pp.).

Cown, D. J., Walford, B., & Kimberley, M. O. (1995). Cross-grain effect on tensile strength and bending stiffness of *Pinus radiata* structural lumber. *New Zealand Journal of Forestry Science, 25*, 256-262

Cown, D. J., Young, G. D., & Kimberley, M. O. (1991). Spiral grain patterns in plantation-grown *Pinus radiata*. *New Zealand Journal of Forestry Science, 21*, 206-216

Dadswell, H. E. (1972). *The anatomy of eucalypt woods*. Melbourne: CSIRO.

Davies, N., & Altaner, C. (2017). SFF grant 407602 - Milestone M-3462: Wood properties (Summer 2016/17). *New Zealand: School of Forestry, University of Canterbury*

Dhondt, S., Vanhaeren, H., Van Loo, D., Cnudde, V., & Inzé, D. (2010). Plant structure visualization by high-resolution X-ray computed tomography. *Trends in Plant Science, 15*, 419-422

Dickson, A., Nanayakkara, B., Sellier, D., Meason, D., Donaldson, L., & Brownlie, R. (2016). Fluorescence imaging of cambial zones to study wood formation in *Pinus radiata* D. Don. *Trees, 31*, 1-12

Donaldson, L. A. (2001). Lignification and lignin topochemistry—an ultrastructural view. *Phytochemistry, 57*, 859-873

Edwards, W., Moles, A. T., & Franks, P. (2007). The global trend in plant twining direction. *Global Ecology and Biogeography, 16*, 795-800

Esau, K. (1965). *Plant Anatomy* (2nd ed.). New York: John Wiley & Sons, Inc.

Esteban, L. G., Palacios, P. d., Fernández, F. G., & Moreno, R. (2009). Wood Anatomy Of The Genus Abies A Review. *30*, 231

Fan, Y., Rupert, K., Wiedenhoeft, A. C., Woeste, K., Lexer, C., & Meilan, R. (2013). Figured grain in aspen is heritable and not affected by graft-transmissible signals. *Trees, 27*, 973-983

Flannery, B. P., Deckman, H. W., Roberge, W. G., & Damico, K. L. (1987). Three-dimensional X-ray microtomography. *Science, 237*, 1439-1444

Forest Owners Association, & Industries, M. f. P. (2017). The New Zealand plantation forest industry: facts and figures. Wellington: Ministry for Primary Industries.

Fry, G. (1983). Eucalypts in New Zealand: a position report. *New Zealand Journal of Forestry, 28*, 394-411

Fuhr, M., Stührk, C., Münch, B., Schwarze, F., & Schubert, M. (2012). Automated quantification of the impact of the wood-decay fungus Physisporinus vitreus on the cell wall structure of Norway spruce by tomographic microscopy. *Wood Science and Technology, 46*, 769-779

Gandolfo, M. A., Hermsen, E. J., Zamaloa, M. C., Nixon, K. C., González, C. C., Wilf, P., . . . Johnson, K. R. (2011). Oldest known *Eucalyptus* macrofossils are from South America. *PLoS One, 6*, e21084

Gapare, W., Hathorn, A., Kain, D., Matheson, C., & Wu, H. (2007). Inheritance of spiral grain in the juvenile core of *Pinus radiata*. *Canadian Journal of Forest Research, 37*, 116-127

Gindl, W., & Teischinger, A. (2007). The potential of Vis-and NIR-spectroscopy for the nondestructive evaluation of grain-angle in wood. *Wood and Fiber Science, 34*, 651-656

Gunning, B. E. S., & Wick, S. M. (1985). Preprophase bands, phragmoplasts, and spatial control of cytokinesis. *Journal of Cell Science, 1985*, 157-179

Hahsler, M., Piekenbrock, M., Arya, S., & Mount, D. (2018) Density Based Clustering of Applications with Noise (DBSCAN) and Related Algorithms, R package (Version 1.1-3) Retrieved from https://cran.r-project.org/web/packages/dbscan/dbscan.pdf

Hannrup, B., Grabner, M., Karlsson, B., Müller, U., Rosner, S., Wilhelmsson, L., & Wimmer, R. (2002). Genetic parameters for spiral-grain angle in two 19-year-old clonal Norway spruce trials. *Annuals of Forest Science, 59*, 551-556

Hansen, J. K., & Roulund, H. (1998). Genetic parameters for spiral grain in two 18-year-old progeny trials with Sitka spruce in Denmark. *Canadian Journal of Forest Research, 28*, 920-931

Harris, J. (1969). On the causes of spiral grain in corewood of radiata pine. *New Zealand Journal of Botany, 7*, 189-213

Harris, J. M. (1973). Spiral grain and xylem polarity in radiata pine: microscopy of cambial reorientation. *New Zealand Journal of Forestry Science, 3*, 363-378

Harris, J. M. (1989). *Spiral grain and wave phenomena in wood formation*. New York: Springer-Verlag.

Hejnowicz, Z., & Romberger, J. (1979). The common basis of wood grain figures is the systematically changing orientation of cambial fusiform cells. *Wood Science and Technology, 13*, 89-96

Hernández, R. E., & Almeida, G. (2007). Effects of wood density and interlocked grain on the shear strength of three Amazonian tropical hardwoods. *Wood and Fiber Science, 35*, 154-166

Iqbal, M., & Ghouse, A. K. M. (1990). Cambial concept and organisation. *The vascular cambium. Research Studies Press: Taunton*1-36

Jacot, A. P. (1931). Tree twist. *Science, 74*, 567-567

Joseleau, J.-P., Imai, T., Kuroda, K., & Ruel, K. (2004). Detection in situ and characterization of lignin in the G-layer of tension wood fibres of *Populus deltoides*. *Planta, 219*, 338-345

Karczewska, D., Karczewski, J., Wloch, W., Jura-Morawiec, J., Kojs, P., Iqbal, M., & Krawczyszyn, J. (2009). Mathematical modeling of intrusive growth of fusiform initials in relation to radial growth and expanding cambial circumference in *Pinus sylvestris L. Acta Biotheoretica, 57*, 331-348

Kawamura, E., Himmelspach, R., Rashbrooke, M. C., Whittington, A. T., Gale, K. R., Collings, D. A., & Wasteneys, G. O. (2006). MICROTUBULE ORGANIZATION 1 regulates structure and function of microtubule arrays during mitosis and cytokinesis in the Arabidopsis root. *Plant Physiology, 140*, 102-114

Kininmonth, J. A., & Whitehouse, L. J. (1991). *Properties and uses of New Zealand radiata pine*. Rotorua: New Zealand Ministry of Forestry: Forest Research Institute.

Ko, B., Vogeler, I., Bolan, N. S., Clothier, B., Green, S., & Kennedy, J. (2007). Mobility of copper, chromium and arsenic from treated timber into grapevines. *Science of The Total Environment, 388*, 35-42

Koehler, A. (1924). *The properties and uses of wood*. New York: McGraw-Hill.

Koehler, A. (1949). *Growing better timber*. Washington: United States Department of Agriculture.

Koehler, A. (1960). Guide to determining slope of grain in lumber and veneer.

Koehler, A., & Luxford, R. F. (1951). *The longitudinal shrinkage of redwood*.

Kojs, P., Wloch, W., & Rusin, A. (2004). Rearrangement of cells in storeyed cambium of *Lonchocarpus sericeus* (Poir.) DC connected with formation of interlocked grain in the xylem. *Trees-Structure and Function, 18*, 136-144

Kojs, P., Włoch, W., Rusin, A., & Szendera, W. (2003). Storeyed structure of cambium as an adaptative strategy to environmental conditions in trees forming canopy and the emergent layer of the tropical rain forests. *Biuletyn Ogrodów Botanicznych, 12*, 23-29

Kollmann, F. F. P., & Côté, W. A. (1968). *Solid wood* (Vol. 1). Berlin: Springer-Verlag.

Krawczyszyn, J. (1972). Movement of the cambial domain pattern and mechanism of formation of interlocked grain in *Platanus*. *Acta Societatis Botanicorum Poloniae, 41*, 443-461

Kubler, H. (1991). Function of spiral grain in trees. *Trees - Structure and Function, 5*, 125-135

Larson, P. R. (1994). *The vascular cambium: development and structure*. New York: Springer-Verlag.

Lausberg, M., Gilchrist, K., & Skipwith, J. (1995). Wood properties of Eucalyptus nitens grown in New Zealand. *New Zealand Journal of Forestry Science, 25*, 147-163

Ledgard, N. J. (2008). Assessing risk of the natural regeneration of introduced conifers or wilding spread. *New Zealand Plant Protection, 61*, 91-97

Lev-Yadun, S. (2001). Intrusive growth - the plant analog of dendrite and axon growth in animals. *New Phytologist, 150*, 508-512

Li, Y., & Altaner, C. (2017). *Improving heartwood quality of durable eucalypts.* Paper presented at the Durable eucalypts on drylands: protecting and enhancing value. Workshop proceedings.

Low, C. B., McKenzie, H. M., Shelbourne, C. J. A., & Gea, L. D. (2005). Sawn timber and wood properties of 21-year-old *Cupressus lusitanica*, *C. macrocarpa*, and *chamaecyparis nootkatensis* χ *c. macrocarpa* hybrids. Part 1: Sawn timber performance. *New Zealand Journal of Forestry Science, 35*, 91-113

Mayo, S., Chen, F., & Evans, R. (2010). Micron-scale 3D imaging of wood and plant microstructure using high-resolution X-ray phase-contrast microtomography. *Journal of Structural Biology, 171*, 182-188

Mazur, E., & Kurczynska, E. U. (2012). Rays, intrusive growth, and storied cambium in the inflorescence stems of *Arabidopsis thaliana* (L.) Heynh. *Protoplasma, 249*, 217-220

Mead, D. J. (2013). *Sustainable management of Pinus radiata plantations*: Food and Agriculture Organization of the United Nations (FAO).

Medhurst, J., Ottenschlaeger, M., Wood, M., Harwood, C., Beadle, C., & Valencia, J. C. (2011). Stem eccentricity, crown dry mass distribution, and longitudinal growth strain of plantation-grown *Eucalyptus nitens* after thinning. *Canadian Journal of Forest Research, 41*, 2209-2218

Mellerowicz, E. J., Baucher, M., Sundberg, B., & Boerjan, W. (2001). Unravelling cell wall formation in the woody dicot stem. *Plant Molecular Biology, 47*, 239-274

Mishiro, A., & Booker, R. E. (1988). Warping in new crop radiata Pine 100× 50mm (2 by 4) Boards. *東京大学農学部演習林報告*37-68

Moore, J. R., Cown, D. J., & McKinley, R. B. (2015). Modelling spiral grain angle variation in New Zealand-grown radiata pine. *New Zealand Journal of Forestry Science, 45*, 15

Moser, L., Fonti, P., Büntgen, U., Esper, J., Luterbacher, J., Franzen, J., & Frank, D. (2009). Timing and duration of European larch growing season along altitudinal gradients in the Swiss Alps. *Tree Physiology, 30*, 225-233

Nanayakkara, B., Manley-Harris, M., Suckling, I. D., & Donaldson, L. A. (2005). *Chemical characterisation of compression wood in Pinus radiata.* Paper presented at the 59th Appita Annual Conference and Exhibition: Incorporating the 13th ISWFPC (International Symposium on Wood, Fibre and Pulping Chemistry), Auckland, New Zealand, 16-19 May 2005: Proceedings.

Newman, R. H., Hill, S. J., & Harris, P. J. (2013). Wide-angle x-ray scattering and solid-state nuclear magnetic resonance data combined to test models for cellulose microfibrils in mung bean cell walls. *Plant Physiology, 163*, 1558-1567

Nick, P. (2007). Control of cell axis *Plant microtubules* (pp. 3-46): Springer.

Northcott, P. (1957). Is spiral grain the normal growth pattern? *The Forestry Chronicle, 33*, 335-352

Norton, D. A. (1998). *Impacts of tree coring on indigenous trees*: Department of Conservation Christchurch.

Ogata, Y., & Fujita, M. (2005). New anatomical method of grain angles measurement using confocal microscopy and image cross-correlation. *Trees-Structure and Function, 19*, 73-80

Ogata, Y., Fujita, M., Nobuchi, T., & Sahri, M. H. (2003). Macroscopic and Anatomical Investigation of Interlocked Grain in *Acacia Mangium*. *24*, 13

Ohba, K. (1993). Clonal forestry with sugi (*Cryptomeria japonica*) *Clonal Forestry II* (pp. 66-90): Springer.

Ohkura, S. (1958). On the macroscopic features of twisted fibre in trees. *Journal of the Faculty of Agriculture Shinshu University, 8*, 59-100

Olson, D. F., Roy, D. F., & Walters, G. A. (1990). *Sequoia sempervirens* (D. Don) Endl. Redwood. *Silvics of North America, 1*, 541-551

Patel, R. N. (1971). Anatomy of stem and root wood of *Pinus radiata* D. Don. *New Zealand Journal of Forestry Science, 1*, 37-49

Paul, S., Gopal, S., Nandi, S. K., & Palni, L. (2015). Eco-morphology and molecular attributes of twisted and straight Chir pine (Pinus roxburghii Sarg.) growing in Uttarakhand: Central Himalaya of Indian Himalayan region. *Inte. J. Advanced Research, 3*, 885-894

Pole, M. (1994). An Eocene macroflora from the Taratu Formation at Livingstone, North Otago, New Zealand. *Australian journal of botany, 42*, 341-367

Ptashnyk, M., & Seguin, B. (2016). The impact of microfibril orientations on the biomechanics of plant cell walls and tissues. *Bulletin of Mathematical Biology, 78*, 2135-2164

Roberds, J. H., Namkoong, G., & Skroppa, T. (1990). Genetic analysis of risk in clonal populations of forest trees. *Theor Appl Genet, 79*, 841-848

Säll, H. (2002). *Spiral grain in Norway spruce.* Växjö University Press.

Schoch-Bodmer, H., & Huber, P. (1952). Local apical growth and forking in secondary fibres. *Proceedings of the Leeds Philosophical Society, 6*, 25-32

Schulgasser, K., & Witztum, A. (2007). The mechanism of spiral grain formation in trees. *Wood Science and Technology, 41*, 133-156

Sepúlveda, P. (2001). Measurement of spiral grain with computed tomography. *Journal of Wood Science, 47*, 289-293

Shelly, J. R., Arganbright, D. G., & Birnbach, M. (2007). Severe warp development in young-growth ponderosa pine studs. *Wood and Fiber Science, 11*, 50-56

Shelly, J. R., & Simpson, W. T. (2000). Analysis of warp in lumber manufactured from suppressed-growth Douglas-fir. *Issues Related to Handling the Influx of Small-Diameter Timber in Western North America*21-27

Silba, J. (1983). *An international census of the Coniferae*. Retrieved from

Skatter, S., & Kucera, B. (1997). Spiral grain - An adaptation of trees to withstand stem breakage caused by wind-induced torsion. *Holz Als Roh-Und Werkstoff, 55*, 207-213

Skatter, S., & Kucera, B. (1998). The cause of the prevalent directions of the spiral grain patterns in conifers. *Trees - Structure and Function, 12*, 265-273

Skolmen, R. G. (1963). Robusta eucalyptus wood: its properties and uses. *Res. Paper PSW-RP-9. Berkeley, CA: Pacific Southwest Forest and Range Experiment Station, Forest Service, US Department of Agriculture; 12 p, 9*,

Sorensson, C. T., & Lausberg, M. J. F. (1996). *Towards genetic improvement of spiral grain*. Queensland: Queensland Forestry Research Institute.

Spear, M., & Walker, J. C. F. (2006). Dimensional instability in timber *Primary Wood Processing: Principles and Practice* (pp. 95-120). Dordrecht: Springer Netherlands.

Steppe, K., Cnudde, V., Girard, C., Lemeur, R., Cnudde, J.-P., & Jacobs, P. (2004). Use of X-ray computed microtomography for non-invasive determination of wood anatomical characteristics. *Journal of Structural Biology, 148*, 11-21

Strabala, T. J., & MacMillan, C. P. (2013). The *Arabidopsis* wood model - the case for the inflorescence stem. *Plant Science, 210*, 193-205

Stuppy, W. H., Maisano, J. A., Colbert, M. W., Rudall, P. J., & Rowe, T. B. (2003). Three-dimensional analysis of plant structure using high-resolution X-ray computed tomography. *Trends in Plant Science, 8*, 2-6

Tarvainen, V. (2005). *Measures for improving quality and shape stability of sawn softwood timber during drying and under service conditions - Best practice manual to improve straightness of sawn timber*. Espoo, Finland: VTT Publications.

Tewari, D. N. (1994). *A monograph on deodar (Cedrus deodara (Roxb.) G. Don)*: International Book Distributors.

Theophrastus. (1916). *Enquiry into Plants, Volume I: Books 1-5*. Translated by Arthur F. Hort. Loeb Classical Library 70. Cambridge, MA: Harvard University Press. (Original work published ca. 350-278 BC).

Thinley, C., Palmer, G., Vanclay, J. K., & Henson, M. (2005). Spiral and interlocking grain in Eucalyptus dunnii. *Holz als Roh- und Werkstoff, 63*, 372-379

Thomas, J. (2014). *An investigation on the formation and occurrance of spiral grain and compression wood in radiata pine (Pinus radiata D. Don.).* (PhD), The University of Canterbury.

Thomas, J., & Collings, D. A. (2016). 3D Visualisation of spiral grain and compression wood in *Pinus radiata* with fluorescence and circular polarised light imaging. *Wood and Fiber Science, 48*, 22-27

Thomas, J., & Collings, D. A. (2017). *Imaging Spiral Grain in Pinus radiata with X-ray Microtomography*, Singapore.

Thurn, M., Lamb, E., & Eshenaur, B. (2018). Juniperus: New York State Integrated Pest Management Program.

Timell, T. E. (1986). *Compression wood in gymnosperms*. Heidelberg: Springer.

Tinevez, J. (2017) Directionality, Plugin for ImageJ (Version 2.0.2) Retrieved from https://imagej.net/Directionality

Traas, J., Bellini, C., Nacry, P., Kronenberger, J., Bouchez, D., & Caboche, M. (1995). Normal differentiation patterns in plants lacking microtubular preprophase bands. *Nature, 375*, 676-677

Trtik, P., Dual, J., Keunecke, D., Mannes, D., Niemz, P., Stähli, P., . . . Stampanoni, M. (2007). 3D imaging of microstructure of spruce wood. *Journal of Structural Biology, 159*, 46-55

Twell, D., Park, S. K., Hawkins, T. J., Schubert, D., Schmidt, R., Smertenko, A., & Hussey, P. J. (2002). MOR1/GEM1 has an essential role in the plant-specific cytokinetic phragmoplast. *Nature Cell Biology, 4*, 711-714

Van Ballekom, S., & Millen, P. (2017, 2017). *NZDFI: Acheivements, Constraints and Opportunities.* Paper presented at the Durable Eucalyptus on Drylands: Protecting and Enhancing Value, Blenheim, New Zealand.

Van den Bulcke, J., Boone, M., Van Acker, J., Stevens, M., & Van Hoorebeke, L. (2009). X-ray tomography as a tool for detailed anatomical analysis. *Annals of Forest Science, 66*, 508-508

Webb, C. D. (1969). Variation of interlocked grain in Sweetgum (*Liquidambar styracifula*). *Forest Products Journal, 19*, 45-48

Weddell, E. (1961). Influence of interlocked grain on the bending strength of timber, with particular reference to utile and greenheart. *Journal of the Institute of Wood Science, 7*, 56-72

Wessels, C., Crafford, P., Du Toit, B., Grahn, T., Johansson, M., Lundqvist, S.-O., . . . Seifert, T. (2016). Variation in physical and mechanical properties from three

drought tolerant Eucalyptus species grown on the dry west coast of Southern Africa. *European Journal of Wood and Wood Products, 74*, 563-575

Whittington, A. T., Vugrek, O., Wei, K. J., Hasenbein, N. G., Sugimoto, K., Rashbrooke, M. C., & Wasteneys, G. O. (2001). MOR1 is essential for organizing cortical microtubules in plants. *Nature, 411*, 610-613

Wilcox, M. (1980). Genetic improvement of eucalypts in New Zealand. *New Zealand Journal of Forestry Science, 10*, 343-359

Włoch, W., Mazur, E., & Beltowski, M. (2002). Formation of spiral grain in the wood of *Pinus sylvestris* L. *Trees - Structure and Function, 16*, 306-312

Włoch, W., Wilczek, A., Jura-Morawiec, J., Kojs, P., & Iqbal, M. (2013). Modelling for rearrangement of fusiform initials during radial growth of the vascular cambium in *Pinus sylvestris* L. *Trees - Structure and Function, 27*, 879-893

Włoch, W., & Zagorskamarek, B. (1982). Reconstruction of storeyed cambium in the linden. *Acta Societatis Botanicorum Poloniae, 51*, 215-228

Wray, N., & Visscher, P. (2008). Estimating trait heritability. *Nature Education, 1*, 29

Wyatt, S. E., Sederoff, R., Flaishman, M. A., & Lev-Yadun, S. (2010). *Arabidopsis thaliana* as a model for gelatinous fiber formation. *Russian Journal of Plant Physiology, 57*, 363-367

Yamanaka, K. (1984). Normal and traumatic resin-canals in the secondary phloem of conifers. *Journal of the Japan Wood Research Society, 30*, 347-353

Young, I. (1999). Seasonal variability of the global ocean wind and wave climate. *International Journal of Climatology: A Journal of the Royal Meteorological Society, 19*, 931-950

Yue, Z. S., & Feng, S. M. (1984). A preliminary report on introduction of *Cupressus torulosa*. *Forest Science and Technology (Linye Keji Tongxun)*6-8

Zobel, B., Stonecypher, R. W., & Browne, C. (1968). Inheritance of spiral grain in young loblolly pine. *Forest Science, 14*, 376-379

Zobel, B. J., & Jett, J. B. (2012). *Genetics of Wood Production*: Springer Berlin Heidelberg.